8-2015

The Effect of Classical Order on the Seismic Behavior of Ancient Masonry Columns

Cody M. Buckley
University of Nebraska-Lincoln, cbuckley@bsestructural.com

THE EFFECT OF CLASSICAL ORDER ON THE SEISMIC BEHAVIOR OF ANCIENT MASONRY COLUMNS

by

Cody Michael Buckley

A THESIS

Presented to the Faculty of

The Graduate College at the University of Nebraska

In Partial Fulfillment of Requirements

For the Degree of Master of Science

Major: Architectural Engineering

Under the Supervision of Professor Ece Erdogmus

Lincoln, Nebraska

August, 2015

THE EFFECT OF CLASSICAL ORDER ON THE SEISMIC BEHAVIOR OF ANCIENT MASONRY COLUMNS

Cody M. Buckley, M.S.

University of Nebraska, 2015

Advisor: Ece Erdogmus

The design and erection of columns in classical Greece and Rome was a deceptively complicated task. Ancient engineers were not guided by a set of building codes, resulting in several regional design variations. The writer Vitruvius condensed these variations into three archetypes or "orders" defined by proportions based on an arbitrary "module".

The goal of this thesis is to better understand the effect of these proportions on the seismic response of ancient columns through the use of Equivalent Lateral Force Procedure and finite element analysis software. To this end, a parametric study of linearly elastic, free-standing columns with homogeneous material properties was conducted. This study considered five typical columns per classical order. Dynamic analysis showed noticeable effects on natural circular frequency (ω_n) and mode of vibration (φ_n) due to both column order and slenderness ratio. Static analysis showed that the deformed shape and location of maximum stress was similar for all test columns.

This newfound understanding was utilized in a case study of the Temple of Antioch ad Cragum front façade. This Corinthian order, pro-style temple: dates back to 1-3rd century AD; is located near modern day Güney Village, Turkey; and is currently being excavated and considered for a partial reconstruction. Dynamic analyses showed that fixed entablature-column connections, similar to ancient clamp connections, cause the

frame to act more rigidly as opposed to pinned connections. Static analyses further illustrated the rigidity of the frame with fixed connections as it tended to resist seismic forces as a single rigid body. The pinned connections allowed for columns to more evenly resist seismic forces.

This study includes several assumptions in order to limit discussion to the effect of geometric proportions on the seismic behavior of ancient columns. The author has reviewed several studies that have approached the analysis of nonlinear, rigid body motion, but none have fully investigated the relationship between seismic behavior and classical order. This thesis is to serve as a basis for future investigation of this relationship under true dry stack conditions.

This thesis is dedicated to Joyce Buckley, Ruth Grannan, and Eldena Palmer; three women who helped me become who I am today.

ACKNOWLEDGEMENTS

To my wife and best friend Lauren: I simply could not have completed this thesis without your (sometimes tough) love and support. In my times of doubt you reminded me of what I can do. Even on my worst days you made me look forward to coming home.

To my family: Thank you for always encouraging me to follow my gut and teaching me that with hard work anything is possible.

To Dr. Ece Erdogmus: Thank you for all your assistance and guidance during my graduate study. I truly appreciate the plethora of opportunities you provided during the course of my study.

To Ariel Kousgaard and the rest of Dr. Erdogmus research team: Thank you for all your assistance and friendship. It is always easier to work when surrounded by a group of like-minded nerds.

To my dog Mikey: Thanks for always finding a way to help me relax and decompress.

Table of Contents

List of Figures

List of Tables

CHAPTER 1: INTRODUCTION

"It's not good because it's old, it's old because it's good." --Anonymous

In this thesis, first a parametric study is carried out on idealized column proportions in the three classical orders (Doric, Ionic, and Corinthian styles) assuming free-standing column scenarios and utilizing idealized linearly elastic models. Then a case study of a prostyle, Corinthian temple façade is analyzed under seismic loads, where Corinthian columns are a part of a frame system. This case study will utilize an actual archeological project ongoing in Southern Turkey (see Section 1.1.1).

1.1. Background and Motivation

The erection of columns in classical Greece and the territories within the Roman Empire, such as those often found in temples and public buildings, was a deceptively complicated task. In addition to the exceptional quality demanded of the builders, there were no governing set of building codes. This often resulted in different regional column variations in proportions and construction style. These columns were composed of numerous masonry blocks of varying size and shape. The size and shape of blocks depended on both design and function (i.e. base, shaft, and capital). Columns were constructed by carefully aligning and stacking these blocks without mortar and with or without dowels, or other reinforcement. This common construction technique without mortar is hereafter referred to as "dry stack".

Large concentrations of dry stack columns can be found in the remains of classical structures dotted throughout the Asia Minor and Mediterranean regions. Many of these

structures have been left in a ruinous state for some time and have little to no documentation regarding their history of structural damage and retrofits. For some of these structures, their location and construction suggests increased susceptibility to seismic events (Ambraseys and Jackson, 1998; Stiros, 2001; Ambraseys, 2006). When paired with the volatile nature of dry stack construction, seismic events are considered a threat to past and future structural stability. Historical accounts of structural health increase in both quality and frequency with a structure's importance. The Parthenon for example has accounts of structural damage due to both explosions and fire (Lawrence, 1996; Spawforth, 2006). However, as previously mentioned there are many structures with little to no documented structural history. A more complete understanding of these structural systems and their response to external threats can result in: 1) more informed explanations of previous structural failures; 2) improved design and employment of successful preservation techniques. It is therefore the goal of this thesis to provide a better understanding of the structural behavior of these columns as their geometries vary with style and proportions.

1.1.1. Temple of *Antioch ad Cragum*

The Temple of *Antioch ad Cragum* was the main imperial temple of the ancient city of *Antiocheia ad Cragum*. The ancient city, once an important provincial coastal city of the Roman Empire, is located in present day Güney Village, near Gazipaşa, Turkey. The temple was in a state of ruin when archaeologists first identified it in the 1960's. It remained in this state until it was re-discovered, by different archeologists, during a surface survey project in the late 1990's (Figure 1.1).

(a) Temple Remains

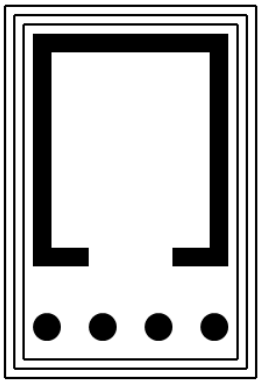

(b) Prostyle Layout

Figure 1.1. Temple of *Antioch ad Cragum*.

The ongoing anastylosis planning for the temple by Erdogmus et al. (2011a, 2011b, 2011, and 2013) has revealed much about the temple's history and original construction. Based on stylistic evidence and sculptural decoration observed on site, researchers have determined that the temple dates approximately to the early 3rd century A.D. It is identified that the temple was of the Corinthian order and featured four columns in its front façade, indicative of a prostyle layout (Figure 1.1). Since 2005, researchers have been systematically removing temple blocks from the collapse site for assessment and cataloging in preparation for a potential partial reconstruction.

1.2. Problem Definition

A wealth of literature regarding the response of classical structures to seismic action is available. However, the lack of dependable structural history increases the challenge of forensic investigations and preservation efforts. With that being said, the role of classical column proportions in the seismic response of classical structures has yet to be investigated in detail. A more focused investigation of such proportions could lead to a better understanding of the problem summarized in the following points:

- ❖ Many classical structures are located in areas prone to seismic excitation.
- ❖ Available historical information on structural health varies between structures.
- ❖ There were no definitive guidelines for ancient column design.

1.3. Goals and Objectives

The goal of this thesis is to better understand the effect of the geometrical differences of classical column orders on the seismic response of classical structures through the use of computer analyses. The objectives of this thesis are listed below:

I. To assess the magnitude of seismic threat to classical columns in both the Asia Minor and Mediterranean regions

II. To create a suite of finite element models representative of free-standing Doric, Ionic, and Corinthian order columns

III. To perform modal analyses to assess and compare the effect of classical proportions on a column's fundamental frequency

IV. To perform static analyses to investigate stresses developing at column component interfaces due to seismic forces

V. To perform a case study extrapolating the analysis methods developed to a Corinthian style façade in order to further investigate the effects of boundary conditions

1.4 Scope & Assumptions

In this paper a parametric study is carried out on idealized column proportions in the three classical orders (Doric, Ionic, and Corinthian) assuming free-standing column scenarios and utilizing idealized linearly elastic models. The models are linearly elastic

as a first step to observe the effects of classical geometrical proportions on free-standing column response in the elastic range. Seismic analyses are performed with the Equivalent Lateral Force Procedure (ELFP). Additionally a case study investigating the effects of mechanical connections on the behavior of the Temple of *Antioch ad Cragum* façade will be investigated. Analyses will be conducted with the following assumptions:

I. Each column in the parametric study is a single rigid body with dimensions determined by classical Vitruvian proportions
II. A single, common diameter is used to limit the parametric study's focus to the effects of typical classical proportions, and slenderness ratios on seismic response
III. Zero imperfections due to initial tilt or damaged cross section are considered
IV. Each column component will have a constant cross section, which neglects taper and ornamentation
V. Viscous damping is not considered with justification from literature (Carydis et al., 1996; Papantonopoulos et al., 2002; Psycharis et al., 2003; Psycharis, 2007)
VI. Idealized pinned and moment connections will be considered for the entablature to column connections of the case study

1.5. Thesis Overview

This thesis is organized into five chapters. The Introduction (Chapter 1) is followed by review of relevant literature (Chapter 2). Chapter 3 details the development and creation of finite element models for analysis. Chapter 4 is analysis results and discussion. Chapter 5 includes conclusions drawn from the thesis and provides suggestions for future research. References and appendices are included at the end of the document.

CHAPTER 2: LITERATURE REVIEW

This chapter provides a critical discussion of the pertinent literature on the following topics: seismicity of ancient structures, dynamic response of rigid blocks, and modeling/analysis techniques for the seismic assessment of ancient structures. The chapter concludes with a summary of key findings and their relation to the goals and methodology of this thesis.

2.1. Classical Temple Design

2.1.1. Terminology

The history of ancient Rome and Greece has been referred to by many terms. The meanings of these terms vary depending on one's discipline. Here the term "classical" refers to the collective architecture of the ancient Roman and Grecian societies. This thesis will reference common components of a classical temple, illustrated in Figure 2.1.

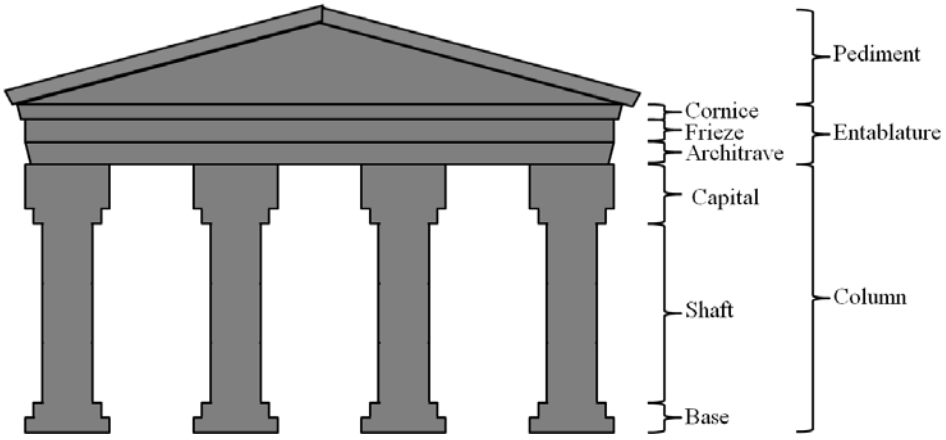

Figure 2.1. Classical Temple Façade Components.

2.1.2. *De Architectura*

Classical temple design was constantly being adjusted and refined. This was due to a variety of reasons such as aesthetics, superstition, and experience. Columns would become slimmer, entablature and roof pitch lower and gentler, and the plan of the

building went from long and thin to more compact over time (Spawforth, 2006). Despite the continual adjustments, the Roman writer Marcus Vitruvius Pollio (commonly known as Vitruvius) used his experience and studies of ancient Greek, and early Roman architecture to, "reduce the whole of this great art to a complete and orderly form of presentation" (Pollio and Morgan, 1960). The result was *De Architectura*, also known as The Ten Books on Architecture.

Of the ten books, two are concerned with the ideal proportion and design of temples. Within these books Vitruvius defines the characteristics of three orders: Doric, Ionic, and Corinthian. The Doric order is the oldest of the three orders. However, in the time of Vitruvius its use had declined significantly. This explains the relatively little attention given to it, including the expression of several Doric proportions in terms of their Ionic counterparts. The Ionic order was the most popular of the three and was described with most detail. This order was described with a completely unique set of proportions that included adjustments in the entablature and pediment based on column height. Although Corinthian was considered a separate order, it is essentially a clone of the Ionic, differing only in the size of its column capital (Pollio and Morgan, 1960).

2.1.3. Vitruvian Temple Design

Vitruvian temple design is based on a set of proportions and a "module". Vitruvius described each of the three orders with a set of ideal proportions. The orders were further divided into "substyles," differentiated primarily by column height, diameter, and spacing. Ultimately, this resulted in twelve temple types, each with a unique set of ideal member proportions based on a common module (Table 2.1).

Table 2.1. Architectural Orders and Substyles (from *De Architectura*).

Order	Substyle	Column Diameter	Column Height	Column Spacing
Doric	Systyle	2M	14M	5.5M (middle) 3M (else)
	Diastyle	2M	14M	8M (middle) 5.5M (else)
Ionic	Pycnostyle	M	10M	1.5M
	Systyle	M	9.5M	2M
	Diastyle	M	8.5M	3M
	Araeostyle	M	8M	4M
	Eustyle	M	9.5M	3M (middle) 2.25M (else)
Corinthian	Pycnostyle	M	10M	1.5M
	Systyle	M	9.5M	2M
	Diastyle	M	8.5M	3M
	Araeostyle	M	8M	4M
	Eustyle	M	9.5M	3M (middle) 2.25M (else)

The module (represented as "M") is an arbitrary base unit used in conjunction with a set of proportions to calculate member dimensions. The relationship between the module and the width of a temple's front colonnade is dependent on the following desired traits: 1) order; 2) substyle; and 3) number of columns in front colonnade. Once these traits have been decided upon, the module can either be determined from a maximum desired colonnade width, or simply chosen. Once the module is determined, the remaining member sizes can be found from the appropriate set of proportions.

2.2. Seismicity and Ancient Structures

Seismicity of ancient structures is a challenging topic for engineers who are charged with restoring or repairing historical entities. Numerous challenges such as: lack of construction documents, primitive (if any) seismic data collection systems, conflicting accounts of historical seismic events, and little to no documentation of other historic

events (i.e. explosions, lightning, or war) set this problem apart from modern seismic investigation. The efforts of previous authors, who have confronted these issues, are summarized in this section.

The Mediterranean and Middle East are home to a plethora of historical monuments, being the location of Mesopotamia, Ancient Greece, and Ancient Rome. In addition, these areas are greatly affected by seismic action. Ambraseys and Jackson (1998) focused on co-seismic surface faulting in a limited area of these regions, highlighted in Figure 2.2. Surface faulting is often associated with large earthquakes and can be used to estimate their size. The authors presented a table of one hundred fifty cases (from 464 BC – 1995 AD) of earthquakes that are associated with surface fault breaks. This table also includes pertinent information for each seismic event, such as date, location, magnitude, and epicenter.

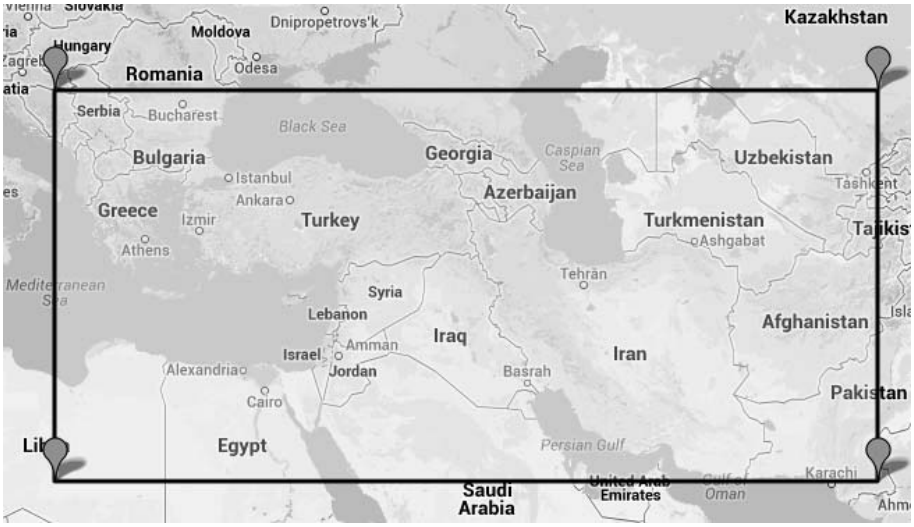

Figure 2.2. Ambraseys and Jackson (1998) - Study Region. The region studied was bound by latitudes 25°N and 45°N and longitudes 18°E and 70°E (Google Maps Engine Lite, 2013a).

A portion of the event magnitude estimations (those closer to 1900) are determined by calibrating felt, or observable, information (macroseismic) information against instrumental (microseismic) values of magnitude. However, macroseismic information was much tougher to come by prior to 1900. As a result, earlier events were categorized into three broad categories of magnitude (6.0-7.0, 7.0-7.8, and 7.8+ on the Richter scale). This "catalogue" of earthquake data provides a valuable look into the seismic history of the region.

Of the one hundred fifty examples of seismic action presented in Ambraseys and Jackson (1998), only six occur between the fourth and sixth centuries. Investigations by Stiros (2001) revealed an "earthquake storm" with over fifty cases of seismic events occurring in the Eastern Mediterranean region during this time period. Of particular note is the 365 AD Crete earthquake, believed to be the most important of the list, and larger than any earthquake that has affected, "the Hellenic Arc and the wider Eastern Mediterranean region in modern or recent historical times." The authors demonstrated how historical and archeological evidence, even conflicting accounts from a difficult period of time (such as the decline of the Roman Empire), can be useful in learning more about historical seismic events. Most importantly, this work highlights the need to investigate the seismic susceptibility of these ancient Eastern Mediterranean structures for preservation or forensic purposes.

Historical documentation can be an invaluable resource if used correctly as in Stiros (2001). However, if used incorrectly, this information can lead to incorrect assumptions and a completely incorrect account of historical events. Ambraseys (2006) demonstrated

this by taking biblical and archeological information at face value, to assess the Jericho and Judea earthquakes that occurred in the Holy Land. These famous earthquakes report statistics that simply cannot be corroborated, be it the 30,000 men killed (excluding women and children) due to the Judea event, or the collapse of Jericho's walls due to the blaring horns of the Israelites. This evidence of embellishment leads the author to caution the reader about catastrophism, the tendency to explain the unknown with major catastrophes (such as earthquakes). Pioneers of "archaeoseismology" used a catastrophe theory to explain the collapse of the Bronze Age, and Ambraseys referred to its revival in recent times as "neo-catastrophism". The downfall to catastrophism, and its revival, is that it causes scientists to ignore, "evidence presented by others or data from outside their own field of expertise." As Ambraseys concluded, the cure to this problem is greater collaborations between disciplines so as glean the truth from historical evidence.

2.3. Case Studies

As work on the dynamics of rigid bodies progressed, researchers saw the opportunity to use that knowledge in the assessment of ancient historic structures. Subsequent sections of this literature review will make reference to specific structures, located across multiple countries. This section consists of background information on each of these structures, as well as what they were used to study. The list of countries in this section is not exhaustive, as such, not all existing historic structures are included.

2.3.1. Greece

The style of architecture described by Vitruvius, known today as classical, originated in Ancient Greece. The ancient structures of this country housed some of history's greatest

minds and were host to countless academic accomplishments. Luckily, many of these structures remain standing today. This section includes examples of several structures that have been utilized by scientists to advance preservation technology.

Figure 2.3. Greek Case Studies. The map above marks the locations of the following case studies located in Greece: a) The Parthenon, Academy of Athens, and Temple of Olympios Zeus; b) Temple of Apollo at Bassae; and c) Temple of Zeus at Nemea (Google Maps Engine Lite, 2013b).

The Parthenon of Athens is quite possibly the most recognizable ancient temple in the world. Construction of the temple lasted from 447-438 BC. The temple experienced structural damage from many sources over the years, primarily from earthquakes, explosions, and fires. Its columns were approximately 10 meters (32.8 feet) high, tapered, and fluted. Multiple drums were used in each column; however the height and number varied between columns. Papers such as Carydis et al. (1996), Papantonopoulos

et al. (2002), Mouzakis et al. (2002), and Psycharis et al. (2003) investigated the seismic behavior of different parts of the temple.

The Academy of Athens was constructed in the late nineteenth century, and consists of a main building and two statue topped columns. The building was completed in 1885, the columns in 1874, and the statues in 1882. The columns are 13.3 meters (43.6 feet) in height and the statues are 3.6 meters (11.8 feet) and 4.1 meters (13.5 feet) tall respectively. Composed entirely of Pentelic marble, the combination of a column, statue, and pedestal weighs approximately 53 tons (77.2 kips) (Ambraseys and Psycharis, 2011). The seismic vulnerability of the statue of Apollo was the focus of a study by Ambraseys and Psycharis (2011).

The Temple of Olympios Zeus is also located in Athens, less than 1 kilometer (3281 feet) from the Parthenon. One of the largest temples of ancient Greece, construction lasted five hundred years and was completed in 131 AD. Originally, the temple consisted of 104 columns, of which only fifteen remain standing today. The columns are typically 16.81 meters (55.2 feet) tall, with the number and size of drums varying from column to column. The temple also featured a small, unique structure built on the architrave of two columns. The authors speculate that the structure was used as an isolation area for Athenian stylite monks. It was demolished in 1886, after a seven to eight century hypothesized life span (Psycharis, 2007). The temple was used by Psycharis (2007) in attempts to extract useful information about the seismic past of Athens.

The Temple of Apollo Epikourios at Bassae is a fifth century Doric style temple, whose first historical description came from Pausanius in 174 AD. The temple then vanished

from the record until its rediscovery by Joachim Bocher in 1765 (Papastamatiou and Psycharis, 1993 & 1996). Today, the temple is described as quite well preserved, despite all the destructive issues it has faced. These issues include: material deterioration, hastened by an elevation approximately 1000 meters (3281 feet) above sea level; leaning structural elements, caused by differential settlement; and its location in a seismically active area of Greece. Thirty-seven columns, all 5.95 meters (19.5 feet) in height and consisting of varying numbers of drums, remain standing. The temple's state of repair and susceptibility to earthquakes provided researchers with an opportunity to gain a better understanding of its seismic resistance. Subsequent sections discuss several studies that utilized this structure, including: 1) a dynamic field study (Papantonopoulos, 1993); 2) numerical investigations of seismic vulnerability in dry-stack structures (Papastamatiou and Psycharis, 1993 & 1996); and 3) parametric studies (Papantonopoulos, 1997 and Psycharis et al., 2000).

The Temple of Zeus at Nemea was built in the Doric style during the late fourth century BC. The columns of the structure are composed of thirteen equal height drums that reach a height of 10.33 meters (33.9 feet). The perimeter of the temple is six columns wide and thirteen long. Within this perimeter is an interior cella. Curiously, the slenderness ratio of these columns is the largest among the ancient Greek temples of continental Greece. This is odd, considering slender columns were not characteristic of the Doric style. The remains of the temple consist of a single column, and a two column colonnade. Cooper et al. (1983) details the excavation efforts carried out on this temple. Psycharis et al. (2000) used the remains of the temple in their study that focused on parameters related to ground motion and geometry of classical columns and colonnades.

2.3.2. Italy

Built in 198 AD, the Antonina Column was created to honor the emperor Marcus Aurelius. It is composed of seventeen blocks of Carrara marble connected by metal dowel – lead filler connections. Unfortunately, these connections were stolen sometime during the Middle Ages. As a result, the 43 meter (141.1 feet) tall, 3.6 meter (11.8 feet) principal diameter column remains standing as a connectionless, dry-stack structure in Rome's Piazza Collona (Krstevska et al. 1996). Experimental dynamic testing on both this column and a scale model was conducted by Krstevska et al. (1996).

2.3.3. Korea

While the influence of classical architecture is widespread, it is fairly minimal in the Far East. However, this does not mean that there are no examples of dry stack masonry. Korean stone pagodas, essentially dry stack, column-like structures, have been subject to a long history of earthquakes. As there is not much in the way of seismograph data, Korea relies very strongly on historic records for seismic hazard analysis. In fact, the intensity of past earthquakes is often estimated by the "inverse method". Kim and Ryu (2003) worked to estimate the intensity of the 1936 Hwagae-myeon, South Korea earthquake with a physical model of such a pagoda.

2.3.4. Macedonia

Bordering Greece to the south, the Republic of Macedonia has at one point been a part of the Roman, Persian, and Ottoman empires. This colorful history has left behind a unique blend of structures, including Mustafa Pasha Mosque in Skopje. Built in 1492, the main mosque structure has a twenty meter by twenty meter footprint, and is twenty-two meters

tall. The slender, column-like minaret encases a spiral staircase and is 47 meters (154.2 feet) tall. The mosque has survived previous seismic events, such as the 1963 Skopje earthquake (6.1 magnitude), but has not done so without damage. Krstevska et al. (2010) used a one to six scale model of the structure to investigate the usefulness of specific repair techniques.

2.3.5. Turkey

The Asian portion of modern day Turkey is a culturally rich region that has been known by many names, including Asia Minor and Anatolia. To this day, academics are discovering more and more evidence of the plethora of cultures that once called it home. Among the relics left behind are a number of ancient structures exhibiting classical architecture. Examples of these structures and the preservation work performed on them are included in this section.

Figure 2.4. Turkish Case Studies. The map above marks the locations of the following case studies located in Turkey: a) Temple of Augustus, b) Aspendos Theatre, c) Temple of Apollo at Claros, and d) Temple of *Antioch ad Cragum* (Google Maps Engine Lite, 2013c).

The Temple of Augustus in Ankara was dedicated to Augustus, the first Roman emperor. The structure is famous for its inscription of the *Res Gestae Divi Augustus*, which

detailed the exploits of the late emperor. The extinction of the original copy on Augustus' mausoleum multiplies the importance of these inscriptions. Originally, the temple was laid out with a width of eight columns and a length of fifteen. Today, the majority of these columns are no longer standing, and a portion of its remaining walls are significantly leaning. The temple's importance stems not only from its Roman past but its later use as a church, and coexistence with a neighboring mosque (Turer and Eroglu, 2006). Structural monitoring and the prevention of further damage was the goal of a study by Turer and Eroglu (2006).

The Aspendos Theatre, located near Antalya, Turkey, is a very well preserved ancient theatre constructed around 200 BC by the architect Xenon. The Romans gained control of the theatre in 129 AD, and the Seljuk Turks around 1200 AD. The Turks repaired the theatre periodically and used it as a roadside inn for caravans (Turer and Boz, 2008). The age of the theatre, coupled with its location in a seismically prone area of the country, attracted the attention of many scientists including Turer and Boz (2008) who conducted a seismic assessment of the structure.

The Temple of Apollo at Claros was an ancient prophecy center, located in the Ionic city of Colophan. In present day, what was Colophan is located in the town of Ahmetbeyli, near Izmir, Turkey. The original columns were 9-11 meters (29.5-36.1 feet) tall, and composed of nine to eleven drums of varying size. Two lead dowels were used as connections between drums (Arisoy et al., 2011). This region of Turkey is given the highest seismic risk category under the Turkish code (Figure 2.5). Given the location, it is highly likely that the temple experienced some form of seismic action during its

history. The remains of this structure will no doubt also experience such forces, which drove Arisoy et al. (2011) to investigate the seismic response of its columns.

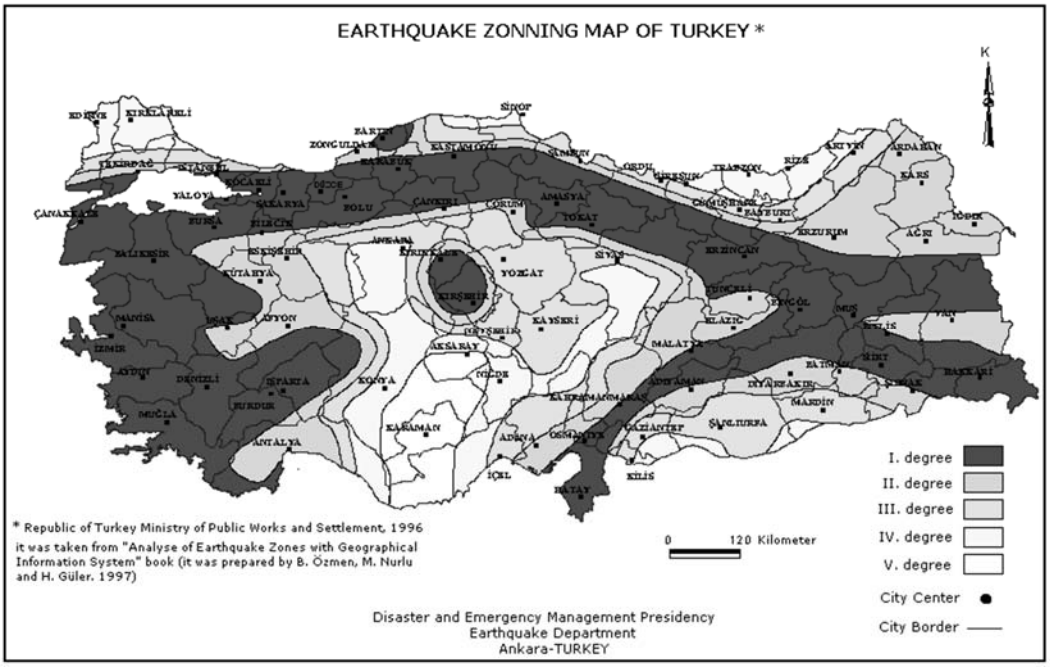

Figure 2.5. Earthquake Zoning Map of Turkey. Above, the earthquake zones of Turkey are classified by expected ground acceleration values (Turkish Republic Disaster and Emergency Management Presedency, Earthquake Department. 2013).

The Temple of *Antioch ad Cragum* was the main imperial temple of the ancient city of *Antiocheia ad Cragum*. The ancient city, once an important provincial coastal city of the Roman Empire, is located in present day Güney Village, near Gazipaşa, Turkey. The temple was in a state of ruin when archaeologists first identified it in the 1960's. It remained in this state until it was re-discovered, by different archeologists, during a surface survey project in the late 1990's. The ongoing anastylosis of the temple by Erdogmus et al. (2011a, 2011b, 2011, and 2013) has revealed much about the temple's history. Researchers have determined, from stylistic evidence and sculptural decoration observed on site, that the temple dates approximately to the early 3rd century A.D. It is also hypothesized that the temple faced the main entry of the city and featured four

columns in its front *façade*, indicative of a *prostyle* layout. While the building served as a temple to the Roman imperial cult, the identity of the first emperor worshipped in the temple is still unknown.

2.4. Dynamic Response of Singular and Stacked Rigid Bodies

The dynamic behavior of rigid bodies is a deceptively difficult problem. Researchers of this problem contend with many issues including: nonlinearity, size effects, and high sensitivity to change. In the literature, this problem has been approached analytically, numerically, and experimentally. The case of a single rigid body, on a rigid base, exposed to some form of excitation, is one that has been analytically examined under a variety of conditions. While such studies of multiple rigid bodies exist, they are fewer in number. As analytical studies became more complex, interest shifted to numerical methods. Researchers utilized both commercial and custom numerical software packages to efficiently test the response of dry stack structures under multiple simulation conditions. Experimental analyses yielded valuable information on the extreme sensitivity of the response. This section includes studies from authors who utilized one or more of these methods to further the understanding of the rigid body response.

The aftermath of a 1960 Chilean earthquake inspired one of the earliest attempts at dynamically analyzing tall, slender rigid body structures. Housner (1963) addressed the elevated "golf ball on a tee" water tanks that outperformed bulkier tanks. In calculations, he modeled these superior structures as single rigid bodies on rigid horizontal bases with a coefficient of friction large enough to prevent sliding. These bodies were then analyzed under a multitude of horizontal motions including: free vibration, constant acceleration,

sinusoidal acceleration, and earthquake motion (Table 2.2). Housner made two very important conclusions: 1) there is a scaling effect that makes the larger of two geometrically similar bodies more stable, 2) the stability of these tall slender monolithic structures subject to earthquake motion is much greater than indicated by their performance against a constant horizontal force.

Papantonopoulos (1993) discussed the results of a dynamic field study conducted on the Temple of Apollo Epikourios at Bassae. The experimental setup consisted of four accelerographs attached to different structural members of the temple. Specifically the devices were placed on the following member types: bedrock, stylobate (a type of foundation member), architrave, and capital. These accelerographs were able to capture data from four separate seismic events over a period of roughly nine months. Inspection of the collected data showed that response behavior was sensitive to both the type of ground motion and the member affected (Table 2.2). Additionally, it was found that the upper members generally had longer predominant periods than the lower members.

Table 2.2. Sensitivity of Temple Element Response.

Element	Horizontal Acceleration	Horizontal Velocity	Vertical Acceleration
Foundation	1.92 - 2.70	1.21 - 1.54	5.79 - 8.12
Architrave	1.55 - 4.91	1.50 - 4.19	5.92 - 12.98
Capital	2.48 - 3.68	3.29 - 3.87	7.14

Kappos et al. (2002) was a comparative study of commonly used techniques for practical analysis of unreinforced masonry structures. The authors utilized SAP 2000 for linear-elastic models and ANSYS for nonlinear models. Due to the cumbersome nature of most non-linear analyses, the authors look at some simplified techniques that can ascertain

useful information about a structure without the high computational cost. Additionally, the authors were able to validate a pushover analysis procedure against shake table results of a half scale building.

Turer and Eroglu (2006) discussed measures taken to prevent further damage to the remains of the Temple of Augustus in Ankara. Ambient vibration testing was performed in order to acquire the first few natural frequencies. This information was used for calibration of a FEM created in SAP 2000. Additionally, long term monitoring procedures were put in place to: assess the tilt of a leaning wall, determine if the tilt was increasing over time, and investigate the effect of temperature on the tilt. The poor state of the temple was confirmed by the numerical models, and structural intervention was needed immediately to prevent collapse due to any seismic motion.

Turer and Boz (2008) worked to evaluate the susceptibility of the Aspendos Theatre to earthquakes using the current Turkish earthquake code. The location of the temple and a seismic map from the Turkish code can be found in Figures 2.4 and 2.5. The authors tested "conglomerate" stone pieces from the site for material properties. Additionally, impact-hammer testing was used to determine the first few dominant vibration frequencies in-situ. This data aided the modeling and verification of a finite element model created in SAP 2000. The response of the theatre to a 475 year return period earthquake generated stresses expected to be three to four times larger than the assumed tensile capacity of the theatre's masonry. This alone proved that the theatre must have seen multiple repairs and restoration, in addition to good maintenance, to be in such great shape today. The authors concluded from their analysis that the theatre is indeed

susceptible to earthquakes and specific recommendations were made to improve its seismic performance.

Ambraseys and Psycharis (2011) focused attention on the seismic vulnerability of monolithic and multi-drum variants of a free standing column topped with a statue. Oftentimes when exposed to earthquakes, the statues would fall but the columns would survive and even be reused. While tempting, and fairly common, the author stressed that overdesign in restoration can actually cause more harm than good to a structure. The remainder of the paper details the authors' case study on the Statue of Apollo at the Academy of Athens. The numerical simulations for this study were conducted using the 3DEC software. During the course of their investigation, the authors made four important observations.

- Seismic codes are not designed with historical buildings in mind and are not suitable for assessing their seismic vulnerability.
- Detailed numerical analyses are necessary to assess vulnerability. These analyses require several informed assumptions regarding the model and the ground motion.
- Understanding the local and regional tectonics is vital when assessing a particular structure. Exciting a model with a random suite of ground motions, with no relation to a particular site, could lead to wrong answers.
- The sensitivity of the problem requires that the numerical model be as accurate as possible.

2.5. Ancient Connections

While dry stack construction is typical of ancient structures, there are several instances of metallic connections being used to connect different members. There are many types of these primitive connections, many of which can be found in the Parthenon of Athens. The following authors have investigated connections on this structure, and others, in order to design appropriate preservation repairs.

Livadefs (1956) looked at the metallurgy behind the Parthenon connections and provided supplementary historical references. Two types of connections are described, the dowel (vertical connections) and the clamp (horizontal connections). The geometry of the dowel was cylindrical, similar to those used today, however the clamp was described as double T or I shaped (Figures 2.6 and 2.7).

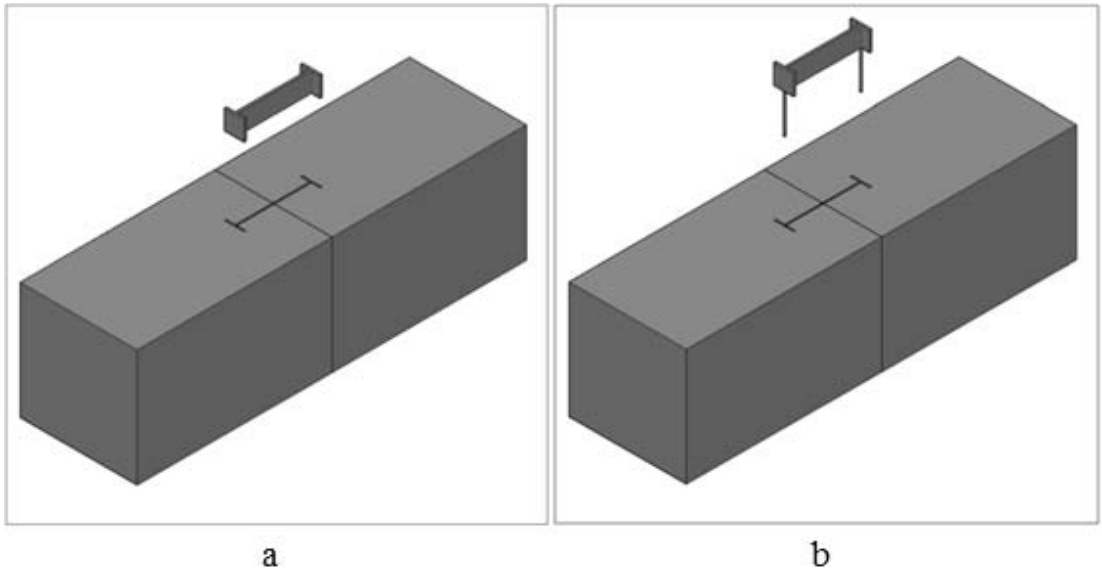

Figure 2.6. Clamp Connections. This figure illustrates different types of clamp connections: a) standard I, b) modified Π.

Despite different geometries, the installation of these connections was rather similar. First, "cuttings" were carved into the stone blocks to fit the shape of the connection.

Typically clamp cuttings were rather shallow and only on the top or bottom face of the block, the dowel cuttings were done so as to fit roughly half the length in each block. Once the connections (properly heated to create snug fit) were placed in the cutting, molten lead was poured into the cutting to ensure a tight fit. The lead had several benefits, most notably it prevented oxidation of the iron and protected the marble from the stresses caused by thermal expansion/contraction of the iron. Joints were made to fit together as closely as possible which was accomplished through polishing. In the case of larger blocks, only a portion of the block was polished in a manner known as "anathyrosis". The column drums utilized an apparatus referred to as "polos-emporion". This apparatus consisted of two plugs and a cylindrical dowel, typically made from wood (Figure 2.7). The plugs were placed into cuttings carved into the face of each drum and the dowel passed through them. The drums were then rotated about this axis until properly polished, and the polos-emporion apparatus left within.

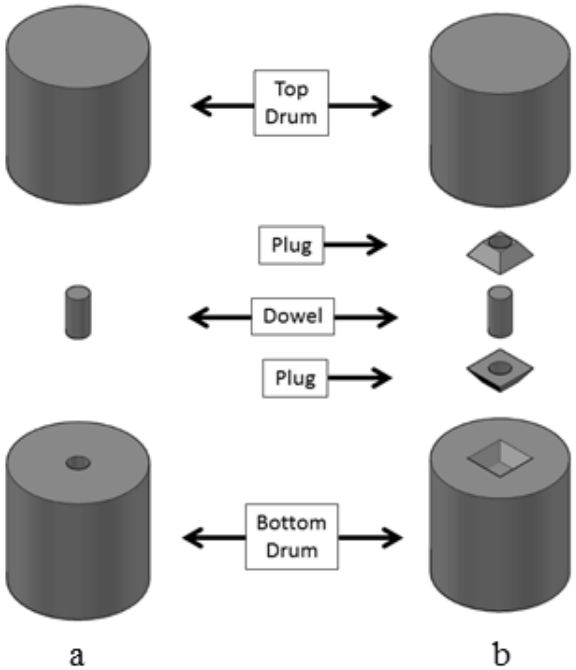

Figure 2.7. Column Connections. This figure illustrates the following connections: a) dowel, b) polos-emporion.

At the time of Zambas (1992), the repair of the Athenian acropolis monuments had been under way for some time. This particular paper was concerned with the structural repair of the Parthenon specifically. The author attributed the damage of previously repaired sections to rusting of the iron connections used in those repairs. The new repairs utilized titanium connectors and a white Portland cement mortar. The choice of titanium was to utilize its resistance to all forms of corrosion. The material properties used by the author can be found in Tables 2.3 and 2.4.

Table 2.3. Marble and Cement Properties from Select Studies.

Authors	Material	E (GPa /ksi)	v	σ_y (MPa /ksi)	σ_u (MPa /ksi)	σ_t (MPa /ksi)	σ_c (MPa /ksi)	σ_f (MPa /ksi)
Zambis (1992)	Pentelic Marble	23/ 3,336	-	-	77.8/ 11.28	19.4/ 2.81	-	-
Kourkoulis and Pasiou (2009)	Dionysos Marble (strong axis)	84.5/ 12,256	0.26	-	-	-	80/ 11.60	10.8/ 1.57
	Dionysos Marble (weak axis)	50/ 7,252	0.11	-	-	-	55/ 7.98	5.3/ 0.77
	White Mortar	15.5/ 2,249	0.26	10/ 1.45	35/ 5.08	2/ 0.29	-	-
Kourkoulis et al. (2010)	Dionysos Marble (strong direction)	84.5/ 12,256	0.26	-	-	10.8/ 1.57	-	-
	Dionysos Marble (interm. direction)	79.5/ 11,531	0.26	-	-	9.5/ 1.38	-	-
	Dionysos Marble (weak direction)	50/ 7,252	0.11	-	-	5.3/ 0.77	-	-
Kourkoulis and Pasiou (2013)	Marble	75.3/ 10,922	0.26	-	-	-	-	-

As previously discussed, the primary materials used for ancient connections were iron and lead. Krstevska et al. (1996) points out that these materials were highly valued at points through history, and oftentimes were stolen. This was in fact the case in their

investigation, as the "metal dowel–lead filler" connections were taken sometime during the Middle Ages. The subsequent shake table testing was then conducted without the connections so as to reflect the current state of the column.

Table 2.4. Metal Material Properties from Select Studies.

Author	Material	Use	E (GPa /ksi)	ν	σ_y (MPa /ksi)	σ_u (MPa /ksi)	τ_u (MPa /ksi)
Zambis (1992)	Titanium	Clamp/ Dowel	105/ 15,229	-	300/ 43.51	420/ 60.92	-
	Ancient Iron	Clamp/ Dowel	220/ 31,909	-	200/ 29.01	360/ 52.21	-
Psycharis (2007)	Steel	Dowel	200/ 29,008	-	-	-	240/ 34.81
Kourkoulis and Pasiou (2009)	Titanium		105/ 15,229	0.32	300/ 43.51	420/ 60.92 tensile	
Toumbakari (2009)	Iron	Clamp	-	-	-	55/ 7.98	29/ 4.21
	Iron	Dowel	-	-	-	-	14/ 2.03
Kourkoulis et al. (2010)	Titanium	Repair	105/ 15,229	0.32			
Kourkoulis and Pasiou (2013)	Steel	Clamp/ Dowel	210/ 30,458	0.27	275/ 39.89	430/ 62.37	-
	Lead	Filler	14/ 2,031	0.43	12/ 1.74	23/ 3.34	-

Studies of individual connections are a valuable first step to the ultimate goal of understanding the combined interaction of all connections in a full structure. Psycharis et al. (2003) investigated the behavior of a "more complete" section of the Parthenon. This model included: three columns, a wall section, and multiple architrave blocks. Vertical

dowels were modeled between the architrave and the capital abacus, clamps between architrave blocks, and polos-emporion between column drums. Material properties used for the clamps and dowels can be found in Table 2.5. When modeled in a single column, the polos-emporion connections were found to resist shear only at very low levels of intensity. Titanium dowels, similar to those found in the architrave and abacus connections, were then modeled in place of the polos-emporion and were found to reduce permanent displacements of the column drums. However, in cases of higher seismic inputs there were instances where the doweled columns were found to cause collapse earlier than unreinforced columns. The full model was analyzed both with and without reinforced architraves. The reinforced model shows significant increase in stability, especially in terms of maximum permanent displacement. Additionally, a model was created using both the reinforced architrave and titanium shear dowels between column drums. This model was not found to significantly improve the response and as such, the dowels were deemed unnecessary.

Table 2.5. Psycharis (2003) Connection Properties. This table contains metal properties used by the author.

Material Properties	Clamps	Dowels
Axial Stiffness	52,000 (kN/m) 3,564 (kip/ft)	
Axial Yield Force	60.00 (kN) 13.49 (kip)	
Ultimate Axial Strain	20%	
Shear Stiffness	26,000 (kN/m) 1,782 (kip/ft)	580,000 (kN/m) 39,743 (kip/ft)
Shear Yield Force	30.00 (kN) 6.74 (kip)	220.00 (kN) 49.46 (kip)

Konstantinidis and Makris (2005) investigated the effects of column behavior, brought on by replacing original polos-emporion connections with titanium dowels. The column model was composed of four drums and a capital. In order to account for the shear

resistance of the polos-emporion, authors superimposed its shear strength to the static friction force. This resulted in an "apparent" coefficient of friction that would take both properties into account. Similar to Psycharis et al. (2003), the polos-emporion were not found to provide substantial shear resistance. This led the authors to conclude that their purpose was limited to polishing the drum surfaces, as described by Livadefs (1956). Small relative sliding in multi-drum columns was shown to be beneficial, since it resulted in a more controlled response than the comparable monolithic column. The authors concluded that the introduction of titanium dowels could be harmful to the columns overall seismic stability, because they prevent energy dissipation from relative sliding.

Psycharis (2007) created another multi-member model, in an attempt to glean information about Athens' seismic history. The model represented a specific section of the Temple of Olympios Zeus, that included: two columns, a section of architrave, and a small building set atop the architrave. This particular temple utilized two steel dowels, of square cross section, oriented randomly between each column drum. Material properties used for the dowels can be found in Table 2.8. Steel clamps were originally present in the architrave, but had been stolen, leading to their exclusion in the model. Curiously, the author stated that the clamps have little effect on the residual displacement of the drums. This statement is interesting to note, because Psycharis et al. (2003) describes titanium connections in the architrave causing "significant" improvement in both the stability and maximum displacement of the architrave blocks.

The behavior of architrave clamp connections under pure shear was investigated by Kourkoulis and Pasiou (2009). This study was conducted in order to fully understand the

effects of shear on both the repaired connection and original marble. Four computer models, consisting of two blocks and a clamp, were created to examine the following parameters: boundary conditions, presence (or not) of mortar filling, and existence (or not) of relieving space. Material properties used by the author can be found in Tables 2.3 and 2.4. The simulation of pure shear was an issue for the author. Due to the asymmetric placement of the connector, additional constraints were needed to enforce pure shear. However, these additional constraints could alter both the location and mode of failure. The uses of mortar filling and a relieving space (near the central cross section) were found to have an important effect. These parameters could influence the magnitude of stress and dictate the location of fracture. The author also observed cases where the marble would fracture before the repaired connection. This is deemed unacceptable, as the ultimate goal is to preserve original material. Further testing was encouraged to: 1) ensure the connection fails before the marble and 2) determine the best arrangement of relieving space and mortar filling composition.

Two types of clamp were investigated by Pavlovcic et al. (2009), the traditional I shape and the modified Π shape (Figure 2.6). Physical testing was conducted at a one to three scale with the clamps designed stronger than the surrounding limestone blocks. In actual reconstruction, the clamp would be designed to fail first. However, the purpose of this experiment was to investigate stone failure under axial loadings. Loadings considered were: monotonic tension, cyclic tension, and cyclic tension/compression. The results of the physical tests were discussed in depth in a companion paper. However, the authors summarized that slot depth (60% capacity increase) and clamp length (80% increase)

were the most influential parameters for standard I clamps, while clamp length and hook depth were found to significantly affect Π clamp performance.

Previous papers working with the Parthenon concentrated on connections in the architraves and columns. Toumbakari (2009) shifted the focus to a portion of the Northern wall. Damage to this wall portion was attributed to fire (267 AD) and explosion (1678 AD). The author argued that the mechanical behavior of the connections, and not rust, was to blame for the failure of the wall. The following five mechanical failure modes were identified: 1) shear induced clamp area failure, 2) dowel area failure due to traction and shear, 3) dowel area failure due to traction, 4) block separation due to out of plane bending, and 5) base shear. The first two failure modes were validated through elastic numerical analysis, however, dynamic analyses is yet to be completed. Material properties utilized in numerical testing can be found in Table 2.4. The author concluded that his findings offer support to the argument of designing interventions based on the bearing of the entire structure, as opposed to a block-by-block analysis.

Kourkoulis et al. (2010) performed an in-depth investigation of the mechanical performance of both intact and repaired architraves. This included careful assessment of both the boundary conditions and loadings that are applied in-situ and in experimental testing. The investigation utilized the FEM and the software ANSYS 9.0. Numerical methods were required due to the difficulties in obtaining a closed form solution. These difficulties included: 1) the length to height ratio of the architrave is not large enough to make classical bending theory applicable; 2) the abacuses (top, flat portion of the capital) were made of the same material as the architrave, and their deformation must be taken

into account; 3) the support conditions of the architrave are not clearly simply supported beams or double cantilever; and 4) the introduction of titanium bars in the repair of fragmented architraves creates several difficulties with the interaction of the titanium and marble, and the marble pieces themselves. Since this work was conducted on Parthenon architraves, material properties for the Dionysus marble and titanium rods used in restoration can be found in Tables 2.3 and 2.4 respectively. For an intact architrave, stresses at mid-span were found to be 70% lower when compared to those developed near abacus corners. Unless the edges were rounded, failure would begin at that location. This sentiment was confirmed by in-situ observations of the Parthenon architraves (unmoved, "from antiquity until the present days"). Possibly aware of this issue, the ancient Greeks sculpted a fillet near the abacus' edge to reduce stress concentrations. In the case of a repaired architrave, danger is present in the immediate vicinity of the reinforcing bars. Finally, it was determined that laboratory simulation of distributed loads using a multiple point loading system did not accurately reflect the stresses in the architraves. The authors recommend engineers increase safety factors to account for this difference. In the specific case of an eight point loading system, the authors found the appropriate factor to be approximately two.

Kourkoulis and Ganniari-Papageorgiou (2010) modified the scope of Kourkoulis et al. (2010) and only studied the mechanical behavior of marble architraves repaired with titanium bars. The repair procedure involved drilling a hole for the titanium bar through the constituent fragments of the architrave. This hole was then filled with a cementitious material to bond the marble to the reinforcement. The bar was then inserted into the hole. The analyses were conducted numerically with the FEM software ANSYS 11.0. The

FEM models were composed of a column abacus and an architrave split vertically through its central cross section, and repaired in the described manner. Focus was placed on several parameters, including: mechanical properties of cementitious filler, geometric features of titanium reinforcing bars, and contact behavior of interfaces composed by marble, cement, and titanium. The results showed that high stress concentrations appear in three regions of the model: 1) central section around the titanium bar; 2) corners of the supporting abacus; 3) upper side of the epistyle in the area of the central section. The cementitious material between the marble and reinforcing bar was found to reduce the high strain discontinuities in the first region. The importance of the composition of such a cementitious material is stressed. The authors suggest a composition that produces a "multi-linear layer, of a slightly ductile nature," such a composition will create smoother stress and strain distributions. A smooth cylindrical reinforcing bar reduced the high stress in the first region significantly. However, this caused the appearances of much higher stresses in region two. This shows that the epistyle will constantly be under the effect of high stress concentrations, and altering the geometric properties of the reinforcing bars will not alleviate, but redistribute these stresses. The authors concluded that there is no definitive solution concerning the optimum combination of reinforcing bar, cement, and architrave. There are too many factors such as the number and shape of fragmented pieces for a single solution.

Arisoy et al. (2011) investigated the effects of lead dowels used in the columns of the Temple of Apollo at Claros. A one to ten scale reproduction of the multi-drum temple column was created. While the original column consisted of nine to eleven drums of varying size, the model used 10 equal height drums. Drums were separated with two lead

dowels. The marble used in the model was described by the authors as "approximately the same material" used in the temple. The dowels were found to cause the column to behave monolithically. Once the dowels broke, the column would respond with nonlinear rigid body motion. The authors note that the response of a rocking system is size-dependant and experimental results cannot be generalized to the original column. The multi-drum column proves much stronger experimentally than in the computer program and the dowels are found to fracture in some cases, but not at any specific location. This leads the authors to conclude that the application of the dowels is important to the column's behavior, and they were installed improperly in this model.

Kourkoulis and Pasiou (2013) is the most current work on the Parthenon connections. It drew upon a large amount of literature, including several of the papers above. The authors described the difficulties encountered with replicating shear tests in the lab, and noted the success of Zambas (1994) and Pavlovcic et al. (2009) in testing the mechanical behavior of connections under pure axial loads. High costs associated with these tests, point to the necessity of reliable numerical models. The expressed goal of this work is to study the behavior, and response, of I shaped connectors under axial loads. In addition, the influence of different parameters was investigated. The materials used in this study include Dionysus marble (remarkably similar to that in the Parthenon), molten lead, and ancient iron. The material properties used for these products, can be found in tables 2.3 and 2.4. The model was validated using the results obtained during the structural testing in Zambas (1994). The finite elements used, and treatment of the interfaces are similar to those used in Kourkoulis and Pasiou (2009). In the parametric analysis, a total of five parameters were investigated: connector length, width of connector flanges, depth of

groove, existence of relieving space, and total volume of lead. The author concludes that long connectors with wide flanges, such as those suggested in Pavlovcic et al. (2009), should not be used as they require additional marble destruction. The depth of the groove requires more investigation as it seems to affect the tensile and compressive stresses oppositely. Finally the role of the relieving space is crucial because it results in a significant relief of the stress field. The relieving space is defined by the authors as, "the gap, intentionally created in the form of absence of filling material along a part of the connector's body, symmetric with respect to the interface between the two marble blocks." The presence of the space results in a reduction of 5% and 25% of the compressive and tensile stresses respectively, without requiring modification of existing groove's volume. Changing any of the connector's parameters, while beneficial in cases, causes additional destruction of the original material making these options the least desirable. The authors concluded by emphasizing that simplifying assumptions were made in their study (particular with regards to material behavior) and that there is substantial future work to be done on the topic.

2.6. Summary

The seismic investigation of historical structures requires an entirely different approach from that of modern structures. Unlike today's structures, ancient structures do not always come with reliable seismic data or construction documents. Instead, a multidisciplinary effort from engineers, archeologists, historians, and geologists is required to sift through structural remains and historical information in order to determine how a structure reached its current state. While historical accounts can be plentiful,

disciplines must work together to glean the truth behind the damage without jumping to premature “catastrophe theories”.

The use of mechanical connections in dry stack structures was not consistent in the ancient world. Some structures have no evidence of these connections while others use them in several situations. Coupled with issues of material theft over the years, good specimens are at a premium. The following points summarize the research on doweled connections.

- *Types* – There are two main types of column connections, the dowel and the polos-emporion. The dowels typically had either a circular or square cross-section. While dowels appeared to have a structural purpose, the use of polos-emporion could have been restricted to alignment or polishing.
- *Materials* – Ancient dowels were composed of a metal rod, typically iron, and molten lead filler. The polos-emporion, however, consisted of three pieces of wood, two plugs and a rod running through them. Modern dowel repairs have utilized a corrosion resistant titanium rod and a white Portland cement mortar as filler.
- *Installation* - Cuttings were carved so as to fit roughly half of the dowel or one plug of the polos-emporion. The dowel rods were heated before being placed in the cutting, to create a snug fit. Molten lead was then poured into the cutting to ensure a tight fit and prevent oxidation of the iron. The polos-emporion plugs were placed into the cuttings, and the wooden rod passed through them.
- *Performance* – The shear resistance of polos-emporion connections was found to be minimal at best. Replacement with titanium-cement connections was found to

reduce permanent displacement at the cost of preventing beneficial energy dissipation due to frictional sliding. The presence of dowels was found to significantly alter the behavior and stability of classical columns.

CHAPTER 3: FINITE ELEMENT MODELING

This chapter focuses on the creation of finite element models and the techniques used for their subsequent analysis. These points are addressed as organized in Figure 3.1.

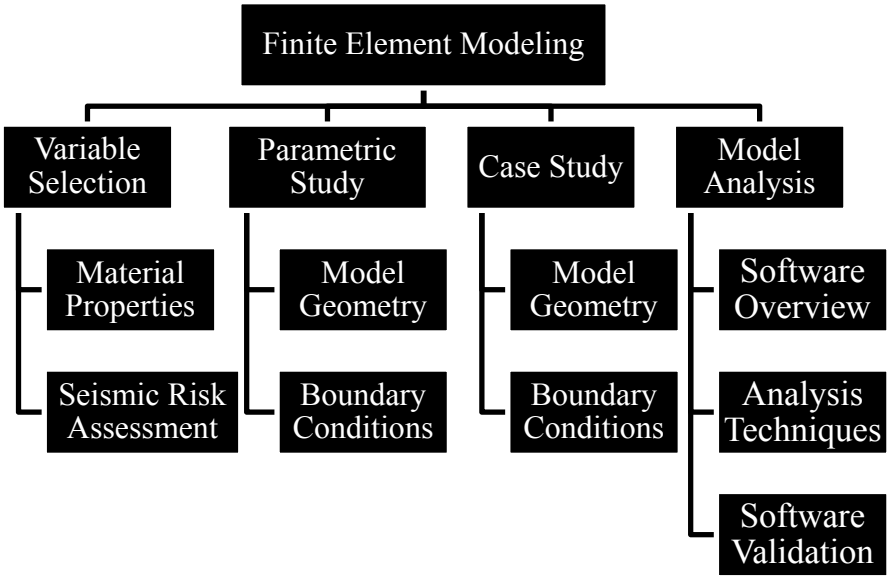

Figure 3.1. Chapter Three Outline.

The first section details the determination of variables common to all finite element models. These variables include material properties as well as seismic properties determined from a site specific seismic risk analysis. This is followed by study specific discussions of model geometry and boundary conditions. The chapter concludes with information on the techniques and software used to analyze the finite element models of this thesis. A known example problem is then used to validate the ability of the software to perform the discussed analysis techniques.

3.1. Variable Selection

In order to create the most realistic finite element models possible, both the parametric study and case study described in Chapter 1 utilized a common set of variables. These variables included material properties determined from the testing of Turkish marble

samples and seismic properties determined from a seismic risk analysis of the Asia Minor and Mediterranean regions.

3.1.1. Material Properties

The marble samples used in material testing were procured from both the Temple of *Antioch ad Cragum* and a nearby, modern quarry (both located near Gazipaşa, Turkey). These samples are hereafter referred to as "Antioch" and "Quarry" respectively. While both samples were rectangular in shape, the Quarry sample had clean, flat faces while the Antioch sample had highly irregular surfaces due to centuries of exposure to the elements (Figure 3.2).

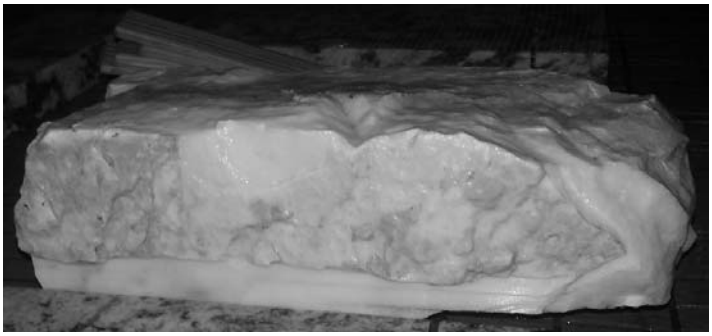

Figure 3.2. Uncut Antioch Marble Sample.

Both samples were cut using a wet saw in order to create 5 cm x 5 cm x 5 cm (2 in x 2 in x 2 in) cubes. The dimensions were determined in accordance with ASTM C170/C170M-09 Standard Test Method for Compressive Strength of Dimension Stone (ASTM Standard C170/C170M, 2009). Fourteen test cubes were produced from the Quarry sample and four from the Antioch sample. The four cubes with the cleanest cuts were taken from each sample and used for testing (Figure 3.3).

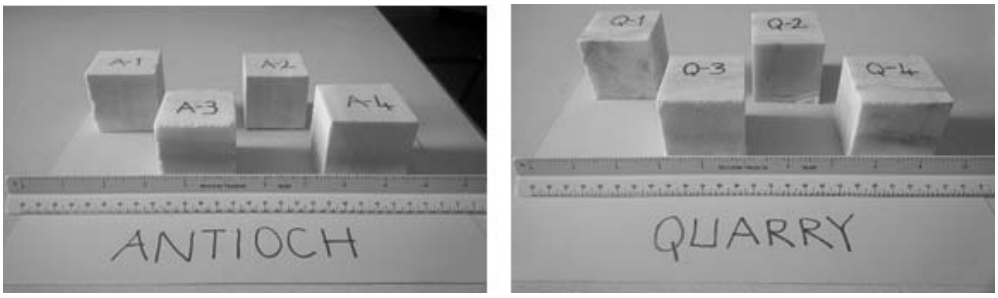

Figure 3.3. Marble Testing Specimens.

First, the density of both the Quarry and Antioch samples was determined by measuring the dimensions and weight of the eight specimens shown in Figure 2. Specimen dimensions were measured using a Chicago Brand 40" Electronic Digital Caliper (PN: 50009) and an Ohaus Explorer digital scale. The density for each sample was taken as the average density of its four specimens. The results indicate that both samples have a density of $2.64e^{-3}$ kg/cm^3 ($9.54e^{-2}$ lb/in^3). The complete data set can be found in Appendix A.

Next, the coefficient of static friction was determined using a simple slip test performed with the scissor lift apparatus in Figure 3.4. The effectiveness of this testing method was proven by its developers, Ghazali and Riddington (Ghazali and Riddington, 1988).

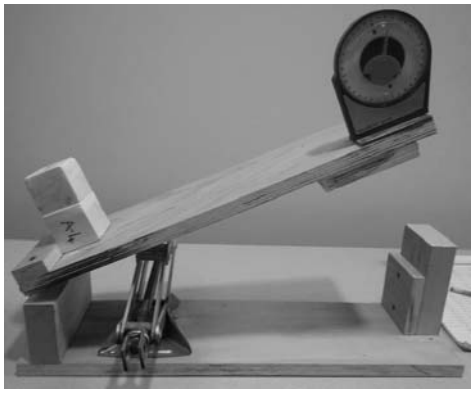

Figure 3.4. Friction Testing Apparatus.

To determine the coefficient of static friction with this apparatus, two specimens were arranged one on top of the other. The bottom specimen is prevented from slipping by the

mounted wooden block. The scissor lift was then used to slowly increase the angle of inclination until slipping of the top specimen was observed. The resulting angle was noted as the angle of friction, whose tangent is equal to the coefficient of static friction. This method was utilized to measure the static friction angle for twelve arrangements of each sample's four cubes. These arrangements utilized the smoothest face of each cube and used this face three times each in the top and bottom blocks. The results showed that the average coefficient of static friction for the samples was very similar, 0.53 for the Quarry sample and 0.54 for the Antioch sample. The complete data set can be found in Appendix B.

Compression testing has shown that the modulus of elasticity for the previously discussed marble samples is approximately 36 GPa (Antioch sample) and 61 GPa (Quarry) (Erdogmus et al., 2014). The finite element models of this thesis utilized a near-average modulus of elasticity of 55 GPa to simulate a non-damaged condition marble. This value was taken as a conservative estimate after taking into account other marble values found in the literature (Table 2.3).

3.1.2. Seismic Threat Assessment

Classically designed columns are present in most of the Asia Minor and Mediterranean regions, with a particularly heavy concentration in modern day Greece, Italy, and Turkey. The seismic threat to these regions can be determined with a response spectra created in accordance with Chapter 11 of the ASCE Standard *Minimum Design Loads for Buildings and Other Structures*, hereafter referred to as ASCE 7-10 (ASCE, 2010) and utilizing the

United States Geological Survey (USGS) website for all locations around the world (Figure 3.5).

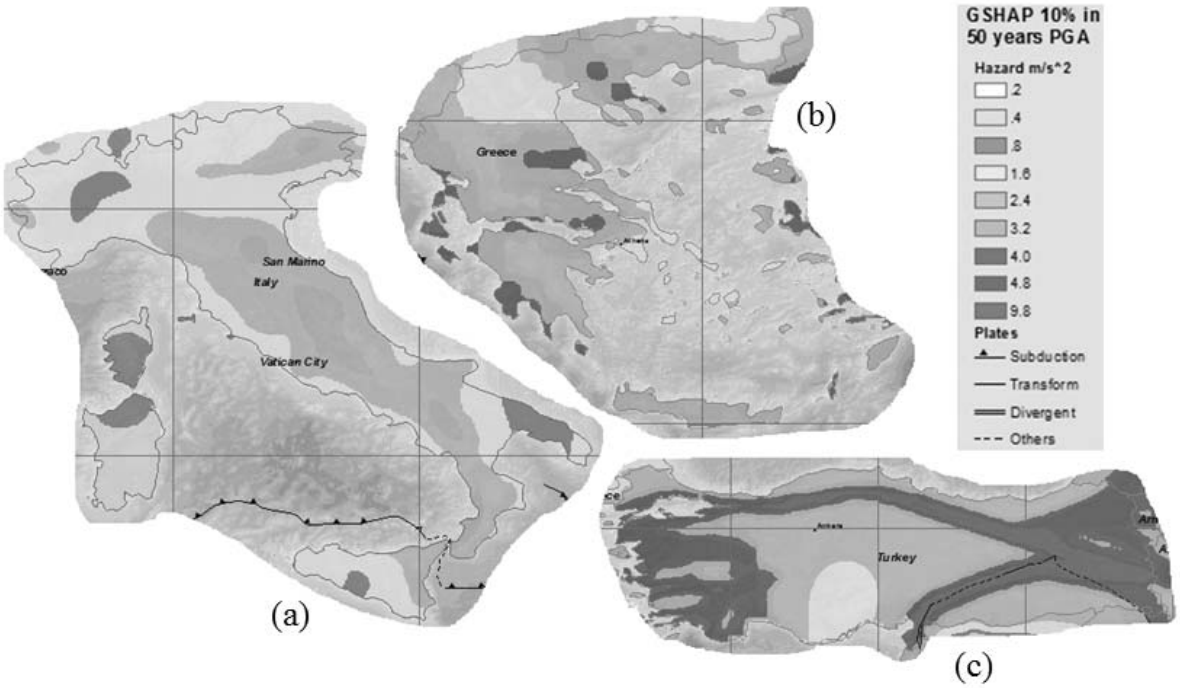

Figure 3.5. Select Seismic Hazard Maps. a) Italy, b) Greece, and c) Turkey (USGS, 2013).

The maps in Figure 3.5 give values for the peak ground acceleration (PGA) with a 10 percent probability of exceedance in 50 years. USGS then suggests the following approximations (Equations 3.1 and 3.2) to obtain values of S_S and S_1 from this data (USGS, 2013).

$$S_S \approx (2.5) * 2\% \text{ in } 50 \text{ PGA} \approx (5.0) * 10\% \text{ in } 50 \text{ PGA} \quad (3.1)$$

$$S_1 \approx (1.0) * 2\% \text{ in } 50 \text{ PGA} \approx (2.0) * 10\% \text{ in } 50 \text{ PGA} \quad (3.2)$$

With the S_S and S_1 values calculated, two design response spectra were created in accordance with ASCE 7-10 (Figure 3.6).

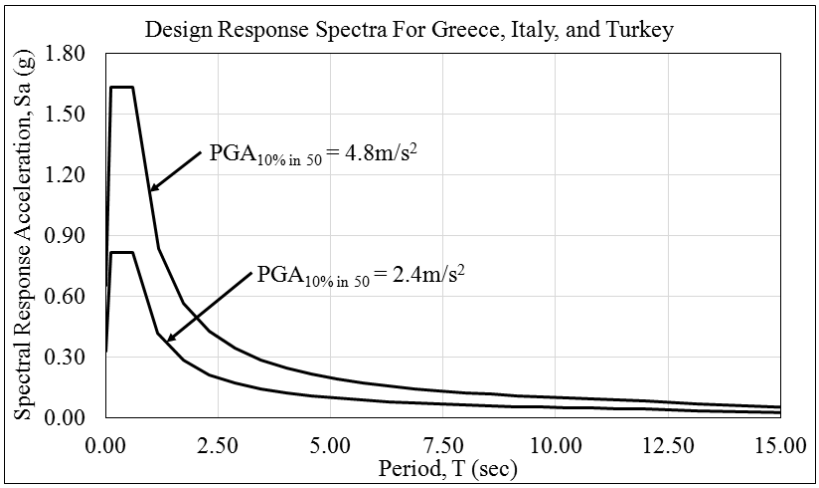

Figure 3.6. Design Response Spectra for Greece, Italy, and Turkey.

The larger spectrum in Figure 3.6 ($PGA_{10\% \text{ in } 50} = 4.8$ m/s^2 (15.7 ft/s^2)) was used in the parametric study of free-standing column models. Excluding the mountainous regions of Turkey, this spectrum defined the worst seismic threat to structures in the three considered countries. The smaller spectrum ($PGA_{10\% \text{ in } 50} = 2.4$ m/s^2 (7.9 ft/s^2)) was specific to the Temple of *Antioch ad Cragum* site and was used in the case study to provide a realistic assessment of the temple façade to seismic forces.

3.2. Parametric Study

The purpose of the parametric study of free-standing classical columns is to determine the effect that classical column geometry has on seismic response. This section will detail the determination of variables specific to this study. Specifically, the model geometry and boundary conditions are discussed.

3.2.1. Model Geometry

Vitruvius described column geometry with a set of proportions based on an arbitrary measurement, the "module". Additionally, each column order was further divided into "substyles" differentiated primarily by column height, diameter, and spacing (Pollio and

Morgan, 1960). With this knowledge, five slenderness ratios typical of each classical column order were deduced. In order to create full proportion sets for each combination of slenderness ratio and order, the shaft diameter (d) of the Ionic and Corinthian orders was utilized as the module. Vitruvius originally detailed the Doric order to have a column shaft diameter twice that of the other orders. In order to utilize a common diameter, the original proportions were scaled down. With the module known, proportions of the capital (L_C:W_C:H_C), cylindrical shaft (H:d), and the column base (L_B:W_B:H_B) were determined based on information presented in *De Architectura* (Table 3.1).

Table 3.1. Classical Column Geometrical Proportions (in terms of d).

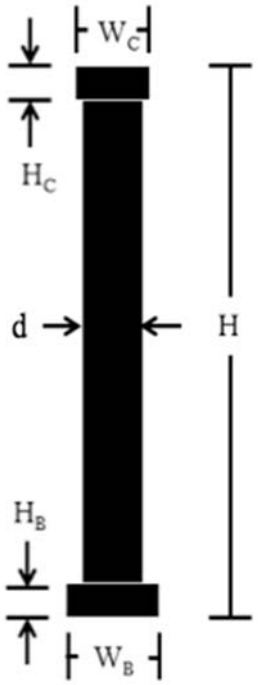

Order	Capital (L_C:W_C:H_C)	Shaft (H:d)	Base (L_B:W_B:H_B)
Doric	1.09 : 1.09 : 0.50	8.00 : 1.00	N/A
		7.50 : 1.00	
		7.00 : 1.00	
		6.50 : 1.00	
		6.00 : 1.00	
Ionic	1.06 : 1.06 : 0.53	10.00 : 1.00	1.50 : 1.50 : 0.50
		9.50 : 1.00	
		9.00 : 1.00	
		8.50 : 1.00	
		8.00 : 1.00	
Corinthian	1.56 : 1.56 : 1.50	See Ionic	See Ionic

Note: L_C and L_B are dimensions in the 3rd orthogonal direction and not shown on figure.

The typical slenderness ratios were based on the substyles of the classical column orders as defined by Vitruvius. The Doric order had the least defined substyles (1 specified slenderness ratio) and as noted in Chapter 2 Vitruvius paid less attention to this order.

With this considered, it was decided to select two larger and two smaller slenderness ratios in addition to the single one specified by Vitruvius. These additional slenderness ratios were spaced similar to those of the Ionic and Corinthian orders. Vitruvius also detailed the proportions of several order specific ornamentations. However, these ornamentations were assumed small enough so as not to affect the overall behavior of the column models.

The beauty of the Vitruvian proportion system is that once a module is selected dimensions are easily obtained. Table 3.1 contains the proportion sets for all 15 free-standing columns that will be tested in this thesis. Since these proportions are all in terms of the Ionic/Corinthian shaft diameter, the column dimensions can be obtained by multiplying the values in Table 3.1 by this shaft diameter (results tabulated in Table 3.2). Vitruvius notes that the module can be any measure including column diameter or specific ornamentation. He also describes specific substyles by noting fraction of their front that should comprise a module. For the purpose of this study, a standard Ionic/Corinthian shaft diameter of 46 cm (18 inches) was chosen. This diameter would be similar to that of smaller structures more likely to be found in less populated areas of the Roman Empire.

Table 3.2. Free-Standing Column Dimensions, d = 46 cm (18 in)

Order	Capital (L_C:W_C:H_C)	Shaft (H:d)	Base (L_B:W_B:H_B)
Doric	99: 99: 45 (cm) 39 : 39 : 18 (in)	3.66 : 0.46 (m) 12.00 : 1.50 (ft)	N/A
		3.45 : 0.46 (m) 11.25 : 1.50 (ft)	
		3.20 : 0.46 (m) 10.50 : 1.50 (ft)	
		2.97 : 0.46 (m) 9.75 : 1.50 (ft)	
		2.75 : 0.46 (m) 9.00 : 1.50 (ft)	
Ionic	48 : 48 : 24 (cm) 19 : 19 : 10 (in)	4.57 : 0.46 (m) 15.00 : 1.50 (ft)	69 : 69 : 23 (cm) 27 : 27 : 9 (in)
		4.34 : 0.46 (m) 14.25 : 1.50 (ft)	
		4.11 : 0.46 (m) 13.50 : 1.50 (ft)	
		3.89 : 0.46 (m) 12.75 : 1.50 (ft)	
		3.66 : 0.46 (m) 12.00 : 1.50 (ft)	
Corinthian	71 : 71 : 69 (cm) 28 : 28 : 27 (in)	See Ionic	See Ionic

As the focus of the parametric study was the proportions of Table 3.1, the diameter was only needed to obtain the final dimensions of Table 3.2. The effect of different shaft diameters is outside the scope of this study.

3.2.2. Boundary Conditions

Classical structures were typically constructed as dry stack. This type of construction relied mostly on the substantial mass of the structure and coulomb friction at each interface to resist lateral motion. In some cases, mechanical connections, such as dowels and clamps were provided in an effort to create a stronger structural system (Section 2).

Free-standing columns have considerably less mass and lack lateral support when compared to those that are part of a building system. Classical free-standing columns typically existed due to one of the following situations: 1) original design, such as the Column of Phocas (Figure 3.7), or columns of Trajan, and Marcus Aurelius in Rome; 2) survival of the column after the rest of the structure's collapse; 3) reconstruction as part of preservation efforts (numerous examples around the world).

Figure 3.7. Column of Phocas in Rome.

The larger columns as described in situation 1 might have fared well due to their large size. However, smaller columns utilized mechanical reinforcement since their mass and friction alone may not be enough to resist lateral loads.

The free-standing column models in this thesis assumed mechanical reinforcement at the base of the column resulting in a cantilever column configuration with one fixed and one free end. This corresponds to restriction of translation and rotation in all directions at the base. This boundary condition assumption allowed the columns to remain structurally stable under lateral loads.

3.3. Case Study

The purpose of the case study is to provide a real life example of the effect classical order and the resulting geometry of columns can have on the seismic response of a structure. Unlike the parametric study, the case study only required the creation of one finite element model. However, this model was tested under multiple boundary conditions. This section will detail the determination of variables specific to this model. Specifically, the model geometry and boundary conditions are discussed.

3.3.1. Model Geometry

Researchers have been systematically studying the temple blocks removed from the Temple of Antioch collapse site for assessment and cataloging. This effort lead to a hypothetical four column, prostyle façade with a column slenderness ratio of approximately 11:1 (Figure 3). When compared to the typical slenderness ratios for the Corinthian order (Table 1) this is on the higher end of the scale.

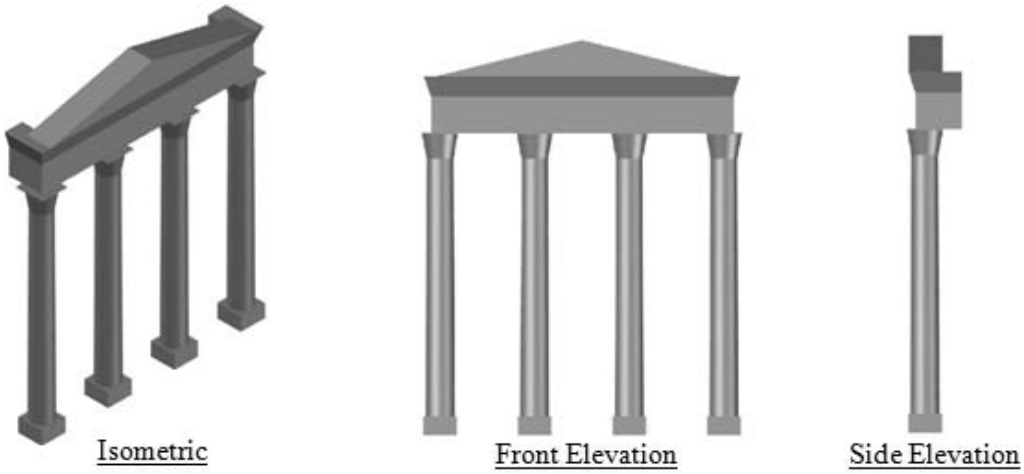

Figure 3.8. Temple of *Antioch ad Cragum* Façade Renderings.

The dimensions of the façade were obtained due to a joint effort from the engineering and art history members of the research team. Column dimensions were obtained from field

measurements of individual temple blocks. These measurements were verified by both engineering and art history members of the research team. The column was found to have both a tapered shaft and Corinthian capital. Dimensions of the façade columns can be found in Table 3.3. This table includes both the actual measured dimensions and dimensions modified to have a constant cross section in the finite element model.

Table 3.3. Temple of *Antioch ad Cragum* Column Dimensions.

Piece	Elevation	Section	Actual Dimensions (cm/in)	Model Dimensions (cm/in)
Capital	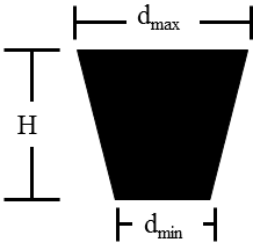	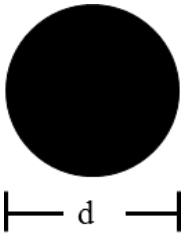	d_{min} = 58 cm (23 in) d_{max} = 79 cm (31 in) H = 57 cm (23 in)	d_{min} = 69 cm (27 in) d_{max} = 69 cm (27 in) H = 57 cm (23 in)
Shaft	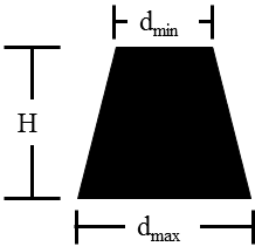	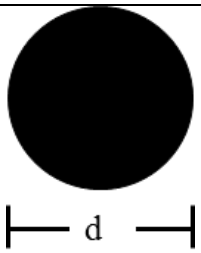	d_{min} = 0.58 m (1.92 ft) d_{max} = 0.64 m (2.08 ft) H = 5.69 m (18.67 ft)	d_{min} = 0.61 m (2.00 ft) d_{max} = 0.61 m (2.00 ft) H = 5.69 m (18.67 ft)
Base	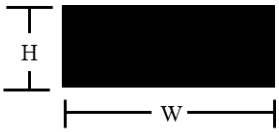	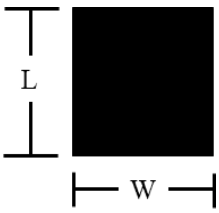	L = 74 cm (29 in) W = 74 cm (29 in) H = 42 m (17 in)	L = 74 cm (29 in) W = 74 cm (29 in) H = 42 cm (17 in)

The column spacing was based off a temple width determined by the Temple of *Antioch ad Cragum* research team. By matching this width and evenly spacing the columns, the center-to-center distance of the columns was found to be 140 cm (55 in). Using a combination of field measurements and three-dimensional photogrammetry, the research team created a set of engineering drawings. The full dimensions of the hypothesized

façade including the entablature and pediment are included in these drawings (Appendix D).

3.3.2. Boundary Conditions

As discussed in Section 3.2, classical structures typically relied on substantial mass and coulomb friction to resist lateral motion. However, without the lateral stability provided by a full structure, the façade model considered in this case study will realistically depend on mechanical reinforcement for lateral stability.

Unlike the free-standing column models that depended solely on the base connection for lateral stability, the façade model also has the beam to column connections to consider. Similar to the parametric study, the case study assumed fixed bases for the columns. With regards to the beam-column connections there were two options: pinned connections and moment connections. The difference between the two is that a pinned connection allows a member to rotate at a joint without affecting the other members at said joint. The moment connection fixes all members at a joint so that any rotation affects all joint members. Each connection type affects the distribution of stresses differently, varying the demands at various connection locations in the façade frame. Both of these options were analyzed with the finite element model and are discussed further in Chapter 4.

3.4. Model Analysis

RAM Elements 13.0 (RAM Elements) was used in this study for the dynamic and static analyses. The models of this thesis were created using members defined by two nodes with six degrees of freedom per node. These members operated similar to 3D beam

elements found in other finite element analysis programs. Since the models were limited to 3D beam elements, the centerline of each component was modeled to ensure that all elements lined up appropriately. To create a model, the centerline is first modeled with nodes and the nodes are connected by members. Once members were created, the appropriate cross sections and material were assigned to complete the structure (Figure 3.9).

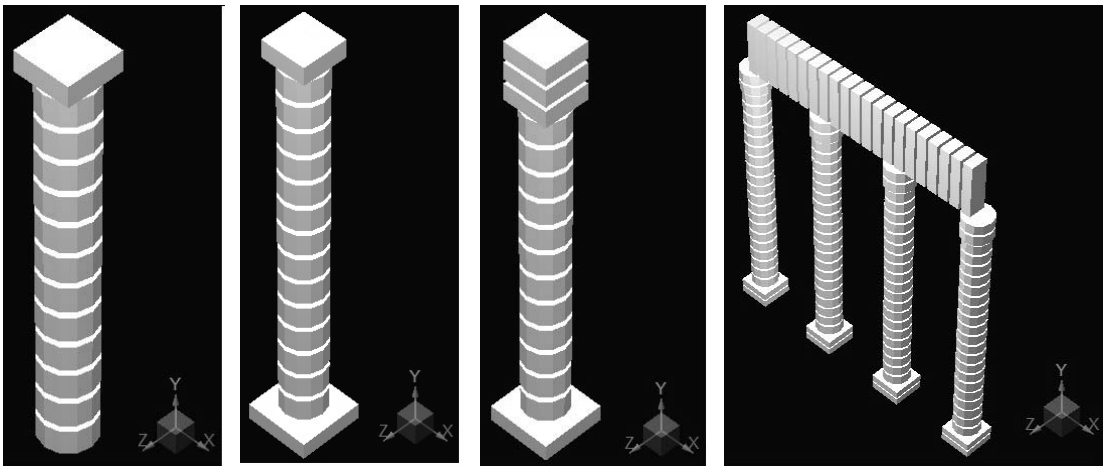

(a) Doric (b) Ionic (c) Corinthian (d) Temple Facade

Figure 3.9. Completed Finite Element Model Renderings.

In total, 15 free-standing column models (5 per order) and 1 façade model were created for this thesis. With the structures modeled, loads and boundary conditions could be applied as required.

In order to perform modal analysis, RAM Elements required that point masses were defined on existing nodes. Rather than lump the mass of any model at a single node, the decision was made to space nodes at approximately 31 cm (12 in) intervals. By increasing the number of nodes and distributing the model mass, a better approximation of the structure was created resulting in a more accurate model. The value for each point mass was determined by considering the tributary member length for each node.

3.4.1. Analysis Techniques

In this thesis, static analyses were performed to investigate the stresses that developed at connection interfaces due to seismic activity. There were three acceptable procedures for seismic analysis detailed in Chapter 12 of ASCE 7-10 (ASCE, 2010). This thesis utilized the Equivalent Lateral Force Procedure (ELFP) in the static analyses of all finite element models. The ELFP requires the determination of the seismic base shear (V) via Equation 3.3.

$$V = C_S * W \tag{3.3}$$

The seismic weight of the structure (W) was taken as the sum of the individual point masses assigned to the nodes of a model. The seismic response coefficient (C_S) was determined according to Equations 3.4 and 3.5.

$$C_S = S_{DS} \div (R/I_E) \tag{3.4}$$

$$C_{S\,MIN} = 0.044 * S_{DS} * I_E \tag{3.5}$$

The response modification factor (R) was dependent on the type of structural system being analyzed and was found in Table 12.2-1 of ASCE 7-10. The importance factor (I_E) was also obtained from ASCE 7-10 from Table 1.5-2. The design spectral response acceleration at short periods (S_{DS}) is a parameter that was determined in the development of the design response spectrum found in Chapter 3.2.2 (Figure 3.8). The factors used to calculate C_S, for both the parametric and case studies, as well as the end result are summarized in Table 3.4.

Table 3.4. Seismic Response Coefficients.

Model	Seismic Force-Resisting System	S_{DS} (g)	R	I_E	C_S
Free-Standing Column	G.5. (Cantilevered Column System)	1.63	1.00	1.00	1.63
Temple of *Antioch ad Cragum* Façade	C.7. (Moment-Resisting Frame System)	0.82	1.00	1.00	0.82

Higher structural stability is reflected in the response modification factor (R), often resulting in smaller C_S coefficients. The seismic force resisting system shown for the façade model in Table 3.4 actually lists a response modification factor (R) of 3.00. While this system is the option that most closely resembles the façade, it is technically for a reinforced concrete frame. Since the façade is not reinforced in the manner implied by ASCE 7-10 (i.e. longitudinal rebar and stirrups) the response modification factor (R) was conservatively taken as 1.00. With C_S calculated, the seismic base shear (V) was determined and vertically distributed along the column with Equations 3.6 and 3.7.

$$F_X = C_{VX} * V \tag{3.6}$$

$$C_{VX} = (w_x * h_x^k) \div (\Sigma w_i * h_i^k) \tag{3.7}$$

To vertically distribute the base shear, at each defined seismic weight (w_x) a horizontal shear (F_x) is applied. The value of this force is found by first calculating C_{VX} (Equation 3.7). This equation takes the individual seismic weight (w_x) and multiplies it by its height (h_x) raised to an exponent based on the structures period (k) before dividing by the sum of all such values for corresponding seismic weights ($\Sigma w_i * h_i^k$). With C_{VX} known, Equation 3.6 can then be solved. The detailed calculation of vertically distributed lateral forces to be applied to finished finite element models can be found in Appendix C

In addition to the static analysis, modal analysis was used to investigate the effect of classical column proportions on the natural circular frequencies (ω_n) and modes of

vibration (φ_n). A natural mode of vibration describes a special deflected shape the structure will maintain while vibrating in simple harmonic motion. Corresponding to the natural mode of vibration is the natural circular frequency, which relates time to the number of simple harmonic cycles undergone by the structure (Chopra, 1995).

The foundation of any structure's dynamic behavior lies with understanding its natural modes and frequencies. In order to determine these properties the eigenvalue problem must be defined and solved. This thesis considered the following: the equation of motion governing free vibration of a linear, undamped multi-degree of freedom system (Equation 3.8), free vibration of such a system in a natural mode (Equation 3.9), and the time variation of displacement described be a simple harmonic function (Equation 3.10). These equations can be combined to form equation 3.11 (Chopra, 1995).

$$[m][\ddot{u}] + [k][u] = 0 \tag{3.8}$$

$$[u(t)] = q_n(t) * \emptyset_n \tag{3.9}$$

$$[u(t)] = \emptyset_n * \{(A_n * \cos \omega_n * t) + (B_n * \sin \omega_n * t)\} \tag{3.10}$$

$$q_n(t) * \{(-\omega_n^2 * [m] * \emptyset_n) + ([k] * \emptyset_n)\} = 0 \tag{3.11}$$

Equation 3.11 has two known variables ([m] and [k]) and can be solved in one of two ways. The first solution is trivial and implies no motion of the system, the second solution is the matrix eigenvalue problem (Equation 3.12). If the characteristic equation (Equation 3.13) is true, then nontrivial solutions exist (Chopra, 1995).

$$\{[k] - (\omega_n^2 * [m])\} * \emptyset_n = 0 \tag{3.12}$$

$$\det\{[k] - (\omega_n^2 * [m])\} = 0 \tag{3.13}$$

In order to find the natural circular frequencies (ω_n), the determinant shown in Equation 3.13 must be expanded. The roots of the resulting polynomial are the natural circular frequencies (ω_n). These frequencies can then be substituted into Equation 3.12 to determine the different vectors describing the natural modes of vibration (φ_n) (Chopra, 1995).

The natural modes of vibration (φ_n) can only be determined to within a multiplicative factor. As such, "any vector proportional to a natural mode is essentially the same natural mode because it also satisfies Equation 3.12 (Chopra, 1995)." The process of normalization is a way to scale natural modes into a form that is easier to understand and compare. Common normalization methods include: taking the largest element as 1, taking a specific degree of freedom as 1, and taking the generalized mass Mn as 1 (Equation 3.14).

$$M_N = \emptyset_n^T * [m] * \emptyset_n \tag{3.14}$$

Normalization to a generalized mass (M_n) of 1 is common in computer software, including the software used in this study and validated in the next section. Often, a structure's deformed shape embodies some combination of the natural modes of vibration. A particular mode's contribution to this deformation can be determined by calculating the effective modal mass participation (Equation 15).

$$M_N^* = \frac{(L_N)^2}{M_N} = \frac{\varphi_n^T * [m] * [i]}{M_N} \tag{3.15}$$

Equation 3.15 utilizes quantities that have already been discussed with the exception of the influence vector (i). This vector, "represents the displacements of the masses resulting from static application of a unit ground displacement (Chopra, 1995)." The

resulting effective modal mass participation can then be taken as a percentage of the total structure mass. ASCE 7-10 states that all modes comprising 90% modal mass participation should be considered in the Modal Response Spectrum Analysis Procedure (ASCE, 2010). However, since the Equivalent Lateral Force Procedure is the method being used for seismic load calculations in this study, 90% mass participation is not sought. Effective modal mass participation is evaluated to determine the dominant mode shapes in the modal analyses.

3.4.2. Software Validation

The ability of the software to accurately calculate the natural modes of vibration and natural circular frequency was verified with an example taken from Anil K. Chopra's textbook *Dynamics of Structures* (Chopra, 1995). This multi-degree of freedom, lumped mass example was chosen for its similarity to the parametric and case studies. The example specifically addressed finding the natural circular frequencies (ω_n) and natural modes of vibration (φ_n) for the structure seen in Figure 3.10.

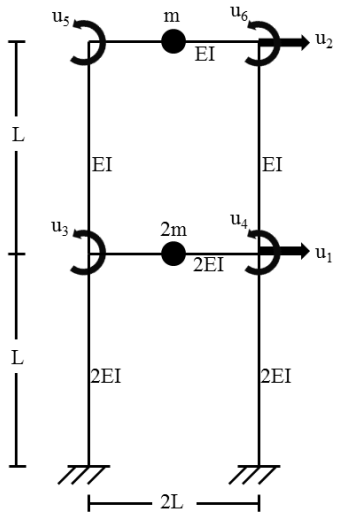

Figure 3.10. Software Validation - Example Structure

The example structure exhibited 6 degrees of freedom and the following variables: mass (m), modulus of elasticity (E), member length (L), and cross sectional moment of inertia (I). The example problem solved for the natural circular frequencies (ω_n) and natural modes of vibration (φ_n) algebraically (i.e. no values given for E, L, and I). In order to obtain numerical results from RAM Elements, arbitrary values based on Figure 3.10 were assumed (Table 3.5).

Table 3.5. Software Validation - Example Structure Assumed Values.

Variable	Assumed Value
Mass (m)	334 kN (2331 slug)
Modulus of Elasticity (E)	55 GPa (7,980 ksi)
Cross Sectional Moment of Inertia (I)	214,480 cm^4 (5,153 in^4)
Member Length (L)	3.05 m (10.00 ft)

The values in Table 3.5 allowed the example structure to be modeled in RAM Elements. Once properly modeled, modal analysis was conducted in RAM Elements. The results of the software's modal analysis were compared to a hand derived MATLAB program. This program was written to solve Equation 3.13 and obtain exact values for the natural circular frequencies (ω_n) and modes of vibration (φ_n) resulting from the values of Table 3.5. The modes of vibration (φ_n) were normalized according to Equation 3.14 in order to compare to the similarly normalized modes of vibration calculated by the software. Finally, the program calculated the effective modal mass participation with Equation 3.15. The results of both the software analysis and MATLAB program are shown in Table 3.6. The derivation of both the mass and stiffness matrices along with the finished MATLAB program can be found in Appendix E.

Table 3.6. Software Validation - Example Structure Results Comparison.

Variable	Symbol	MATLAB	RAM Elements
Natural Circular Frequency	$\omega_{1\ (rad/sec}$	24.32	23.91
	$\omega_{2\ (rad/sec)}$	64.75	62.73
Natural Mode of Vibration	$\phi_{1\ (unitless)}$	-0.222, -0.575	0.223, 0.574
	$\phi_{2\ (unitless}$	-0.406, 0.315	0.406, -0.315
Effective Mass Participation %	$\phi_{1\ (unitless)}$	80.73	80.78
	$\phi_{2\ (unitless}$	19.27	19.22

The results show that the software was able to successfully replicate the hand calculated results within a 3% error margin. After the software's validation, the parametric study was conducted using the same software settings and assumptions.

CHAPTER 4: RESULTS AND DISCUSSION

This chapter presents the results of the static and dynamic analyses of the models described in Chapter 3. A discussion of these results in terms of their impact on the understanding of classical column geometries and their effect on the seismic behavior is also included.

4.1. Parametric Study of Free-Standing Classical Columns

The 15 free-standing column finite element models were created and analyzed with techniques discussed in Chapter 3. This section contains the results of this parametric study.

4.1.1. Dynamic Analysis

The purpose of the dynamic analysis is to investigate the effect of classical column proportions on the natural circular frequencies (ω_n) and modes of vibration (φ_n) of a free-standing column. The software RAM Elements (verified in Chapter 3.4.3) was utilized to calculate these properties for all 15 free-standing columns. The resulting 1st natural circular frequencies (ω_1) are summarized in Figure 4.1.

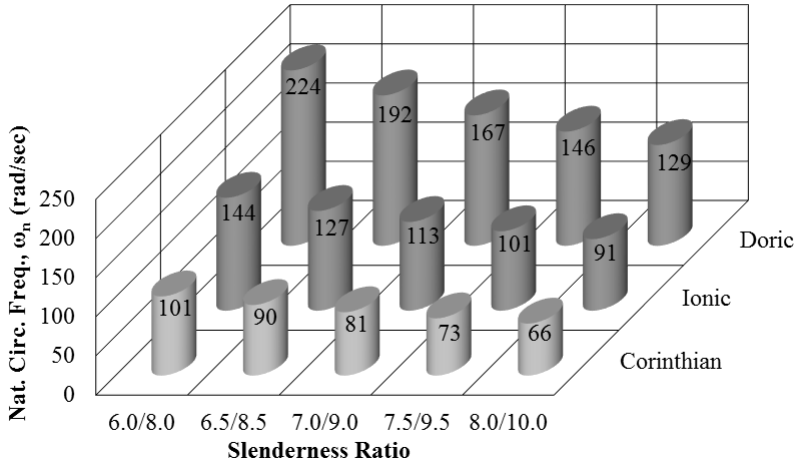

Figure 4.1. 1st Natural Circular Frequency Results Comparison

Figure 4.1 shows that for a given column order, an increase in slenderness ratio leads to a decrease in the natural circular frequency (ω_n). To better understand this result consider the natural circular frequency of vibration (ω_n) for an undamped single degree of freedom system (Equation 4.1). The subject of viscous damping in dry stack structures has been discussed at length in the literature (Carydis et al., 1996; Papantonopoulos et al., 2002; Psycharis et al., 2003; Psycharis, 2007). However, no consensus has been reached regarding when and how much damping to use. As such this thesis will assume zero damping while acknowledging that the addition of a small amount of damping should be considered in the future and may affect the results when this variable is considered.

$$\omega_n = (2\pi / T_n) = \sqrt{\frac{k}{m}} \tag{4.1}$$

Equation 4.1 shows that the natural circular frequencies (ω_n) and modes of vibration (φ_n) for a structure are dependent on two factors: stiffness and mass. As seen in Chapter 3.4.1. the determination of these two factors is necessary to the successful solution of the eigenvalue problem. The determination of mass is self-explanatory, however, the stiffness is more involved. Utilizing slope-deflection and fixed end moments, the

stiffness coefficients can be derived for flexural elements (Chopra, 1995). Independently derived in Appendix E, these coefficients consist of a numerical constant, modulus of elasticity (E), member length (L), and cross sectional moment of inertia (I). Within each stiffness coefficient, the variables take the form (constant*E*I/L). Substituting these variable back into Equation 4.1 one obtains Equation 4.2.

$$\omega_n = \sqrt{\frac{\text{constant} * E * I}{L * m}} \tag{4.2}$$

Equation 4.2 is a qualitative expression meant to illustrate the effect of the variable on the natural circular frequency (ω_n). From this expression it can be determined that, with all other variables being equal, increases in member length (L) and mass (m) would decrease the natural circular frequency (ω_n). Returning to the results of Figure 4.1, and given the study assumes a fixed column shaft diameter, the increase of slenderness ratio for a given column order leads to increases in both member length (L) and mass (m). Across the three classical orders and its substyles, the modulus of elasticity (E) remains constant (no change in material), and cross sectional moment of inertia (I) varies slightly (due to lack or existence of base and size and location of the capital). As such, the observed effect of slenderness ratio on natural circular frequency (ω_n) in Figure 4.1 is valid.

Similarly, the differences observed between the natural circular frequencies (ω_n) of the different column orders can be assessed. Consider the results at the median slenderness ratio for each column order (Doric - 7.0, Ionic/Corinthian – 9.0) (Figure 4.2). The natural circular frequency is highest in the Doric column and lowest in the Corinthian column. This implies that the Corinthian is the most flexible of the three classical orders.

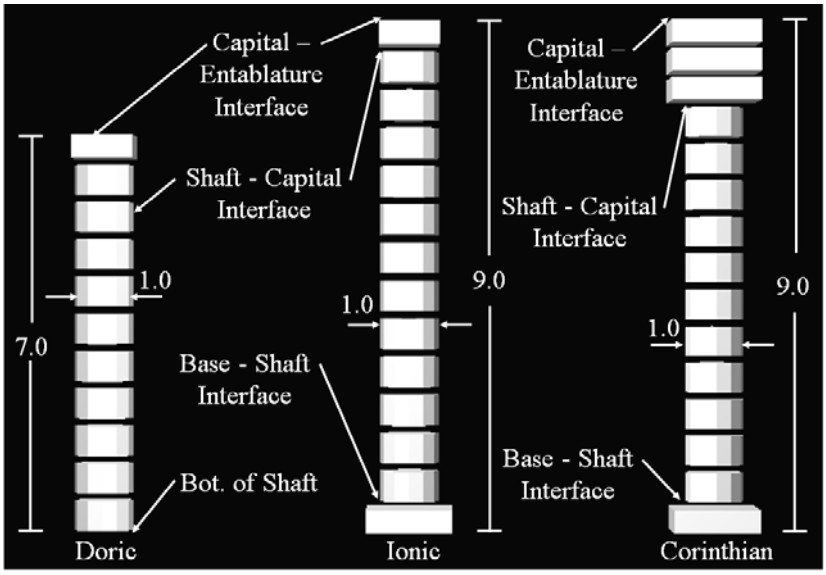

Figure 4.2. Column Order Comparison – Median Slenderness Ratio

In addition to the natural circular frequencies (ω_n) RAM elements calculated the natural modes of vibration (φ_n) and normalized them to a generalized mass (M_n) of 1. The mode shapes were taken from RAM Elements and re-normalized so that the largest modal displacement value encountered in all results was equal to 1. As such the mode shapes exhibited in Figure 4.3 show displacement values less than or equal to 1. Similar to the natural circular frequencies (ω_n), the results were first compared across all slenderness ratios for a specific mode and column order (Figure 4.3).

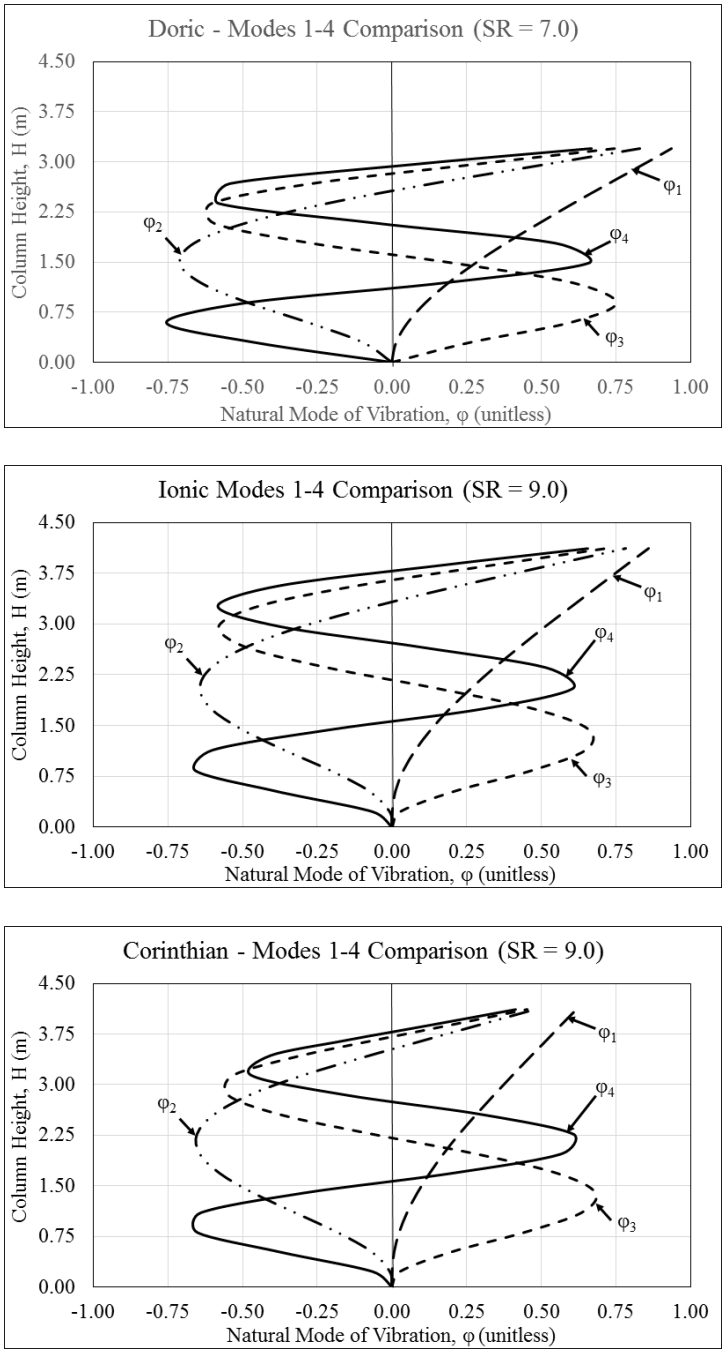

Figure 4.3. Modes 1-4 Comparison (Slenderness Ratio = 7.0/9.0).

Figure 4.4 illustrates the small effect of slenderness ratio on the natural dynamic properties of columns under the first fundamental mode.

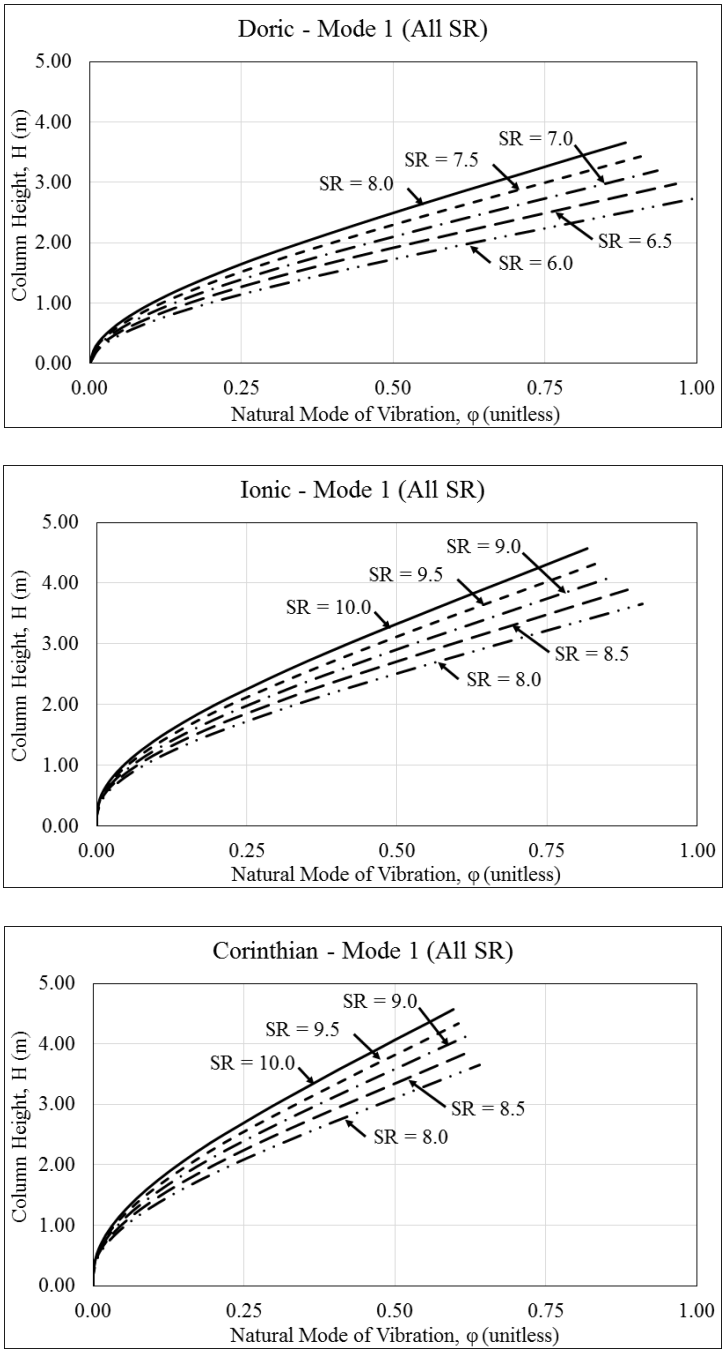

Figure 4.4. Mode 1 Shape (All Slenderness Ratios).

This small change between slenderness ratios is typical of all column orders at each of the four considered modes. As such, it is more interesting to compare the results between different column orders, at the median slenderness ratio for each of the first four modes (Figure 4.5).

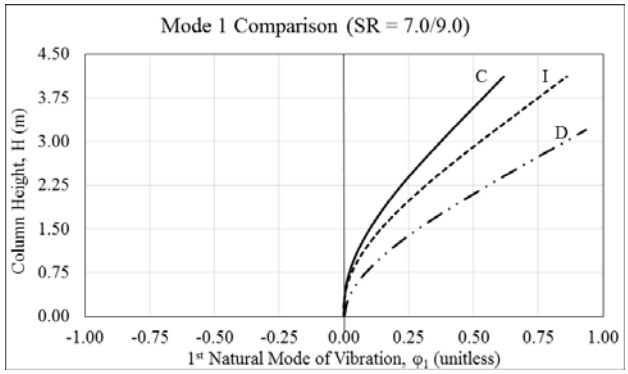

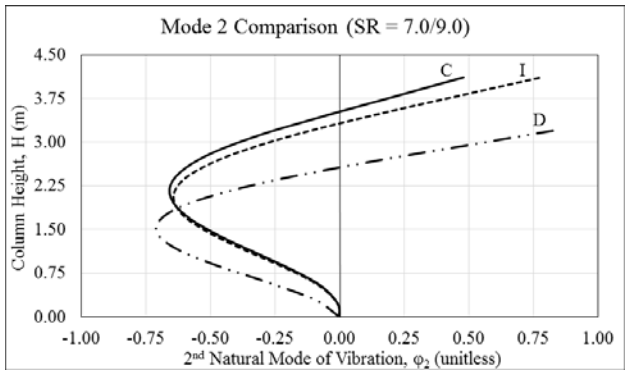

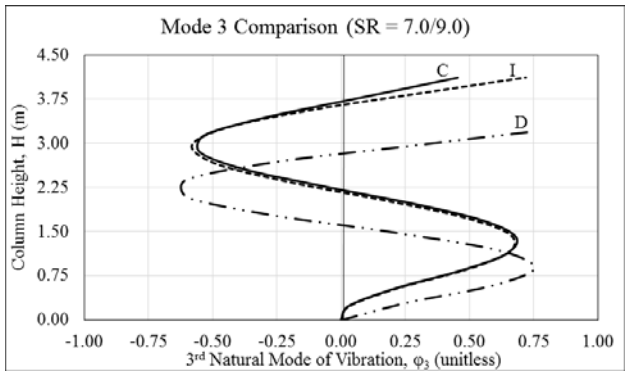

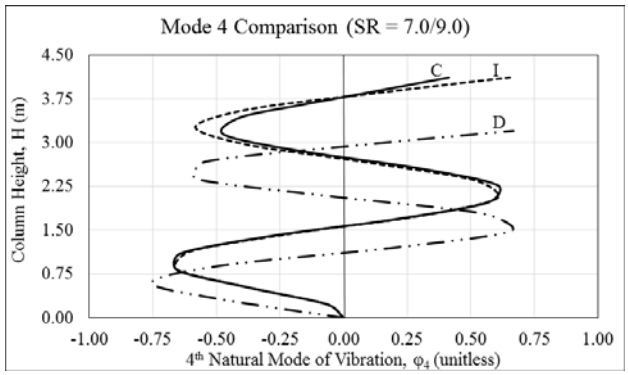

Figure 4.5. Mode Shape Comparison (Modes 1-4)

Figure 4.5 shows that the general modal behavior is consistent across all three column orders for the first four natural circular frequencies (ω_n) considered. This is to be expected as all columns have the same fixed-free boundary conditions. The effect of variances in both geometry and location of mass can be seen in the more subtle differences between the mode shapes of the column orders. Notice that in each graph of Figure 13 the smaller modal displacements belong to the order with the smaller natural circular frequencies (ω_n). When Equation 3.12 is considered, this direct relationship between natural circular frequencies (ω_n) and natural modes of vibration (φ_n) is to be expected.

4.1.2. Static Analysis

As discussed in Chapter 3.4.1 the Equivalent Lateral Force Procedure (ELFP) was utilized for all static analysis. Once the equivalent lateral forces were calculated according to ASCE 7-10 (Appendix C) they were applied to the finite element models and a static analysis was performed. The axial reaction data taken from the fixed column base is tabulated in Table 4.1.

Table 4.1. Free-Standing Column - Axial Reaction Results.

Order	Slenderness Ratio				
	6.0/8.0	**6.5/8.5**	**7.0/9.0**	**7.5/9.5**	**8.0/10.0**
Doric	12.1 kN (2.7 kip)	13.1 kN (2.9 kip)	14.1 (kN) (3.2 (kip)	15.1 (kN) (3.4 (kip)	16.0 (kN) (3.6 (kip)
Ionic	17.8 kN (4.0 kip)	18.8 kN (4.2 kip)	19.7 kN (4.4 kip)	20.7 kN (4.7 kip)	21.7 kN (4.9 kip)
Corinthian	23.5 kN (5.3 kip)	24.5 kN (5.5 kip)	25.4 kN (5.7 kip)	26.4 kN (5.9 kip)	27.4 kN (6.2 kip)

As the slenderness ratio increases, the fixed diameter assumption results in more column volume and thus more mass. The axial reaction is a direct representation of the

difference in mass between the columns. The Corinthian column proved to have higher reactions due primarily to the extra mass attributed to its larger capital. With self-weight being the only applied vertical force, the axial reaction was equal to the total weight of the column. The expected output axial reactions were verified in Appendix C.

The lateral thrust (or shear at the support) were also analyzed using seismic loads calculated by the Equivalent Lateral Force Procedure (Appendix C). The calculated shear reaction data is tabulated in Table 4.2.

Table 4.2. Free-Standing Column - Shear Reaction Results.

Order	Slenderness Ratio				
	6.0/8.0	**6.5/8.5**	**7.0/9.0**	**7.5/9.5**	**8.0/10.0**
Doric	19.8 kN (4.5 kip)	21.4 kN (4.8 kip)	23.0 kN (5.2 kip)	24.5 kN (5.5 kip)	26.1 kN (5.9 kip)
Ionic	29.0 kN (6.5 kip)	30.6 kN (6.9 kip)	32.2 kN (7.2 kip)	33.8 kN (7.6 kip)	35.3 kN (7.9 kip)
Corinthian	38.3 kN (8.6 kip)	39.9 kN (9.0 kip)	41.5 kN (9.3 kip)	43.1 kN (9.7 kip)	44.6 kN (10.0 kip)

Since the lateral force is proportional to the seismic weight, the results summarized in Figure 4.6 are as expected with columns of larger mass exhibiting higher shear reactions (Appendix C).

The moment reactions were a result of the equivalent lateral forces and their points of application along a column height. The moment reaction data is tabulated in Table 4.3.

Table 4.3. Free-Standing Column - Moment Reaction Results.

Order	Slenderness Ratio				
	6.0/8.0	**6.5/8.5**	**7.0/9.0**	**7.5/9.5**	**8.0/10.0**
Doric	37.5 kN-m (27.7 kip-ft)	43.8 kN-m (32.3 kip-ft)	50.6 kN-m (37.3 kip-ft)	57.8 kN-m (42.6 kip-ft)	65.5 kN-m (48.3 kip-ft)
Ionic	72.1 kN-m (53.2 kip-ft)	80.7 kN-m (59.5 kip-ft)	89.8 kN-m (66.3 kip-ft)	99.4 kN-m (73.3 kip-ft)	109.5 kN-m (80.8 kip-ft)
Corinthian	107.4 kN-m (79.2 kip-ft)	118.6 kN-m (87.5 kip-ft)	130.4 kN-m (96.2 kip-ft)	142.6 kN-m (105.2 kip-ft)	155.4 kN-m (114.6 kip-ft)

As expected, the Corinthian columns resulted in the largest moment reactions among the three orders. This was again a product of the Corinthian columns' larger size and higher center of gravity (Appendix C).

The deformed shapes that resulted from the static analysis proved to be fairly consistent among all 15 test columns (Figure 4.6).

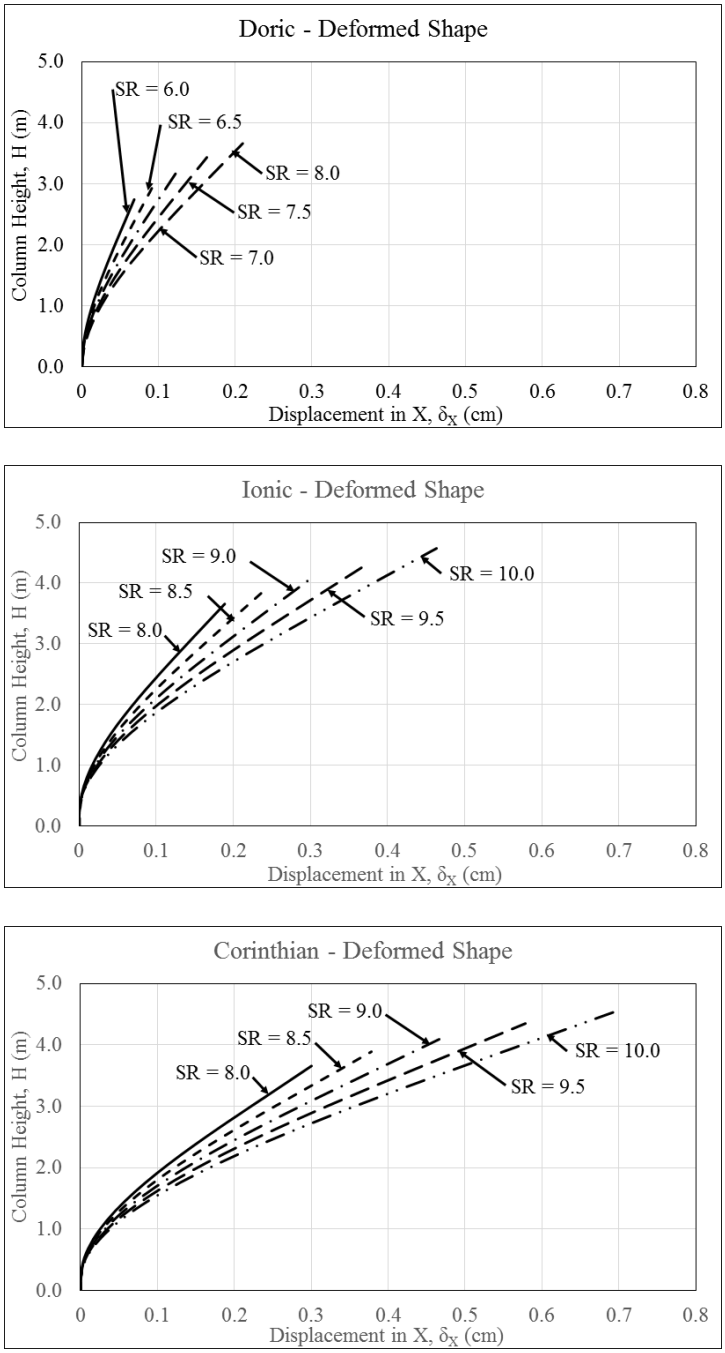

Figure 4.6. Deformed Shape – Free Standing Columns

Figure 14 illustrates that the maximum lateral displacement occurs at the top of the capital as expected. The similarity of the deformed shape to the 1st natural mode of vibration (φ_n) is apparent. This can be explained by an effective mass participation

percentage of 54-63% for the first natural mode of vibration. The maximum displacement data is tabulated in Table 4.4

Table 4.4. Free-Standing Column – Maximum Displacement Results.

Order	Slenderness Ratio				
	6.0/8.0	**6.5/8.5**	**7.0/9.0**	**7.5/9.5**	**8.0/10.0**
Doric	0.28 (cm) 0.11 (in)	0.38 (cm) 0.15 (in)	0.51 (cm) 0.20 (in)	0.66 (cm) 0.26 (in)	0.84 (cm) 0.33 (in)
Ionic	0.18 (cm) 0.07 (in)	0.23 (cm) 0.09 (in)	0.30 (cm) 0.12 (in)	0.38 (cm) 0.15 (in)	0.46 (cm) 0.18 (in)
Corinthian	0.30 (cm) 0.12 (in)	0.38 (cm) 0.15 (in)	0.48 (cm) 0.19 (in)	0.58 (cm) 0.23 (in)	0.71 (cm) 0.28 (in)

It was shown in the results of the three reactions above (Tables 4.1-4.3) that the larger columns are subjected to higher lateral forces. It comes as no surprise that as these forces increase, so too does the maximum lateral displacement.

The final results comparison for the parametric study involves the maximum member stresses on the column (Figure 4.7).

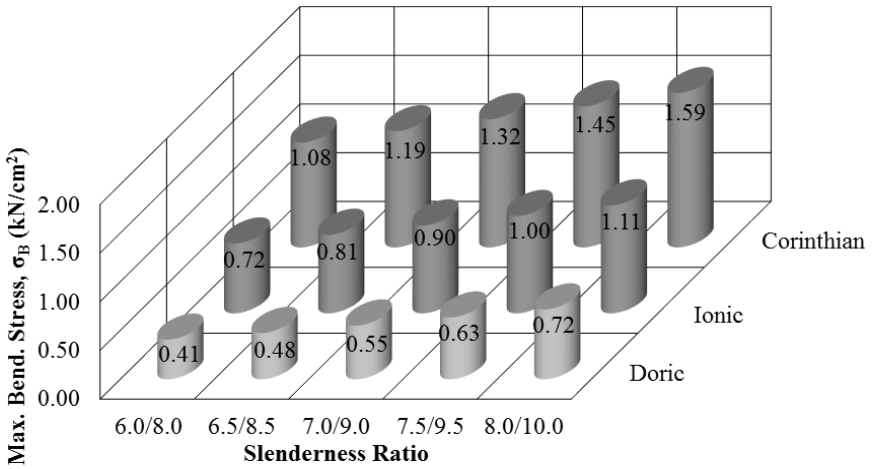

Figure 4.7. Maximum Bending Stress Results Summary

The maximum bending stresses exhibited in Figure 4.7 show that the bending stress increases (along with applied forces) from Doric to Ionic to Corinthian. However, the

location of the maximum bending stress is also of note. For models without a base (Doric) it occurs at the bottom of the column shaft (Figures 4.2 and 4.8).

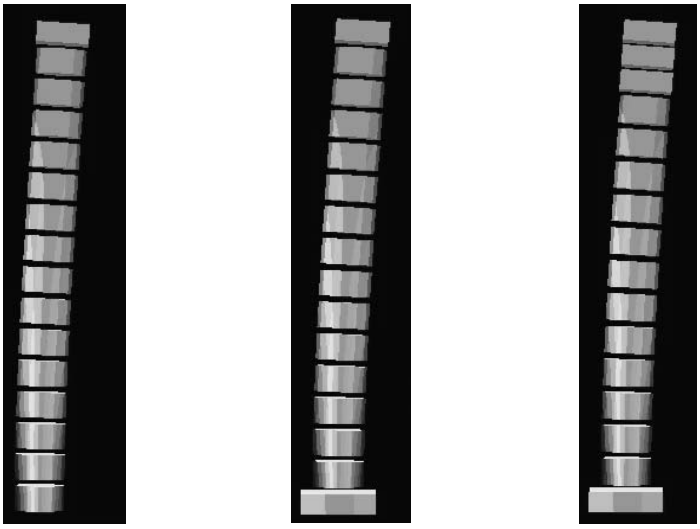

(a) Doric (b) Ionic (c) Corinthian

Figure 4.8. Parametric Study – Typical Member Bending Stress Distributions

For columns with a base, it occurs not at the bottom of the column (where the fixed connection was assumed) but in the column shaft at the base – shaft interface (Figures 4.2 and 4.8). This is due to the smaller cross-section of the shaft being asked to carry nearly the same force as the base in this location. This location of maximum member stress is true for axial, shear, and bending principal stresses.

4.2. Case Study - *Temple of Antioch ad Cragum Façade*

Finite element models were created for the Temple of *Antioch ad Cragum* façade and analyzed with techniques discussed in Chapter 3. This section contains the results of the case study analyses.

4.2.1. Dynamic Analysis

The purpose of the dynamic analysis is to better understand the dynamic characteristics of a classical frame system. Unlike the parametric study, this case study will investigate

a single structure but pay special attention to the effects of beam to column connections (pinned connections vs. moment connections) on the overall dynamic behavior. Similar to the parametric study, the goal of this analysis is to determine the natural circular frequencies (ω_n) and modes of vibration (φ_n) of the structure utilizing RAM Elements.

As discussed in Chapter 3.4. RAM Elements calculates the natural circular frequencies (ω_n) and modes of vibration (φ_n) based on point masses defined on existing nodes. In addition to the typical point masses that were defined for the columns of the parametric study, point masses were also calculated for the triangular pediment. The shape of the pediment made accurate modeling difficult, therefore its weight (48 kN or 11 kip) and distribution was simulated via a stair step loading scheme and point masses applied at the entablature height (Appendix D). The total pediment weight was accurate to within 2%. The values for each point mass were determined by considering the pediment shape, density, and the tributary member length for each node. While the location of the pediment point masses are not completely accurate (they should be located higher) they will provide a suitable approximation. The effective mass participation percentages are reported along with the natural circular frequencies (ω_n) in Table 4.5.

Table 4.5. Case Study - Natural Circular Frequency Results.

Mode	Moment Connections		Pinned Connections	
	Nat. Circ. Freq. ω_n	Mass Partic.%	Nat. Circ. Freq. ω_n	Mass Partic.%
1	57.44	75.29	27.97	66.77
2	342.34	0.00	212.31	0.00
3	355.50	0.31	213.39	0.00
4	365.74	0.00	214.13	0.00
5	403.80	8.50	235.32	14.64
6	824.49	0.00	666.87	0.00
7	881.14	0.40	673.75	0.11
8	921.64	0.00	678.38	0.00
9	992.25	3.40	700.16	4.97

Table 4.6 shows that of the nine modes calculated, only three contribute significant modal mass participation. These three dominant mode shapes are shown for the moment connection model in Figure 4.11.

Of the nine modes shown in Table 4.5, only three were found to contribute significant modal mass participation (> 0.5%). The three mode shapes shown are similar to the first three mode shapes of the free standing columns analyzed in the parametric study (Figure 4.9).

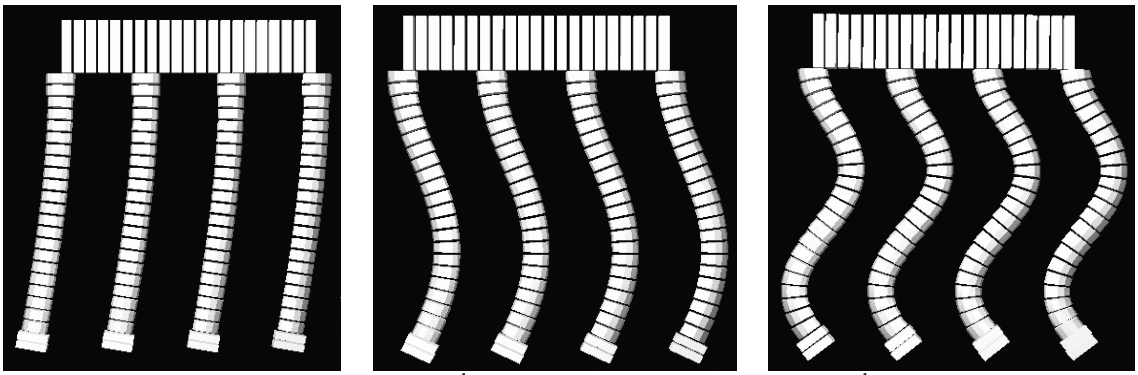

(a) 1st Natural Mode (φ_1) (b) 5th Natural Mode (φ_5) (c) 9th Natural Mode (φ_9)

Figure 4.9. Façade Frame Modes of Vibration – Moment Connections

A similar relationship can be seen in the mode shapes for the pinned connections (Figure 4.10).

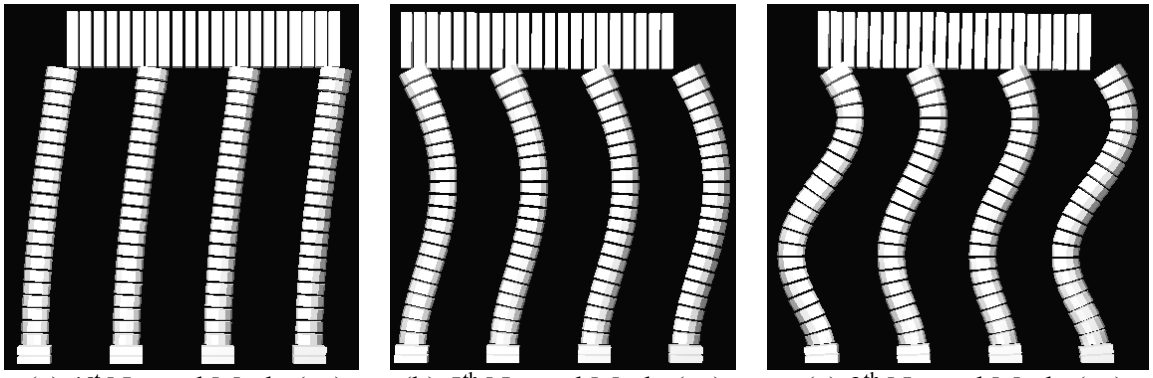

(a) 1st Natural Mode (φ_1) (b) 5th Natural Mode (φ_5) (c) 9th Natural Mode (φ_9)

Figure 4.10. Façade Frame Modes of Vibration – Pinned Connections

The remaining mode shapes combine different column deformed shapes with respect to one another.

4.2.2. Static Analysis

In the parametric case study the only loads applied to the models were gravity and the equivalent lateral forces determined according to ASCE 7-10 (Appendix C). The simulation of pinned connections at the beam-column connection site was accomplished by creating hinges at the ends of the entablature elements connecting to the columns. The base reactions for both connection cases are tabulated in Table 4.6.

Table 4.6. Case Study – Axial, Shear, and Moment Reactions.

Connection Type	Column	Moment Connections		
		Axial, P	Shear, V	Moment, M
Moment	Column 1	-17.4 (kN)	59.9 (kN)	188.3 (kN-M)
	Column 2	95.5 (kN)	62.2 (kN)	194.2 (kN-M)
	Column 3	104.1 (kN)	62.6 (kN)	195.2 (kN-M)
	Column 4	164.5 (kN)	60.8 (kN)	190.7 (kN-M)
Pinned	Column 1	81.0 (kN)	61.2 (kN)	349.8 (kN-M)
	Column 2	101.7 (kN)	62.6 (kN)	350.4 (kN-M)
	Column 3	101.7 (kN)	62.6 (kN)	350.4 (kN-M)
	Column 4	62.4 (kN)	61.2 (kN)	349.5 (kN-M)

As expected, the beam-column connection conditions had a significant effect on the resulting base reactions. By utilizing moment connections, a portion of the moment that

would have to be resisted by the base connection is resisted by the moment connection. The result is lower moment reactions at the base than those of pinned connection case. However, by resisting this moment at the moment connection, the overall frame tends to overturn as a single unit. This can be seen in the fact that the axial reactions increase as the columns get nearer to the point of overturning. The pinned connection simply allows the entirety of the moment to transfer to the base where it resisted by the fixed connection. With regards to the maximum lateral displacement, the moment connection outperformed the pinned-pinned connection. The moment connection only allowed a maximum lateral displacement of 0.31 cm (0.12 in) compared to the pinned connection which allowed 1.32 cm (0.52 in).

The maximum member stresses on the column were also affected by the selection of column-entablature connection. The stress distributions show that for the moment connection case there are three areas of high stress, located in (in order of severity): the shaft at the base – shaft interface, in the shaft at the capital – shaft interface, and in the capital at the capital – entablature interfaces (Figures 4.2 and 4.11).

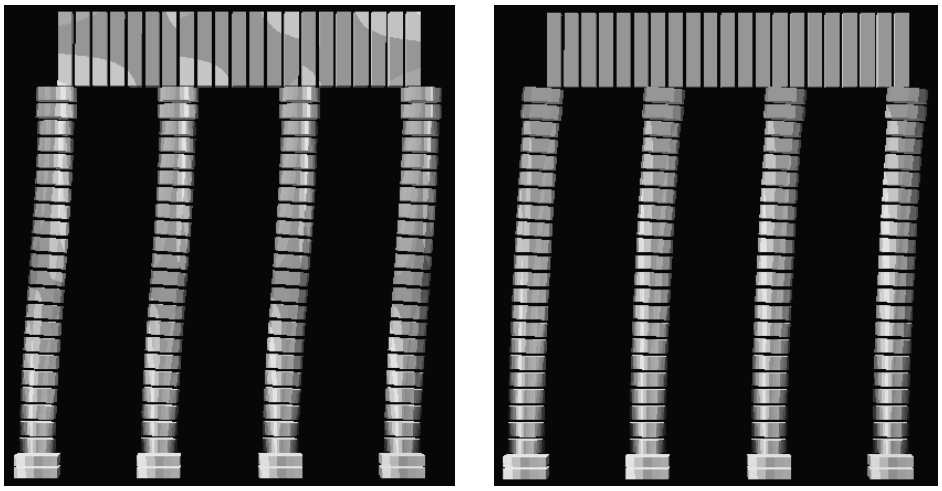

(a) Moment Connections (b) Pinned Connections

Figure 4.11. Case Study –Member Bending Stress Distribution.

These areas are of particular concern because they coincide with possible column component connection sites. The principal stresses at the column component interfaces are summarized in Table 4.7.

Table 4.7. Case Study - Maximum Member Stress.

Connection Type	Interface	Moment Connections		
		Axial, σ	Shear, τ	Bending, σ_b
Moment	Base-Shaft	0.55 MPa (0.08 ksi)	0.21 MPa (0.03 ksi)	7.79 MPa (1.13 ksi)
	Shaft-Capital	0.41 MPa (0.06 ksi)	0.14 MPa (0.02 ksi)	6.00 MPa (0.87 (ksi)
	Capital - Entablature	0.28 MPa (0.04 ksi)	0.21 MPa (0.03 ksi)	4.83 MPa (0.70 ksi)
Pinned	Base-Shaft	0.34 MPa (0.05 ksi)	0.21 MPa (0.03 ksi)	14.96 MPa (2.17 ksi)
	Shaft-Capital	0.21 MPa (0.03 ksi)	0.14 MPa (0.02 ksi)	1.93 MPa (0.28 ksi)
	Capital - Entablature	0.14 MPa (0.02 ksi)	0.07 MPa (0.01 ksi)	0.76 MPa (0.11 ksi)

The data in Table 4.7 echoes the findings of the parametric study for the Corinthian order, showing that the worst member stresses occur in the shaft at the base - shaft interface. Recall that the higher stresses at this location are due to the smaller cross-section of the shaft being asked to carry nearly the same force as the base. The flexibility of the pinned connection frame is again showcased by the location of its maximum member stresses in the shaft at the base - shaft interface and a better distribution of axial and shear stress among its columns. This is in contrast to the rigidity of the moment connection frame that distributes the bending stress into three primary areas (see above) and acts as a single unit to resist overturning.

CHAPTER 5: CONCLUSIONS AND RECOMMENDATIONS FOR FUTURE WORK

This study includes several assumptions in order to limit discussion to the effect of geometric proportions on the seismic behavior of ancient columns. The authors concede that several studies have attempted to accurately capture the dynamic behavior of nonlinear, rigid body motion indicative of true dry stack behavior with varying levels of success. The relationship between seismic behavior and classical order has yet to be fully investigated. This study is to serve as a basis for the investigation of this relationship.

5.1. Conclusions

As stated in Chapter 1, the overall goal of this thesis is to better understand the effect of the geometrical differences of classical column orders on the seismic response of classical structures through the use of computer analyses. This goal was broken down into two separate studies: 1) Parametric Study of Free-Standing Classical Columns; 2) Case Study – *Temple of Antioch ad Cragum Façade*. Both of these studies utilized the finite element software *RAM Elements 13.0* to perform static and dynamic analyses. This software was verified with an example structure in Chapter 3.4.2. The following conclusions are derived for each of the objectives listed in Section 1.

I. The design response spectra was created for countries with a high density of dry stack structures (Greece, Italy, and Turkey). The factors used in the creation of this spectra were also necessary in the calculation of the seismic response coefficient (C_S). This factor was central to the calculation of the equivalent lateral forces used in the Equivalent Lateral Force Procedure.

II. The parametric study considered 15 total free-standing columns, 5 per classical column order. The geometries of these columns were determined by utilizing the proportions of the author Vitruvius and an Ionic/Corinthian shaft diameter of 46 cm (18.00 in) which is representative of smaller structures (more likely to be found in more remote areas of the Roman Empire).

III. Modal analysis showed that the classical proportions of Vitruvius had a noticeable effect on the natural circular frequencies (ω_n) and modes of vibration (φ_n) of the test columns. When the columns from each order at the median slenderness ratio were compared, the larger columns were found to result in decreased fundamental frequencies and increased flexibility due to their increase in both mass and height. Additionally, the slenderness ratio was found to have a noticeable, yet predictable effect on the natural circular frequencies (ω_n) and modes of vibration (φ_n).

IV. Static analysis showed that the deformed shape for all 15 test columns was similar. This deformed shape was shown to be nearly proportional to the 1st natural mode of vibration (φ_n), verified by the approximately 60% effective mass participation percentages provided by this mode. The location of maximum stress was found to be identical for all principle stresses: axial, shear, and bending. This location was in the column shaft at the base – shaft interface (Ionic/Corinthian) and also in the column shaft at the bottom of the column shaft (Doric). This was due to both the magnitude of force at these locations and the smaller cross-sectional areas of the column shaft when compared to the base.

V. The case study modal analysis showed that the fixed and pinned connection frame models exhibited similar natural modes of vibration (φ_n). Only three of the modes

contributed significant modal mass participation (> 0.5%) and they were similar to the first three natural modes of vibration (φ_n) found in the parametric study. However, the connection was found to have a large effect on the natural circular frequency (ω_n). Pinned connections were found to greatly reduce the natural circular frequency (ω_n) and result in a much more flexible structure.

The static analysis reinforced the findings that the pinned connections allowed the frame to be more flexible, allowing the reactions to evenly distribute at the base columns. This resulted in the maximum principle stresses being located in the column shaft at the base - shaft interface for the same reasons detailed for the parametric study. However, these connections led to a larger base moment reaction when compared to the moment connections. The moment connections shared the large moment reaction between the base and the beam-entablature connection resulting in smaller stresses. This lead to principal stress concentrations in the column shaft at the base – shaft interface and shaft - capital interfaces in addition to the capital at the capital – entablature interface. Unlike the pinned connections, the moment connections resulted in a rigid structure that acted to resist overturning forces as a single unit. This resulted in axial reactions that varied with the distance from the point of overturning. Finally, with regards to maximum displacement, the moment connection (0.31 cm) was found to outperform the pinned connection (1.32 cm). Considering the literature regarding ancient connections, it is likely that if a connection between the column and entablature existed it was a moment connection. This is due to the method and installation of both the dowels and I-shaped clamps that have been discovered.

Continual refinement of the Temple of *Antioch ad Cragum* façade model will be vital to the successful design of connections should the reconstruction take place.

5.2. Recommendations for Future Work

The conclusions above have provided additional insight to the seismic behavior of classical colonnaded structures. The results of this thesis could lead to several avenues of research including the following possibilities.

Effect of Classical Column Orders in Non-Linear Dry Stack Columns

The results of this thesis showed that classical column geometries can have a noticeable effect on seismic response. The next logical step would be to extend this research utilizing nonlinear analysis of the same arrangements to incorporate cracking, crushing, sliding, and rocking. The removal of mechanical fastening adds layers of complication to the analysis due to the frictional interaction between component column pieces. While several authors have approached the subject of dry stack column behavior, the effect of classical column orders in dry stack columns without mechanical fastening has not been specifically addressed. Therefore the next phase of this project will utilize the findings of this study but incorporate these complications incrementally.

Restoration of Temple of *Antioch ad Cragum* Façade

This thesis performed the first step of analysis for a resurrected façade. However, the model will constantly need to be updated with continued findings in the field. The model detailed here was only the current iteration of the façade. The research team is continually refining the dimensions, layout, and composition of the façade. The model must be updated to reflect these findings.

The most critical piece of a successful restoration will be the connection design. With the size of component blocks varying considerably, the location of connections in the façade will likely not have a logical pattern. As such it is vital to have an updated column model in order to know what forces the connections will need to resist in order to hold the structure together.

REFERENCES

Ambraseys, N. N. 2006. Earthquakes and Archaeology. *Journal of Archaeological Science* 33 (7): 1008, http://www.sciencedirect.com.leo.lib.unomaha.edu/science/article/pii/S030544030500244X.

Ambraseys, N. N., and J. A. Jackson. 1998. Faulting Associated With Historical and Recent Earthquakes in the Eastern Mediterranean Region. *Geophysical Journal International* 133 (2): 390-406, http://dx.doi.org.leo.lib.unomaha.edu/10.1046/j.1365-246X.1998.00508.x.

Ambraseys, Nicholas, and Ioannis N. Psycharis. 2011. Earthquake Stability of Columns and Statues. *Journal of Earthquake Engineering* 15 (5) (06/01; 2012/10): 685-710, http://dx.doi.org.leo.lib.unomaha.edu/10.1080/13632469.2010.541549.

Arisoy, Bengi, Ayhan Nuhoglu, and Emre Ercan. 2011. Seismic Response of Multi-drum Classical Columns of Apollo Temple at Claros. *Scientific Research and Essays* 6 (2): 283-92.

ASCE. 2010. "Minimum Design Loads for Buildings and Other Structures." *ASCE 7-10*, New York.

ASTM Standard C170/C170M. 2009. "Standard Test Method for Compressive Strength of Dimension Stone." ASTM International. West Conshohocken, PA. 2003. DOI: 10.1520/C0170_C0170M-09. www.astm.org.

Carydis, P. G., H. P. Mouzakis, C. L. Papantonopoulos, D. J. Papastamatiou, I. N. Psycharis, E. A. Vougioukas, and C. Zambas. 1996. Experimental and Numerical Investigations of the Earthquake Response of Classical Monuments. Paper presented at Proceedings of the 11th World Conference on Earthquake Engineering (CD-ROM), Acapulco, Mexico.

Chopra, A. K. 1995. *Dynamics of structures: Theory and applications to earthquake engineering*. Englewood Cliffs, N.J: Prentice Hall.

Cooper, Frederick A., Stella G. Miller, Stephen G. Miller, and Candace Smith. 1983. *The Temple of Zeus at Nemea: Perspectives and Prospects*. Athens, Greece: Benaki Museum.

Erdogmus, E., C. M. Buckley, and H. Brink. 2011a. Restoration of the Temple of Antioch. Paper presented at Proceedings of 11th North American Masonry Conference, Minneapolis, Minnesota.

———. 2011b. The Temple of Antioch: A Study Abroad Internship for Architectural Engineering Students. Paper presented at AEI 2011: Building Integration Solutions. Oakland, CA, http://dx.doi.org/10.1061/41168(399)1.

Erdogmus, E., K. Fickle, A. Kousgaard, and J. Freedland. 2014. Assessment and Preservation of Ancient Roman Marble Blocks. Paper presented at Proceedings of 12th North American Masonry Conference, Denver, Colorado.

Erdogmus, E., J. Freedland, A. Jording, A. Kousgaard, and C. M. Buckley. 2013. Material Condition and Deterioration Assessment Program for a 3rd Century Roman

Temple. Paper presented at AEI 2013: Building Solutions for Architectural Engineering, State College, PA, http://dx.doi.org/10.1061/9780784412909.084.

Erdogmus, E., T. Norton, C. M. Buckley, B. Petersen, and K. Kauzlarich. 2011. Seismic Investigation for the Temple of Antioch Reconstruction. Paper presented at Vulnerability, Uncertainty, and Risk: Analysis, Modeling, and Management. Hyattsville, MD, http://dx.doi.org/10.1061/41170(400)33.

Ghazali, M. Z., and J. R. Riddington. 1988. Simple Test Method for Masonry Shear Strength. *Proceedings of the Institution of Civil Engineers, Part 2*: 567-74.

Google Maps Engine Lite. 2013a. Ambraseys and Jackson Study. [cited 6/18 2013]. Available from https://mapsengine-google-com.leo.lib.unomaha.edu.

———. 2013b. Greece. [cited 6/18 2013]. Available from https://mapsengine-google-com.leo.lib.unomaha.edu.

———. 2013c. Turkey. [cited 6/18 2013]. Available from https://mapsengine-google-com.leo.lib.unomaha.edu.

Housner, George W. 1963. The Behavior of Inverted Pendulum Structures During Earthquakes. *Bulletin of the Seismological Society of America* 53 (2): 403-17.

Kappos, A. J., G. G. Penelis, and C. G. Drakopoulos. 2002. Evaluation of Simplified Models for Lateral Load Analysis of Unreinforced Masonry Buildings. *Journal of Structural Engineering* 128 (7): 890-7.

Kim, Jae Kwan, and Hyeuk Ryu. 2003. Seismic Test of a Full-scale Model of a Five-storey Stone Pagoda. *Earthquake Engineering & Structural Dynamics* 32 (5): 731-50, http://dx.doi.org.leo.lib.unomaha.edu/10.1002/eqe.246.

Konstantinidis, Dimitrios, and Nicos Makris. 2005. Seismic Response Analysis of Multidrum Classical Columns. *Earthquake Engineering & Structural Dynamics* 34 (10): 1243-70, http://dx.doi.org.leo.lib.unomaha.edu/10.1002/eqe.478.

Kourkoulis, S. K., E. Ganniari-Papageorgiou, and M. Mentzini. 2010. Dionysos Marble Beams Under Bending: A Contribution Towards Understanding the Fracture of the Parthenon Architraves. *Engineering Geology* 115 (3-4): 246, http://www.sciencedirect.com.leo.lib.unomaha.edu/science/article/pii/S0013795209001665.

Kourkoulis, Stavros K., and Evangelia Ganniari-Papageorgiou. 2010. Restoring Fragmented Marble Epistyles: Some Critical Points. *Journal of Cultural Heritage* 11 (4): 420, http://www.sciencedirect.com.leo.lib.unomaha.edu/science/article/pii/S1296207410000130.

Kourkoulis, S. K., and E. D. Pasiou. 2009. Epistyles Connected with "I" Connectors Under Pure Shear. *Journal of the Serbian Society for Computational Mechanics* 2 (2): 81-99.

Kourkoulis, Stavros K., and Ermioni D. Pasiou. 2013. Interconnected Epistyles of Marble Monuments Under Axial Loads. *International Journal of Architectural Heritage* 0 (ja):

nu, http://www.tandfonline.com.leo.lib.unomaha.edu/doi/abs/10.1080/15583058.2012.756079.

Krstevska, Lidija, Vladimir Mihailov, Enzo Boschi, and Antonio Rovelli. 1996. Experimental Dynamic Testing of Prototype and Model of the Antonina Column in Roma. Paper presented at Proceedings of the Eleventh World Conference on Earthquake Engineering, Acapulco, Mexico.

Krstevska, Lidija, Ljubomir Tashkov, Kiril Gramatikov, Raffaele Landolfo, Oreste Mammana, Francesco Portioli, and Federico Mazzolani. 2010. Large-scale Experimental Investigation on Mustafa Pasha Mosque. *Journal of Earthquake Engineering* 14 (6): 842-73, http://www.tandfonline.com.leo.lib.unomaha.edu/doi/abs/10.1080/13632460903338528.

Lawrence, A. W. 1996. *Greek Architecture*, ed. R. A. Tomlinson. 5th ed.Yale University Press.

Livadefs, C. J. 1956. The Structural Iron of the Parthenon. *Journal of the Iron and Steel Institute*(182): 49-66.

Mouzakis, H. P., I. N. Psycharis, D. Y. Papastamatiou, P. G. Carydis, C. Papantonopoulos, and C. Zambas. 2002. Experimental Investigation of the Earthquake Response of a Model of a Marble Classical Column. *Earthquake Engineering & Structural Dynamics* 31 (9): 1681-98.

Papantonopoulos, C., I. N. Psycharis, D. Y. Papastamatiou, J. V. Lemos, and H. P. Mouzakis. 2002. Numerical Prediction of the Earthquake Response of Classical Columns Using the Distinct Element Method. *Earthquake Engineering & Structural Dynamics* 31 (9): 1699-717.

Papantonopoulos, C. L. 1997. The Earthquake Resistance of Ancient Columns: A Numerical Perspective Developed at the Classical Temple of Apollo Epikourios. Paper presented at Structural Studies, Repairs and Maintenance of Historical Buildings, San Sebastian, Spain.

———. 1993. The Articulated Structural System: Studying the Earthquake Response of a Classical Temple. Paper presented at Structural Repair and Maintenance of Historical Buildings III, Bath, U.K.

Papastamatiou, D., and I. N. Psycharis. 1996. Numerical Simulation of the Seismic Response of Megalithic Monuments: Preliminary Investigations Related to the Apollo Temple at Vassai. In *Archaeoseismology.*, eds. S. Stiros, R. E. Jones, 225-236Institute of Geology and Mineral Exploration, The British School at Athens.

Papastamatiou, Dimitri, and Loannis Psycharis. 1993. Seismic Response of Classical Monuments-a Numerical Perspective Developed at the Temple of Apollo in Bassae, Greece. *Terra Nova* 5 (6): 591-601 (accessed 9/12/2012 4:41:17 PM).

Pavlovcic, L., F. Sinur, and D. Beg. 2009. Analysis of Architrave Connection. Paper presented at Protection of Historical Buildings, PROHITECH 09, Rome, Italy.

Pollio, Vitruvius, and M. H. Morgan. 1960. *The Ten Books on Architecture*. New York: Dover Publications.

Psycharis, I. N., J. V. Lemos, D. Y. Papastamatiou, C. Zambas, and C. Papantonopoulos. 2003. Numerical Study of the Seismic Behaviour of a Part of the Parthenon Pronaos. *Earthquake Engineering & Structural Dynamics* 32 (13): 2063-84.

Psycharis, I. N., D. Y. Papastamatiou, and A. P. Alexandris. 2000. Parametric Investigation of the Stability of Classical Columns Under Harmonic and Earthquake Excitations. *Earthquake Engineering & Structural Dynamics* 29 (8): 1093-109.

Psycharis, Ioannis N. 2007. A Probe into the Seismic History of Athens, Greece from the Current State of a Classical Monument. *Earthquake Spectra* 23 (2) (05/01; 2012/10): 393-415, http://dx.doi.org.leo.lib.unomaha.edu/10.1193/1.2722794.

Spawforth, Tony. 2006. *The Complete Greek Temples*. London: Thames and Hudson.

Stiros, Stathis C. 2001. The AD 365 Crete Earthquake and Possible Seismic Clustering During the Fourth to Sixth Centuries AD in the Eastern Mediterranean: A Review of Historical and Archaeological Data. *Journal of Stuctural Geology* 23 : 545-62.

Toumbakari, E. E. 2009. Analysis and Interpretation of the Structural Failures of the Orthostate in the Northern Wall of the Athens Parthenon. *Strain* 45 (5): 456-67, http://dx.doi.org.leo.lib.unomaha.edu/10.1111/j.1475-1305.2008.00529.x.

Turer, A., and T. Eroglu. 2006. Structural Analysis of Historic Temple of Augustus in Ankara, Turkey. New Delhi, India.

Turer, Ahmet, and Berk Boz. 2008. Computer Modeling and Seismic Performance Assessment of Historic Aspendos Theatre in Antalya, Turkey. *Engineering Structures* 30 (8): 2127-39.

Turkish Republic Disaster and Emergency Management Presedency, Earthquake Department. 2013. Earthquake Zoning Map of Turkey. [cited 6/27 2013]. Available from http://www.deprem.gov.tr/SarbisEng/Shared/DepremHaritalari.aspx.

United States Geological Survey. 2013. Earthquake Hazards Program. [cited 1/6 2014]. Available from http://earthquake.usgs.gov.

Zambas, C. 1992. Structural Repairs to the Monuments of the Acropolis-the Parthenon. *Proceedings of the ICE-Civil Engineering* 92 (4): 166-76.

APPENDIX A: MARBLE SAMPLE DENSITY MEASUREMENTS

Date	11/4/2013
Time	1:00 PM - 1:30PM
Tester	Cody Buckley

Specimen	Dimension 1			Dimension 2			Dimension 3			Weight (lb)	Density (lb/in^3)	Density (kg/cm^3)
	1 (in)	2 (in)	Avg	1 (in)	2 (in)	Avg	1 (in)	2 (in)	Avg			
A-1	2.103	2.135	2.119	2.066	2.098	2.082	2.080	2.097	2.089	0.8805	0.09556	0.002645
A-2	2.045	2.032	2.039	1.996	2.010	2.003	2.022	2.007	2.015	0.7865	0.09562	0.002647
A-3	2.003	2.036	2.020	2.051	2.051	2.051	2.007	2.022	2.015	0.7965	0.09546	0.002642
A-4	2.183	2.171	2.177	2.040	2.076	2.058	2.181	2.150	2.166	0.9265	0.09550	0.002643
Q-1	2.019	1.997	2.008	2.013	2.021	2.017	2.031	2.016	2.024	0.7870	0.09603	0.002658
Q-2	2.069	2.130	2.100	2.036	2.032	2.034	2.016	2.022	2.019	0.8260	0.09580	0.002652
Q-3	2.002	1.993	1.998	1.996	2.008	2.002	2.051	2.045	2.048	0.7775	0.09493	0.002628
Q-4	2.013	2.013	2.013	2.016	2.030	2.023	2.017	2.043	2.030	0.7830	0.09472	0.002622

Average Density (kg/cm3)	
Antioch Sample	0.00264
Quarry Sample	0.00264

APPENDIX B: COEFFICIENT OF STATIC FRICTION MEASUREMENTS

Date	10/29/2013
Time	3:00 PM - 4:30PM
Tester	Cody Buckley
Notes	Grain orientation is measured relative to apparatus
	θ_1 is angle at first slide, θ_F is angle at sliding failure
	The term "hiccup" refers to a slight movement

Specimen		*Grain Orientation*		*Measurements*			$\mu_1 = \tan(\theta_1 - \theta_1)$	*Behavioral Observations*
Bottom	*Top*	*Bottom*	*Top*	θ_1	θ_1	θ_F		
Q-1	Q-2	Par	Perp	0.05	32.0		0.62	Smooth and quick
Q-1	Q-3	Par	Par	0.05	33.0	35.0	0.65	Hiccup twice at 33, then failure
Q-1	Q-4	Par	Par	0.05	29.0	32.5	0.55	Hiccup, then quick
Q-2	Q-1	Perp	Par	0.05	29.0		0.55	Smooth and quick
Q-2	Q-3	Perp	Par	0.05	30.5	35.0	0.59	Several hiccups, slid off in a torsional manner
Q-2	Q-4	Perp	Par	0.05	24.0	27.5	0.44	Hiccup, then go
Q-3	Q-1	Par	Par	0.05	27.5		0.52	Smooth and quick
Q-3	Q-2	Par	Perp	0.05	27.5	30.5	0.52	Several hiccups before going
Q-3	Q-4	Par	Par	0.05	27.5	29.5	0.52	Slow continual slide
Q-4	Q-1	Par	Par	0.05	25.5		0.48	Quick
Q-4	Q-2	Par	Perp	0.05	26.0		0.49	Slower continual
Q-4	Q-3	Par	Par	0.05	25.5	27.0	0.48	One hiccup
A-1	A-2	Perp	Par	0.05	32.5	35.5	0.64	Several hiccups, torsional slide
A-1	A-3	Perp	Par	0.05	29.0	34.0	0.55	Several false starts, more of a tip over
A-1	A-4	Perp	Par	0.05	33.5		0.66	Pretty smooth
A-2	A-1	Perp	Perp	0.05	29.5		0.56	Brief hiccup
A-2	A-3	Perp	Par	0.05	29.0	30.0	0.55	Slow continual slide
A-2	A-4	Perp	Perp	0.05	24.0	26.5	0.44	Hiccup followed by torsional slide off
A-3	A-1	Perp	Perp	0.05	29.5	31.5	0.56	Hiccups
A-3	A-2	Perp	Par	0.05	29.0	33.5	0.55	One hiccup
A-3	A-4	Perp	Par	0.05	22.5		0.41	Almost no slide
A-4	A-1	Par	Perp	0.05	28.5		0.54	Smooth quick
A-4	A-2	Par	Par	0.05	29.5		0.56	One hiccup
A-4	A-3	Par	Par	0.05	21.5	33.0	0.39	One hiccup

$(\mu_1)_{Quarry}$	
Average	**0.53**
Range	**0.44-0.65**

$(\mu_1)_{Antioch}$	
Average	**0.54**
Range	**0.39-0.66**

APPENDIX C: EQUIVALENT LATERAL FORCE PROCEDURE CALCULATIONS

Column	Cs	W (kips)	Node	h_x (ft)	w_x (kips)	k	$w_x h_x^k$	$Cvx = w_x h_x^k / \Sigma w_i h_i^k$	$Fx = Cvx*V$ (kip)	M_z (k-ft)
C8	1.63	5.282	1	0.00	0.313	1.00	0.000	0.000	0.000	0.000
			2	12.00	0.339	1.00	4.068	0.113	0.970	11.636
			3	0.75	0.459	1.00	0.344	0.010	0.082	0.061
			4	9.75	0.485	1.00	4.725	0.131	1.126	10.982
			5	10.50	0.678	1.00	7.119	0.197	1.697	17.817
			6	11.25	0.678	1.00	7.627	0.211	1.818	20.454
			7	1.75	0.291	1.00	0.510	0.014	0.122	0.213
			8	2.75	0.291	1.00	0.801	0.022	0.191	0.525
			9	3.75	0.291	1.00	1.092	0.030	0.260	0.977
			10	4.75	0.291	1.00	1.384	0.038	0.330	1.567
			11	5.75	0.291	1.00	1.675	0.046	0.399	2.296
			12	6.75	0.291	1.00	1.966	0.054	0.469	3.164
			13	7.75	0.291	1.00	2.258	0.063	0.538	4.171
			14	8.75	0.291	1.00	2.549	0.071	0.608	5.317
					5.282		36.118		8.610	79.180
C8.5	1.63	5.500	1	0.00	0.313	1.00	0.000	0.000	0.000	0.000
			2	12.75	0.339	1.00	4.322	0.108	0.972	12.396
			3	0.75	0.455	1.00	0.341	0.009	0.077	0.058
			4	10.50	0.481	1.00	5.050	0.127	1.136	11.929
			5	11.25	0.678	1.00	7.627	0.191	1.716	19.301
			6	12.00	0.678	1.00	8.136	0.204	1.830	21.960
			7	1.73	0.284	1.00	0.490	0.012	0.110	0.190
			8	2.70	0.284	1.00	0.767	0.019	0.173	0.466
			9	3.68	0.284	1.00	1.044	0.026	0.235	0.863
			10	4.65	0.284	1.00	1.321	0.033	0.297	1.381
			11	5.63	0.284	1.00	1.598	0.040	0.359	2.022
			12	6.60	0.284	1.00	1.875	0.047	0.422	2.783
			13	7.58	0.284	1.00	2.152	0.054	0.484	3.666
			14	8.55	0.284	1.00	2.428	0.061	0.546	4.671
			15	9.53	0.284	1.00	2.705	0.068	0.609	5.797
					5.500		39.855		8.965	87.482
C9	1.63	5.719	1	0.00	0.313	1.00	0.000	0.000	0.000	0.000
			2	13.50	0.339	1.00	4.576	0.105	0.975	13.161
			3	0.75	0.452	1.00	0.339	0.008	0.072	0.054
			4	11.25	0.478	1.00	5.378	0.123	1.146	12.888
			5	12.00	0.678	1.00	8.136	0.186	1.733	20.797
			6	12.75	0.678	1.00	8.644	0.198	1.841	23.478
			7	10.30	0.278	1.00	2.863	0.065	0.610	6.279
			8	9.34	0.278	1.00	2.597	0.059	0.553	5.169
			9	8.39	0.278	1.00	2.332	0.053	0.497	4.166
			10	7.43	0.278	1.00	2.067	0.047	0.440	3.272
			11	6.48	0.278	1.00	1.801	0.041	0.384	2.485

			12	5.52	0.278	1.00	1.536	0.035	0.327	1.807
			13	4.57	0.278	1.00	1.270	0.029	0.271	1.236
			14	3.61	0.278	1.00	1.005	0.023	0.214	0.774
			15	2.66	0.278	1.00	0.739	0.017	0.158	0.419
			16	1.70	0.278	1.00	0.474	0.011	0.101	0.172
					5.719		43.757		9.321	96.155
C9.5	1.63	5.937	1	0.00	0.313	1.00	0.000	0.000	0.000	0.000
			2	14.25	0.339	1.00	4.830	0.101	0.978	13.930
			3	0.75	0.450	1.00	0.337	0.007	0.068	0.051
			4	12.00	0.476	1.00	5.706	0.119	1.155	13.857
			5	12.75	0.678	1.00	8.644	0.181	1.749	22.303
			6	13.50	0.678	1.00	9.152	0.191	1.852	25.004
			7	1.69	0.273	1.00	0.461	0.010	0.093	0.157
			8	2.63	0.273	1.00	0.717	0.015	0.145	0.381
			9	3.56	0.273	1.00	0.973	0.020	0.197	0.701
			10	4.50	0.273	1.00	1.229	0.026	0.249	1.119
			11	5.44	0.273	1.00	1.485	0.031	0.301	1.634
			12	6.38	0.273	1.00	1.741	0.036	0.352	2.246
			13	7.31	0.273	1.00	1.997	0.042	0.404	2.955
			14	8.25	0.273	1.00	2.253	0.047	0.456	3.762
			15	9.19	0.273	1.00	2.509	0.052	0.508	4.665
			16	10.13	0.273	1.00	2.765	0.058	0.560	5.666
			17	11.06	0.273	1.00	3.021	0.063	0.611	6.764
					5.937		47.822		9.677	105.195
C10	1.63	6.156	1	0.00	0.313	1.00	0.000	0.000	0.000	0.000
			2	15.00	0.339	1.00	5.085	0.098	0.980	14.702
			3	0.75	0.459	1.00	0.344	0.007	0.066	0.050
			4	12.75	0.485	1.00	6.179	0.119	1.191	15.187
			5	13.50	0.678	1.00	9.152	0.176	1.764	23.817
			6	14.25	0.678	1.00	9.661	0.186	1.862	26.537
			7	11.75	0.291	1.00	3.423	0.066	0.660	7.753
			8	10.75	0.291	1.00	3.132	0.060	0.604	6.489
			9	9.75	0.291	1.00	2.840	0.055	0.548	5.338
			10	8.75	0.291	1.00	2.549	0.049	0.491	4.299
			11	7.75	0.291	1.00	2.258	0.043	0.435	3.373
			12	6.75	0.291	1.00	1.966	0.038	0.379	2.559
			13	5.75	0.291	1.00	1.675	0.032	0.323	1.857
			14	4.75	0.291	1.00	1.384	0.027	0.267	1.267
			15	3.75	0.291	1.00	1.092	0.021	0.211	0.790
			16	2.75	0.291	1.00	0.801	0.015	0.154	0.425
			17	1.75	0.291	1.00	0.510	0.010	0.098	0.172
					6.156		52.051		10.034	114.615
I8	1.63	4.000	1	0.00	0.313	1.00	0.000	0.000	0.000	0.000

			2	12.00	0.164	1.00	1.964		0.088	0.575	6.906
			3	0.75	0.451	1.00	0.339		0.015	0.099	0.074
			4	11.21	0.302	1.00	3.386		0.152	0.992	11.122
			5	1.70	0.277	1.00	0.471		0.021	0.138	0.235
			6	2.65	0.277	1.00	0.734		0.033	0.215	0.571
			7	3.60	0.277	1.00	0.998		0.045	0.292	1.053
			8	4.55	0.277	1.00	1.261		0.057	0.370	1.682
			9	5.50	0.277	1.00	1.524		0.069	0.447	2.458
			10	6.45	0.277	1.00	1.788		0.080	0.524	3.381
			11	7.41	0.277	1.00	2.051		0.092	0.601	4.451
			12	8.36	0.277	1.00	2.314		0.104	0.678	5.667
			13	9.31	0.277	1.00	2.578		0.116	0.755	7.030
			14	10.26	0.277	1.00	2.841		0.128	0.832	8.539
					4.000		22.248			6.520	53.169
I8.5	1.63	4.218	1	0.00	0.313	1.00	0.000		0.000	0.000	0.000
			2	12.75	0.164	1.00	2.087		0.083	0.573	7.310
			3	0.75	0.449	1.00	0.337		0.013	0.093	0.069
			4	11.96	0.300	1.00	3.584		0.143	0.985	11.775
			5	1.68	0.272	1.00	0.458		0.018	0.126	0.212
			6	2.62	0.272	1.00	0.712		0.028	0.196	0.512
			7	3.55	0.272	1.00	0.966		0.039	0.266	0.943
			8	4.49	0.272	1.00	1.221		0.049	0.335	1.504
			9	5.42	0.272	1.00	1.475		0.059	0.405	2.196
			10	6.35	0.272	1.00	1.729		0.069	0.475	3.018
			11	7.29	0.272	1.00	1.983		0.079	0.545	3.971
			12	8.22	0.272	1.00	2.237		0.089	0.615	5.054
			13	9.16	0.272	1.00	2.491		0.100	0.685	6.267
			14	10.09	0.272	1.00	2.745		0.110	0.754	7.611
			15	11.02	0.272	1.00	3.000		0.120	0.824	9.085
					4.218		25.025			6.876	59.530
I9	1.63	4.437	1	0.00	0.313	1.00	0.000		0.000	0.000	0.000
			2	13.50	0.164	1.00	2.209		0.079	0.571	7.713
			3	0.75	0.458	1.00	0.344		0.012	0.089	0.067
			4	12.71	0.309	1.00	3.924		0.140	1.015	12.897
			5	1.75	0.290	1.00	0.507		0.018	0.131	0.229
			6	2.74	0.290	1.00	0.796		0.028	0.206	0.565
			7	3.74	0.290	1.00	1.086		0.039	0.281	1.050
			8	4.74	0.290	1.00	1.375		0.049	0.356	1.684
			9	5.73	0.290	1.00	1.664		0.060	0.430	2.467
			10	6.73	0.290	1.00	1.953		0.070	0.505	3.399
			11	7.73	0.290	1.00	2.243		0.080	0.580	4.481
			12	8.72	0.290	1.00	2.532		0.091	0.655	5.711
			13	9.72	0.290	1.00	2.821		0.101	0.730	7.091
			14	10.72	0.290	1.00	3.111		0.111	0.804	8.619

			15	11.71	0.290	1.00	3.400	0.122	0.879	10.297
					4.437		27.965		7.232	66.270
I9.5	1.63	4.655	1	0.00	0.313	1.00	0.000	0.000	0.000	0.000
			2	14.25	0.164	1.00	2.332	0.075	0.570	8.117
			3	0.75	0.455	1.00	0.342	0.011	0.083	0.063
			4	13.46	0.306	1.00	4.119	0.133	1.006	13.538
			5	1.73	0.285	1.00	0.492	0.016	0.120	0.208
			6	2.71	0.285	1.00	0.770	0.025	0.188	0.509
			7	3.68	0.285	1.00	1.049	0.034	0.256	0.943
			8	4.66	0.285	1.00	1.327	0.043	0.324	1.510
			9	5.64	0.285	1.00	1.605	0.052	0.392	2.211
			10	6.62	0.285	1.00	1.884	0.061	0.460	3.044
			11	7.59	0.285	1.00	2.162	0.070	0.528	4.010
			12	8.57	0.285	1.00	2.441	0.079	0.596	5.109
			13	9.55	0.285	1.00	2.719	0.088	0.664	6.340
			14	10.53	0.285	1.00	2.997	0.096	0.732	7.705
			15	11.50	0.285	1.00	3.276	0.105	0.800	9.203
			16	12.48	0.285	1.00	3.554	0.114	0.868	10.834
					4.655		31.069		7.588	73.342
I10	1.63	4.874	1	0.00	0.313	1.00	0.000	0.000	0.000	0.000
			2	15.00	0.164	1.00	2.455	0.071	0.568	8.519
			3	0.75	0.453	1.00	0.340	0.010	0.079	0.059
			4	14.21	0.304	1.00	4.315	0.126	0.998	14.183
			5	1.71	0.280	1.00	0.479	0.014	0.111	0.190
			6	2.67	0.280	1.00	0.748	0.022	0.173	0.463
			7	3.63	0.280	1.00	1.018	0.030	0.235	0.856
			8	4.60	0.280	1.00	1.287	0.037	0.298	1.368
			9	5.56	0.280	1.00	1.556	0.045	0.360	2.000
			10	6.52	0.280	1.00	1.825	0.053	0.422	2.752
			11	7.48	0.280	1.00	2.094	0.061	0.485	3.624
			12	8.44	0.280	1.00	2.364	0.069	0.547	4.616
			13	9.40	0.280	1.00	2.633	0.077	0.609	5.727
			14	10.36	0.280	1.00	2.902	0.085	0.671	6.958
			15	11.32	0.280	1.00	3.171	0.092	0.734	8.309
			16	12.29	0.280	1.00	3.440	0.100	0.796	9.779
			17	13.25	0.280	1.00	3.710	0.108	0.858	11.369
					4.874		34.337		7.944	80.772
D6	1.63	2.730	1	0.00	0.134	1.00	0.000	0.000	0.000	0.000
			2	9.00	0.163	1.00	1.469	0.115	0.514	4.622
			4	8.25	0.297	1.00	2.448	0.192	0.856	7.060
			5	0.92	0.267	1.00	0.245	0.019	0.086	0.078
			6	1.83	0.267	1.00	0.490	0.038	0.171	0.314
			7	2.75	0.267	1.00	0.734	0.058	0.257	0.706

			8	3.67	0.267	1.00	0.979	0.077	0.342	1.255
			9	4.58	0.267	1.00	1.224	0.096	0.428	1.961
			10	5.50	0.267	1.00	1.469	0.115	0.513	2.824
			11	6.42	0.267	1.00	1.714	0.135	0.599	3.843
			12	7.33	0.267	1.00	1.958	0.154	0.685	5.020
					2.730		12.730		4.450	27.683
D6.5	1.63	2.948	1	0.00	0.146	1.00	0.000	0.000	0.000	0.000
			2	9.75	0.163	1.00	1.592	0.107	0.515	5.019
			4	9.00	0.309	1.00	2.780	0.187	0.899	8.092
			5	1.00	0.291	1.00	0.291	0.020	0.094	0.094
			6	2.00	0.291	1.00	0.583	0.039	0.188	0.377
			7	3.00	0.291	1.00	0.874	0.059	0.283	0.848
			8	4.00	0.291	1.00	1.165	0.078	0.377	1.507
			9	5.00	0.291	1.00	1.457	0.098	0.471	2.355
			10	6.00	0.291	1.00	1.748	0.118	0.565	3.392
			11	7.00	0.291	1.00	2.039	0.137	0.660	4.617
			12	8.00	0.291	1.00	2.331	0.157	0.754	6.030
					2.948		14.859		4.806	32.332
D7	1.63	3.167	1	0.00	0.142	1.00	0.000	0.000	0.000	0.000
			2	10.50	0.163	1.00	1.714	0.100	0.516	5.416
			4	9.75	0.305	1.00	2.976	0.174	0.896	8.733
			5	0.98	0.284	1.00	0.277	0.016	0.083	0.081
			6	1.95	0.284	1.00	0.554	0.032	0.167	0.325
			7	2.93	0.284	1.00	0.831	0.048	0.250	0.731
			8	3.90	0.284	1.00	1.108	0.065	0.333	1.300
			9	4.88	0.284	1.00	1.385	0.081	0.417	2.031
			10	5.85	0.284	1.00	1.662	0.097	0.500	2.925
			11	6.83	0.284	1.00	1.939	0.113	0.583	3.982
			12	7.80	0.284	1.00	2.215	0.129	0.667	5.201
			13	8.78	0.284	1.00	2.492	0.145	0.750	6.582
					3.167		17.152		5.162	37.308
D7.5	1.63	3.385	1	0.00	0.139	1.00	0.000	0.000	0.000	0.000
			2	11.25	0.163	1.00	1.836	0.094	0.517	5.814
			4	10.50	0.302	1.00	3.174	0.162	0.893	9.378
			5	0.95	0.278	1.00	0.265	0.014	0.075	0.071
			6	1.91	0.278	1.00	0.531	0.027	0.149	0.285
			7	2.86	0.278	1.00	0.796	0.041	0.224	0.642
			8	3.82	0.278	1.00	1.062	0.054	0.299	1.141
			9	4.77	0.278	1.00	1.327	0.068	0.373	1.782
			10	5.73	0.278	1.00	1.593	0.081	0.448	2.567
			11	6.68	0.278	1.00	1.858	0.095	0.523	3.494
			12	7.64	0.278	1.00	2.123	0.108	0.598	4.563
			13	8.59	0.278	1.00	2.389	0.122	0.672	5.775

			14	9.55	0.278	1.00	2.654	0.135	0.747	7.130
					3.385		19.609		5.518	42.641
D8	1.63	3.604	1	0.00	0.137	1.00	0.000	0.000	0.000	0.000
			2	12.00	0.163	1.00	1.959	0.088	0.518	6.211
			4	11.25	0.300	1.00	3.373	0.152	0.891	10.026
			5	0.94	0.273	1.00	0.256	0.012	0.068	0.063
			6	1.88	0.273	1.00	0.512	0.023	0.135	0.254
			7	2.81	0.273	1.00	0.768	0.035	0.203	0.571
			8	3.75	0.273	1.00	1.024	0.046	0.271	1.015
			9	4.69	0.273	1.00	1.280	0.058	0.338	1.586
			10	5.63	0.273	1.00	1.536	0.069	0.406	2.283
			11	6.56	0.273	1.00	1.792	0.081	0.474	3.108
			12	7.50	0.273	1.00	2.048	0.092	0.541	4.059
			13	8.44	0.273	1.00	2.304	0.104	0.609	5.138
			14	9.38	0.273	1.00	2.560	0.115	0.677	6.343
			15	10.31	0.273	1.00	2.816	0.127	0.744	7.675
					3.604		22.230		5.874	48.332

Node	Cs	W (kips)	h_x (ft)	w_x (kips)	k	$w_x h_x^k$	$Cvx = w_x h_x^k / \Sigma w_i h_i^k$	Fx = Cvx*V (kip)	M_Z (k-ft)
1	0.82	67.310	0.00	0.331	1.00	0.000	0.000	0.000	0.000
2			21.92	0.746	1.00	16.351	0.018	0.976	21.388
4			20.04	0.549	1.00	11.002	0.012	0.657	13.160
5			1.38	0.573	1.00	0.787	0.001	0.047	0.065
6			0.00	0.331	1.00	0.000	0.000	0.000	0.000
7			21.92	1.185	1.00	25.968	0.028	1.550	33.968
8			20.04	0.549	1.00	11.002	0.012	0.657	13.160
9			1.38	0.573	1.00	0.787	0.001	0.047	0.065
10			0.00	0.331	1.00	0.000	0.000	0.000	0.000
11			21.92	1.185	1.00	25.968	0.028	1.550	33.968
12			20.04	0.549	1.00	11.002	0.012	0.657	13.160
13			1.38	0.573	1.00	0.787	0.001	0.047	0.065
14			0.00	0.331	1.00	0.000	0.000	0.000	0.000
15			21.92	0.746	1.00	16.351	0.018	0.976	21.388
16			20.04	0.549	1.00	11.002	0.012	0.657	13.160
17			1.38	0.573	1.00	0.787	0.001	0.047	0.065
18			0.69	0.662	1.00	0.455	0.000	0.027	0.019
19			0.69	0.662	1.00	0.455	0.000	0.027	0.019
20			0.69	0.662	1.00	0.455	0.000	0.027	0.019
21			0.69	0.662	1.00	0.455	0.000	0.027	0.019
22			20.98	0.614	1.00	12.892	0.014	0.769	16.142
23			20.98	0.614	1.00	12.892	0.014	0.769	16.142
24			20.98	0.614	1.00	12.892	0.014	0.769	16.142
25			20.98	0.614	1.00	12.892	0.014	0.769	16.142
26			2.31	0.483	1.00	1.116	0.001	0.067	0.154
27			3.24	0.483	1.00	1.567	0.002	0.094	0.303
28			4.18	0.483	1.00	2.018	0.002	0.120	0.503
29			5.11	0.483	1.00	2.469	0.003	0.147	0.753
30			6.04	0.483	1.00	2.920	0.003	0.174	1.053
31			6.98	0.483	1.00	3.372	0.004	0.201	1.404
32			7.91	0.483	1.00	3.823	0.004	0.228	1.804
33			8.84	0.483	1.00	4.274	0.005	0.255	2.255
34			9.78	0.483	1.00	4.725	0.005	0.282	2.757
35			10.71	0.483	1.00	5.176	0.006	0.309	3.308
36			11.64	0.483	1.00	5.627	0.006	0.336	3.910
37			12.58	0.483	1.00	6.079	0.007	0.363	4.562
38			13.51	0.483	1.00	6.530	0.007	0.390	5.265
39			14.44	0.483	1.00	6.981	0.008	0.417	6.017
40			15.38	0.483	1.00	7.432	0.008	0.444	6.820
41			16.31	0.483	1.00	7.883	0.009	0.470	7.673
42			17.24	0.483	1.00	8.334	0.009	0.497	8.577
43			18.18	0.483	1.00	8.786	0.010	0.524	9.530
44			19.11	0.483	1.00	9.237	0.010	0.551	10.534
45			2.31	0.483	1.00	1.116	0.001	0.067	0.154

46	3.24	0.483	1.00	1.567	0.002	0.094	0.303
47	4.18	0.483	1.00	2.018	0.002	0.120	0.503
48	5.11	0.483	1.00	2.469	0.003	0.147	0.753
49	6.04	0.483	1.00	2.920	0.003	0.174	1.053
50	6.98	0.483	1.00	3.372	0.004	0.201	1.404
51	7.91	0.483	1.00	3.823	0.004	0.228	1.804
52	8.84	0.483	1.00	4.274	0.005	0.255	2.255
53	9.78	0.483	1.00	4.725	0.005	0.282	2.757
54	10.71	0.483	1.00	5.176	0.006	0.309	3.308
55	11.64	0.483	1.00	5.627	0.006	0.336	3.910
56	12.58	0.483	1.00	6.079	0.007	0.363	4.562
57	13.51	0.483	1.00	6.530	0.007	0.390	5.265
58	14.44	0.483	1.00	6.981	0.008	0.417	6.017
59	15.38	0.483	1.00	7.432	0.008	0.444	6.820
60	16.31	0.483	1.00	7.883	0.009	0.470	7.673
61	17.24	0.483	1.00	8.334	0.009	0.497	8.577
62	18.18	0.483	1.00	8.786	0.010	0.524	9.530
63	19.11	0.483	1.00	9.237	0.010	0.551	10.534
64	2.31	0.483	1.00	1.116	0.001	0.067	0.154
65	3.24	0.483	1.00	1.567	0.002	0.094	0.303
66	4.18	0.483	1.00	2.018	0.002	0.120	0.503
67	5.11	0.483	1.00	2.469	0.003	0.147	0.753
68	6.04	0.483	1.00	2.920	0.003	0.174	1.053
69	6.98	0.483	1.00	3.372	0.004	0.201	1.404
70	7.91	0.483	1.00	3.823	0.004	0.228	1.804
71	8.84	0.483	1.00	4.274	0.005	0.255	2.255
72	9.78	0.483	1.00	4.725	0.005	0.282	2.757
73	10.71	0.483	1.00	5.176	0.006	0.309	3.308
74	11.64	0.483	1.00	5.627	0.006	0.336	3.910
75	12.58	0.483	1.00	6.079	0.007	0.363	4.562
76	13.51	0.483	1.00	6.530	0.007	0.390	5.265
77	14.44	0.483	1.00	6.981	0.008	0.417	6.017
78	15.38	0.483	1.00	7.432	0.008	0.444	6.820
79	16.31	0.483	1.00	7.883	0.009	0.470	7.673
80	17.24	0.483	1.00	8.334	0.009	0.497	8.577
81	18.18	0.483	1.00	8.786	0.010	0.524	9.530
82	19.11	0.483	1.00	9.237	0.010	0.551	10.534
83	2.31	0.483	1.00	1.116	0.001	0.067	0.154
84	3.24	0.483	1.00	1.567	0.002	0.094	0.303
85	4.18	0.483	1.00	2.018	0.002	0.120	0.503
86	5.11	0.483	1.00	2.469	0.003	0.147	0.753
87	6.04	0.483	1.00	2.920	0.003	0.174	1.053
88	6.98	0.483	1.00	3.372	0.004	0.201	1.404
89	7.91	0.483	1.00	3.823	0.004	0.228	1.804
90	8.84	0.483	1.00	4.274	0.005	0.255	2.255
91	9.78	0.483	1.00	4.725	0.005	0.282	2.757
92	10.71	0.483	1.00	5.176	0.006	0.309	3.308

93	11.64	0.483	1.00	5.627	0.006	0.336	3.910
94	12.58	0.483	1.00	6.079	0.007	0.363	4.562
95	13.51	0.483	1.00	6.530	0.007	0.390	5.265
96	14.44	0.483	1.00	6.981	0.008	0.417	6.017
97	15.38	0.483	1.00	7.432	0.008	0.444	6.820
98	16.31	0.483	1.00	7.883	0.009	0.470	7.673
99	17.24	0.483	1.00	8.334	0.009	0.497	8.577
100	18.18	0.483	1.00	8.786	0.010	0.524	9.530
101	19.11	0.483	1.00	9.237	0.010	0.551	10.534
109	21.92	0.878	1.00	19.234	0.021	1.148	25.159
110	21.92	0.878	1.00	19.234	0.021	1.148	25.159
111	21.92	0.878	1.00	19.234	0.021	1.148	25.159
112	21.92	0.878	1.00	19.234	0.021	1.148	25.159
113	21.92	0.878	1.00	19.234	0.021	1.148	25.159
114	21.92	0.878	1.00	19.234	0.021	1.148	25.159
115	21.92	0.878	1.00	19.234	0.021	1.148	25.159
116	21.92	0.878	1.00	19.234	0.021	1.148	25.159
117	21.92	0.878	1.00	19.234	0.021	1.148	25.159
118	21.92	0.878	1.00	19.234	0.021	1.148	25.159
119	21.92	0.878	1.00	19.234	0.021	1.148	25.159
120	21.92	0.878	1.00	19.234	0.021	1.148	25.159
121	21.92	0.878	1.00	19.234	0.021	1.148	25.159
122	21.92	0.878	1.00	19.234	0.021	1.148	25.159
123	21.92	0.878	1.00	19.234	0.021	1.148	25.159
124	21.92	0.878	1.00	19.234	0.021	1.148	25.159
125	21.92	0.878	1.00	19.234	0.021	1.148	25.159
126	21.92	0.878	1.00	19.234	0.021	1.148	25.159
		67.310		924.781		55.194	989.849

APPENDIX D: TEMPLE OF *ANTIOCH AD CRAGUM*

ENGINEERING DRAWINGS

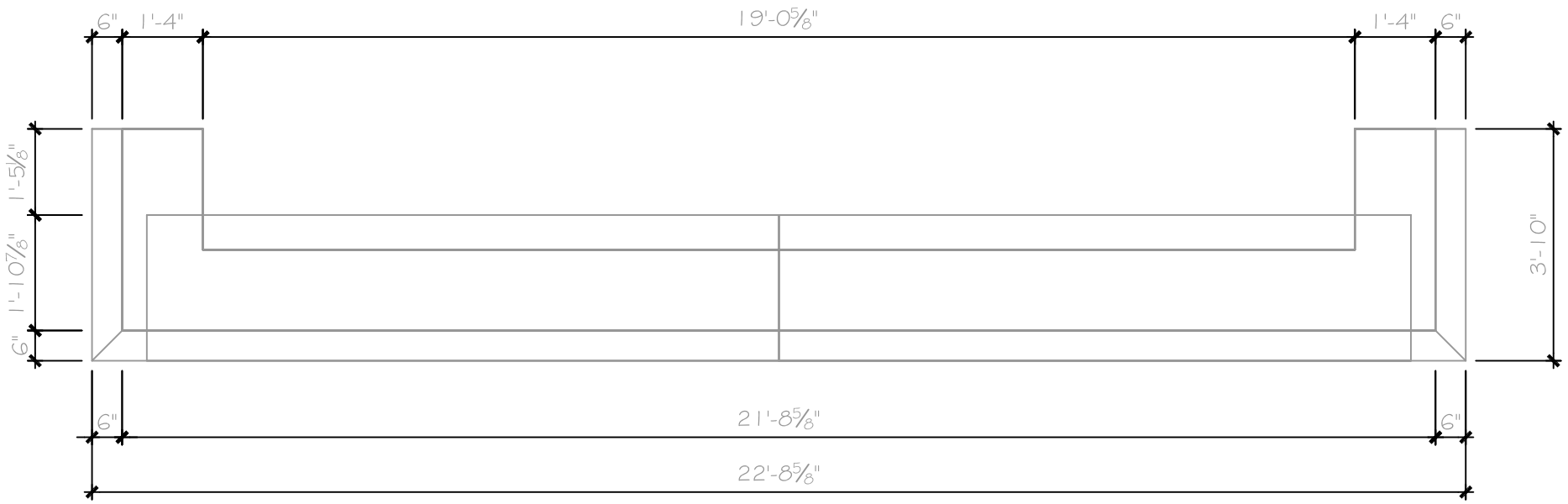

ELEV. B

ELEV. A

ISOMETRIC

SCALE: NTS

PLAN

SCALE: 3/8" = 1'-0"

Ece Erdogmus, Ph.D., P.E.
Associate Professor
Architectural Engineering
205A Peter Kiewit Institute
1110 S. 67th St.
Omaha, NE 68182-0816

TEMPLE OF ANTIOCH PARTIAL RECONSTRUCTION

GÜNEY VILLAGE, TURKEY

Date: 03/16/15
Drawn By: CMB
Sheet: 1 of 2

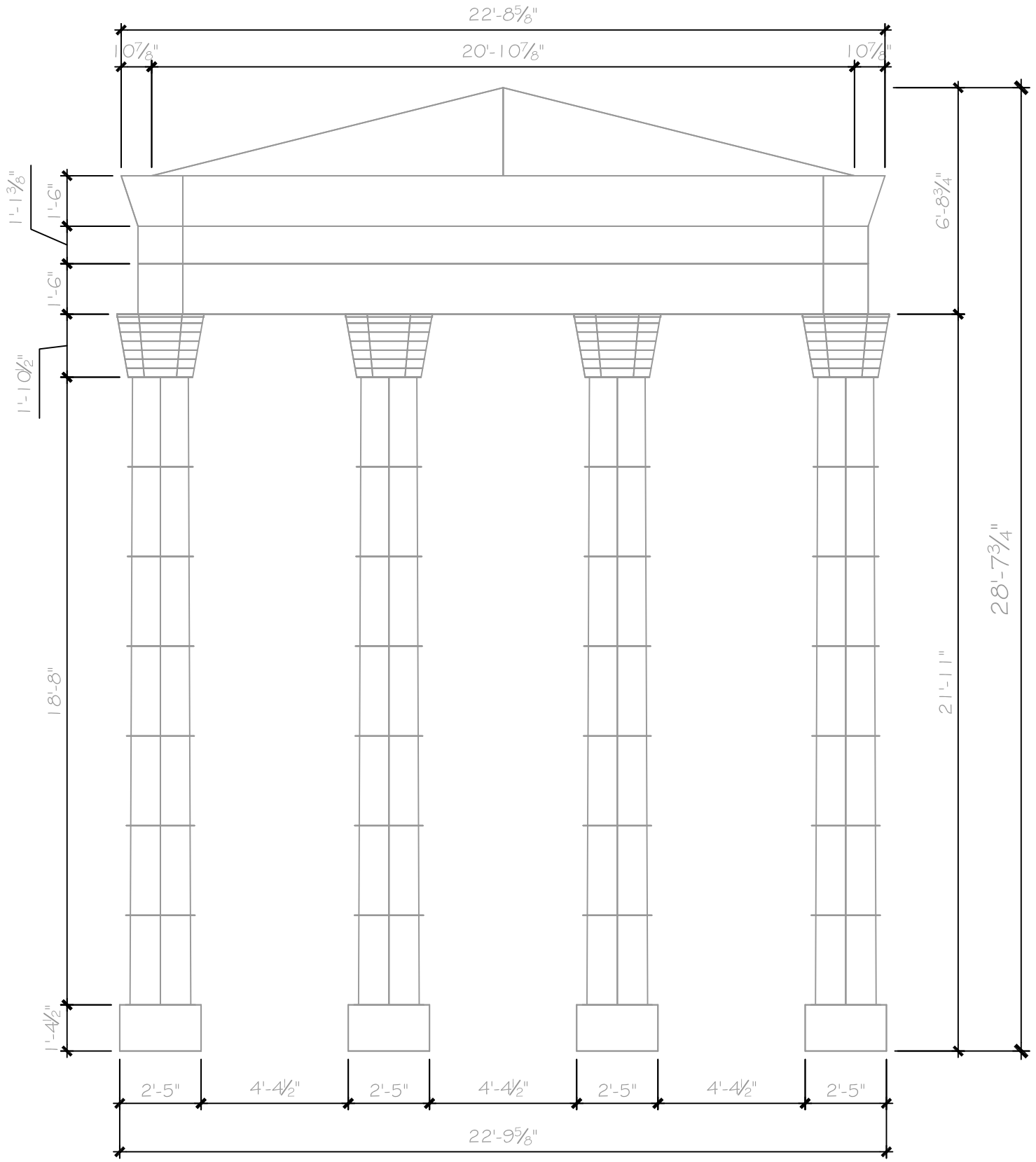

ELEVATION A

SCALE: ¼" = 1'-0"

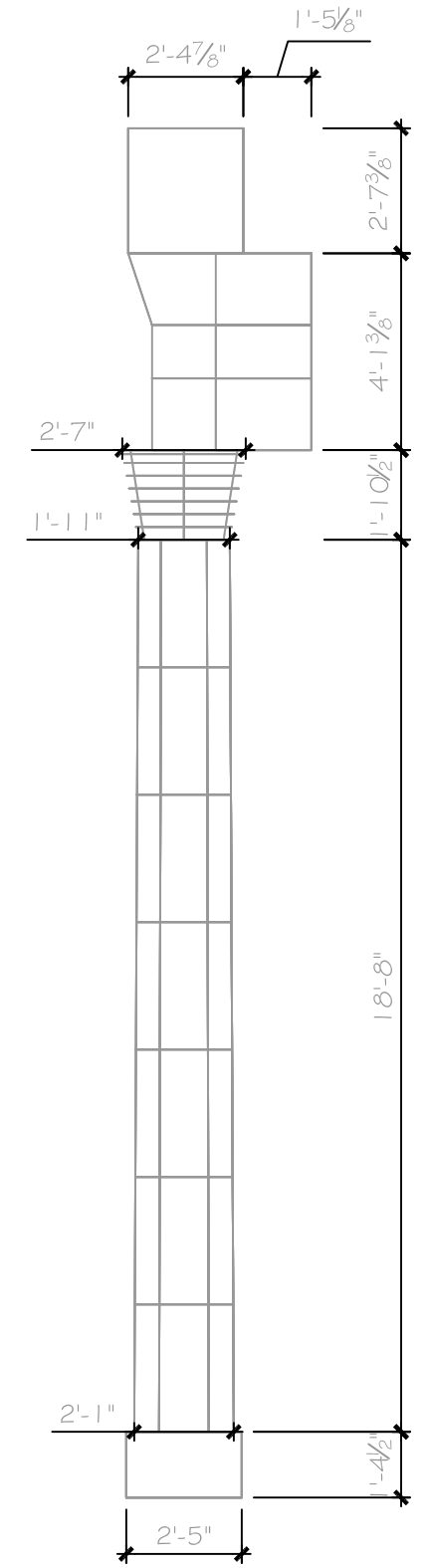

ELEVATION B

SCALE: ¼" = 1'-0"

Ece Erdogmus, Ph.D., P.E.
Associate Professor
Architectural Engineering
205A Peter Kiewit Institute
1110 S. 67th St.
Omaha, NE 68182-0816

TEMPLE OF ANTIOCH PARTIAL RECONSTRUCTION

GÜNEY VILLAGE, TURKEY

Date: 03/16/15
Drawn By: CMB
Sheet: 2 of 2

InfraStructure, LLC
ENGINEERING CONSULTING GROUP

COMPUTED BY CMB	DATE	SHEET 1 OF 4
CHECKED BY	DATE	PROJ. NO.
PROJECT		
SUBJECT Structural Analysis Review		

Derivation of Appendix I in Chopra (stiffness coefficients)

– review of slope-deflection
- relates unknown slopes & deflections to applied loads on structure
- moments & angular displacements are positive when acting clockwise on the span
- linear displacements are positive when they cause cord of span & cord angle (ψ) to rotate clockwise
- slope deflection equations can be obtained by using the principle of superposition by considering seperately the moments developed at each support due to each of the displacements θ_A, θ_B, & Δ & then the loads

- Angular displacement @ A, θ_A

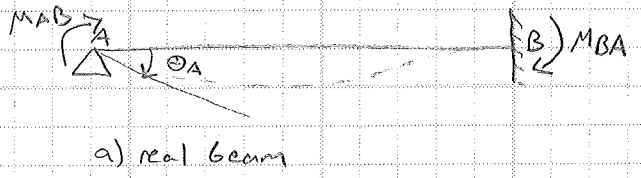

a) real beam

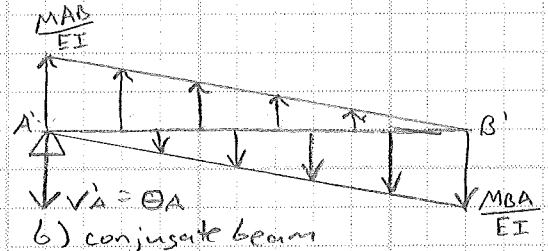

b) conjugate beam

* moment diagram determined by superposition

– deflection of real beam is zero @ A & B, so corresponding sum of moments at each end of conjugate beam must also be zero, so

$\Sigma M_{A'} = 0$

$$\left(\frac{1}{2}\right)\left(\frac{M_{AB}}{EI}\right)(L)\left(\frac{1}{3}\right)(L) - \left(\frac{1}{2}\right)\left(\frac{M_{BA}}{EI}\right)(L)\left(\frac{2}{3}\right)(L) = 0$$

$$\left(\frac{L^2}{6EI}\right) M_{AB} = M_{BA}\left(\frac{L^2}{3EI}\right)$$

$$M_{AB} = 2M_{BA}$$

$$\boxed{M_{AB} = \left[\frac{4EI}{L}\right]\theta_A}$$

$\Sigma M_{B'} = 0$

$$-\left(\frac{1}{2}\right)\left(\frac{M_{AB}}{EI}\right)(L)\left(\frac{2}{3}\right)(L) + \left(\frac{1}{2}\right)\left(\frac{M_{BA}}{EI}\right)(L)\left(\frac{1}{3}\right)L + V'_A(L) = 0$$

$$\left(\frac{L^2}{3EI}\right) M_{AB} = \left(\frac{L^2}{6EI}\right) M_{BA} + \theta_A(L)$$

$$M_{BA}\left(\frac{2L^2}{3EI}\right) - M_{BA}\left(\frac{L^2}{6EI}\right) = \theta_A(L)$$

$$M_{BA}\left(\frac{4L^2}{6EI} - \frac{L^2}{6EI}\right) = \theta_A(L)$$

$$M_{BA} = \left(\frac{2EI}{L^2}\right)\theta_A(L)$$

$$\boxed{M_{BA} = \left[\frac{2EI}{L}\right]\theta_A}$$

InfraStructure, LLC
ENGINEERING CONSULTING GROUP

COMPUTED BY CMB	DATE	SHEET 2 OF 4
CHECKED BY	DATE	PROJ. NO.
PROJECT		
SUBJECT Structural Analysis Review		

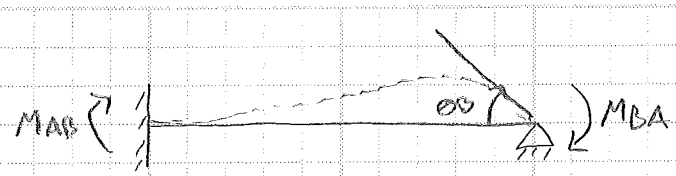

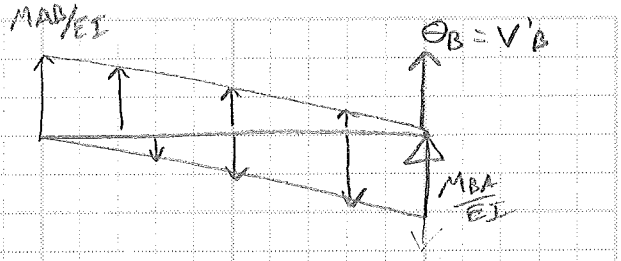

$\zeta \sum M_B = 0$

$$\left(\frac{1}{2}\right)\left(\frac{M_{BA}}{EI}\right)(L)\left(\frac{L}{3}\right) - \left(\frac{1}{2}\right)\left(\frac{M_{AB}}{EI}\right)(L)\left(\frac{2L}{3}\right) = 0$$

$$\left(\frac{L^2}{6EI}\right) M_{BA} = \left(\frac{L^2}{3EI}\right) M_{AB}$$

$$M_{BA} = 2 M_{AB}$$

$$\boxed{M_{BA} = \left(\frac{4EI}{L}\right)\theta_B}$$

$\zeta \sum M_A = 0$

$$-\left(\frac{1}{2}\right)\left(\frac{M_{BA}}{EI}\right)(L)\left(\frac{2L}{3}\right) + \left(\frac{1}{2}\right)\left(\frac{M_{AB}}{EI}\right)(L)\left(\frac{L}{3}\right) + \theta_B(L) = 0$$

$$-\left(\frac{L^2}{3EI}\right) M_{BA} + \left(\frac{L^2}{6EI}\right) M_{AB} + \theta_B(L) = 0$$

$$M_{AB}\left(\frac{2L^2}{3EI} - \frac{L^2}{6EI}\right) = \theta_B(L)$$

$$\boxed{M_{AB} = \left(\frac{2EI}{L}\right)\theta_B}$$

InfraStructure, LLC
ENGINEERING CONSULTING GROUP

COMPUTED BY CMB	DATE	SHEET 3 OF 4
CHECKED BY	DATE	PROJ. NO.
PROJECT		
SUBJECT Structural Analysis Review		

- Angular displacement @ B, θ_B
  - similar to θ_A, only this time A is fixed & B is pinned

$$M_{AB} = \left[\frac{2EI}{L}\right]\theta_B \qquad M_{BA} = \left[\frac{4EI}{L}\right]\theta_B$$

- Relative Linear displacement, Δ
  - if the far node B of the member is displaced relative to A so that the cord of member rotates clockwise (positive displacement) & both ends do not rotate equal & opposite shear & moment reactions are developed in the member as shown below

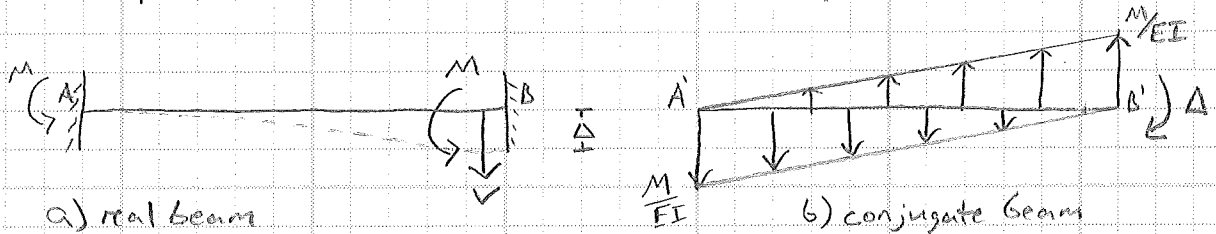

a) real beam b) conjugate beam

$$\circlearrowleft \Sigma M_{B'} = 0$$

$$\left(\frac{1}{2}\right)\left(\frac{M}{EI}\right)(L)\left(\frac{2}{3}\right)(L) - \left(\frac{1}{2}\right)\left(\frac{M}{EI}\right)(L)\left(\frac{1}{3}\right)L - \Delta = 0$$

$$M\left(\frac{2L^2}{6EI}\right) - M\left(\frac{L^2}{6EI}\right) = \Delta$$

$$\boxed{M = -\left[\frac{6EI}{L^2}\right]\Delta}$$

* this moment has a negative sign due to sign convention, since for equilibrium it acts counterclockwise on the member

- Fixed-End Moments
  - previously we considered relationships between displacements & necessary moments M_{AB}, M_{BA} acting at nodes A & B respectively
  - in general, linear or angular displacements of nodes are caused by loadings acting on the span not by moments acting at the nodes
  - in order to develop the slope deflection equations we must transform these span loadings into equivalent moments acting at the nodes & then use the load-displacement relationships just derived
  - to do this we find the reaction moment that each load develops at the nodes
  - consider the example below a fixed-fixed beam w/ a point load @ center

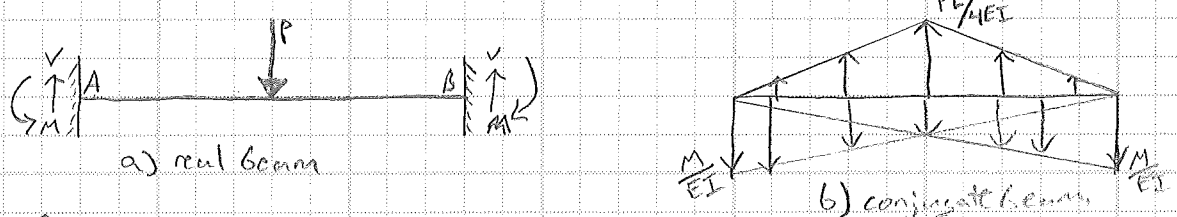

a) real beam b) conjugate beam

$$\uparrow \Sigma F_y = 0$$

$$\left(\frac{1}{2}\right)\left(\frac{PL}{4EI}\right)(L) - (2)\left(\frac{1}{2}\right)(L)\left(\frac{M}{EI}\right) = 0 \Rightarrow \boxed{M = \frac{PL}{8}}$$

InfraStructure, LLC
ENGINEERING CONSULTING GROUP

COMPUTED BY CMB	DATE	SHEET 4 OF 4
CHECKED BY	DATE	PROJ. NO.
PROJECT		
SUBJECT Structural Analysis Review		

- the previous moment found is called a fixed-end moment (FEM)
  - also note that due to sign convention M is negative at node A (CCW) & positive @ Node B (CW)
  - fixed end moments change depending on loadings, a variety of FEM's for different loadings are tabulated on back cover of H-66 Clue book
- the FEM (load specific) are added to end moments due to each displacement (derived earlier) to obtain resultant moments

- Generalized slope deflection equations
  - be extremely careful when using these to apply sign convention correctly & know which way things are pointing

$$M_{AB} = \left[\frac{4EI}{L}\right]\theta_A + \left[\frac{2EI}{L}\right]\theta_B - \left[\frac{6EI}{L^2}\right]\Delta + (FEM)_{AB}$$

$$M_{BA} = \left[\frac{2EI}{L}\right]\theta_A + \left[\frac{4EI}{L}\right]\theta_B - \left[\frac{6EI}{L^2}\right]\Delta + (FEM)_{BA}$$

* Deriving Appendix 1

a)

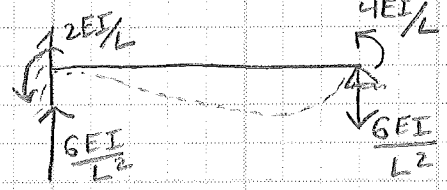

- Taking left as A & right as B
- $M_{BA} = \left[\frac{2EI}{L}\right]\theta_A + \left[\frac{4EI}{L}\right]\theta_B - \left[\frac{6EI}{L^2}\right]\Delta$
- no FEM needed, only 1/2 of derivation

b)

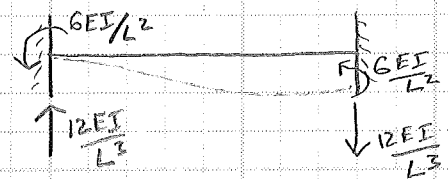

- Taking left as A & right as B
- need full derivation

InfraStructure, LLC
ENGINEERING CONSULTING GROUP

COMPUTED BY CMB	DATE	SHEET 13 OF 24
CHECKED BY	DATE	PROJ. NO.
PROJECT Chapter 9		
SUBJECT Structural Dynamics (Chopra)		

* Example 9.8
- starting with EOM from example 9.4 derive EOM in example 9.5
- simply put the EOM in example 9.5 are the statically condensed version of the EOM in example 9.4. So example 9.5 has the Dynamic DOF EOM

$$[u] = \begin{bmatrix} u_t \\ u_o \end{bmatrix} = \begin{bmatrix} u_1 \\ u_2 \\ u_3 \\ u_4 \end{bmatrix} \qquad [p(t)] = \begin{bmatrix} p_t(t) \\ 0 \end{bmatrix} = \begin{bmatrix} p_1(t) \\ p_2(t) \\ p_3(t) \\ p_4(t) \end{bmatrix}$$

$$[m] = \begin{bmatrix} m_{tt} & 0 \\ 0 & 0 \end{bmatrix} = \begin{bmatrix} m/4 & 0 & 0 & 0 \\ 0 & m/2 & 0 & 0 \\ 0 & 0 & 0 & 0 \\ 0 & 0 & 0 & 0 \end{bmatrix}$$

$$[K] = \begin{bmatrix} K_{tt} & K_{to} \\ K_{ot} & K_{oo} \end{bmatrix} = \frac{8EI}{L^3} \begin{bmatrix} 12 & -12 & -3L & -3L \\ -12 & 24 & 3L & 0 \\ -3L & 3L & L^2 & L^2/2 \\ -3L & 0 & L^2/2 & 2L^2 \end{bmatrix}$$

- find condensed stiffness matrix

$$[\hat{K}_{tt}] = [K_{tt}] - [K_{ot}]^T [K_{oo}]^{-1} [K_{ot}] = \frac{8EI}{L^3} \left\{ \begin{bmatrix} 12 & -12 \\ -12 & 24 \end{bmatrix} - \begin{bmatrix} -3L & -3L \\ 3L & 0 \end{bmatrix} \begin{bmatrix} L^2 & L^2/2 \\ L^2/2 & 2L^2 \end{bmatrix}^{-1} \begin{bmatrix} -3L & 3L \\ -3L & 0 \end{bmatrix} \right\}$$

- $[K_{ot}]^T = [K_{to}]$

$$[\hat{K}_{tt}] = \frac{48EI}{7L^3} \begin{bmatrix} 2 & -5 \\ -5 & 16 \end{bmatrix}$$ * EOM from example 9.5

- final relation between condensed DOF & dynamic DOF

$$[u_o] = -[K_{oo}]^{-1} [K_{ot}] [u_t] = [T][u_t]$$

$$[T] = \frac{1}{L} \begin{bmatrix} 2.57 & -3.43 \\ 0.857 & 0.857 \end{bmatrix}$$ * note this hasn't been multiplied by the $(8EI/L^3)$ out front of $[K]$

* Example 9.9
- formulate EOM for frame in example 9.7 governing the lateral floor displacements

$$[K] = \begin{bmatrix} K_{tt} & K_{to} \\ K_{ot} & K_{oo} \end{bmatrix} = \frac{EI}{h^3} \begin{bmatrix} 72 & -24 & 6h & 6h & -6h & -6h \\ -24 & 24 & 6h & 6h & 6h & 6h \\ 6h & 6h & 16h^2 & 2h^2 & 2h^2 & 0 \\ 6h & 6h & 2h^2 & 16h^2 & 0 & 2h^2 \\ -6h & 6h & 2h^2 & 0 & 6h^2 & h^2 \\ -6h & 6h & 0 & 2h^2 & h^2 & 6h^2 \end{bmatrix}$$

InfraStructure, LLC
ENGINEERING CONSULTING GROUP

COMPUTED BY CMB	DATE	SHEET 14 OF 24
CHECKED BY	DATE	PROJ. NO.
PROJECT Chapter 9		
SUBJECT Structural Dynamics (Chopra)		

- $[\hat{K}_{tt}] = [K_{tt}] - [K_{ot}]^T [K_{oo}]^{-1} [K_{ot}] = \frac{EI}{h^3}\begin{bmatrix} 54.88 & -17.51 \\ -17.51 & 11.61 \end{bmatrix}$
  - this matrix is also known as the lateral stiffness matrix, because DOF are the lateral displacements of the floor
  - used in equake analysis
- $[u_o] = -[K_{oo}]^{-1}[K_{ot}][u_t] = [T][u_t]$
- $[T] = \frac{1}{h}\begin{bmatrix} -0.4426 & -0.2459 \\ -0.4426 & -0.2459 \\ 0.9836 & -0.7869 \\ 0.9836 & -0.7869 \end{bmatrix}$
- EOM are written using $[m_{tt}]$; $[P_t]$; & $[\hat{K}_{tt}]$

$$m\begin{bmatrix} 2 & 0 \\ 0 & 1 \end{bmatrix}\begin{bmatrix} \ddot{u}_1 \\ \ddot{u}_2 \end{bmatrix} + \frac{EI}{h^3}\begin{bmatrix} 54.88 & -17.51 \\ -17.51 & 11.61 \end{bmatrix}\begin{bmatrix} u_1 \\ u_2 \end{bmatrix} = \begin{bmatrix} p_1(t) \\ p_2(t) \end{bmatrix}$$ // Final

9.4 Planar or Symetric Plan systems; Ground Motion

9.4.1 Planar Systems; Translational Ground Motion

- start w/ simplest case. All dynamic DOF are displacements in the same direction as ground motion
- 2 examples, a tower & building frame shown below

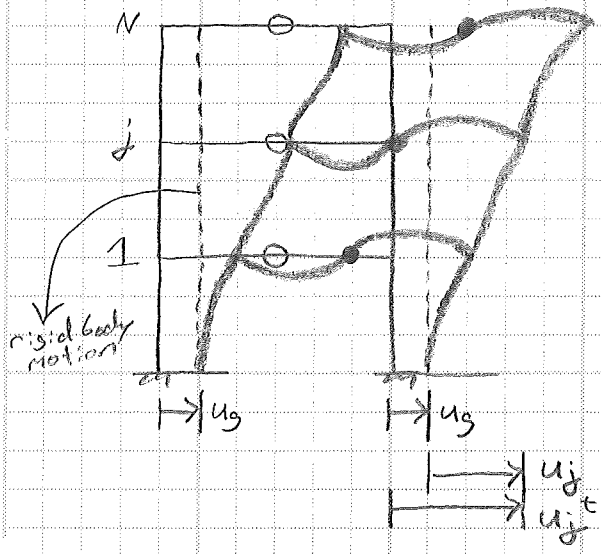

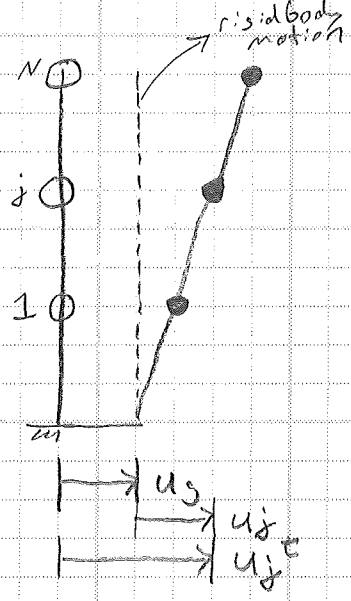

- $u_j^t = u_j + u_g$
  - u_j^t: absolute displacement of mass
  - u_j: relative displacement between mass & ground
  - u_g: displacement of ground

InfraStructure, LLC
ENGINEERING CONSULTING GROUP

COMPUTED BY CMB	DATE	SHEET 10 OF 24
CHECKED BY	DATE	PROJ. NO.
PROJECT Chapter 9		
SUBJECT Structural Dynamics (Chopra)		

- invert flexibility matrix to get [K]

$$[K] = \frac{6EI}{7L^3}\begin{bmatrix} 8 & -3 \\ -3 & 2 \end{bmatrix}$$

- free vibration EOM

$$\begin{bmatrix} 3m & 0 \\ 0 & m \end{bmatrix}\begin{bmatrix} \ddot{u}_1 \\ \ddot{u}_2 \end{bmatrix} + \frac{6EI}{7L^3}\begin{bmatrix} 8 & -3 \\ -3 & 2 \end{bmatrix}\begin{bmatrix} u_1 \\ u_2 \end{bmatrix} = \begin{bmatrix} 0 \\ 0 \end{bmatrix} \quad // \text{ Final}$$

* Example 9.7
- formulate EOM for the two story frame below

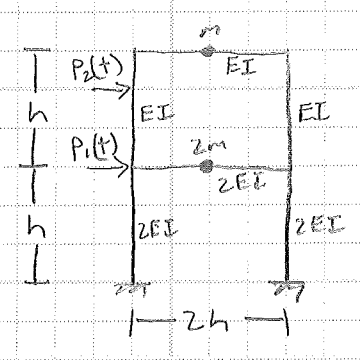

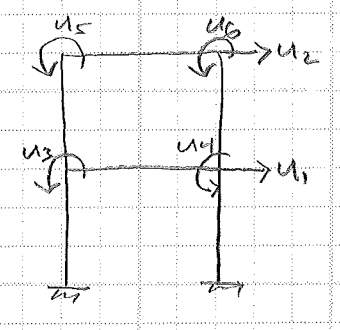

$$[u] = [u_1\ u_2\ u_3\ u_4\ u_5\ u_6]^T$$

$$[\ddot{u}] = [\ddot{u}_1\ \ddot{u}_2\ \ddot{u}_3\ \ddot{u}_4\ \ddot{u}_5\ \ddot{u}_6]^T$$

$$[p(t)] = [p_1(t)\ p_2(t)\ 0\ 0\ 0\ 0]^T$$

$$m = \begin{bmatrix} 2m & 0 & 0 & 0 & 0 & 0 \\ 0 & m & 0 & 0 & 0 & 0 \\ 0 & 0 & 0 & 0 & 0 & 0 \\ 0 & 0 & 0 & 0 & 0 & 0 \\ 0 & 0 & 0 & 0 & 0 & 0 \\ 0 & 0 & 0 & 0 & 0 & 0 \end{bmatrix}$$

- define stiffness matrix
  - $u_1 = 1$

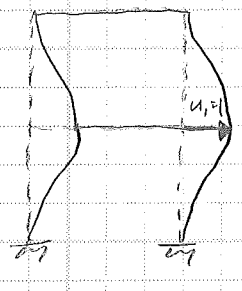

$$K_{11} = \left(\frac{12(2EI)}{h^3}\right)2 + \left(\frac{12EI}{h^3}\right)2 = \frac{72EI}{h^3} \qquad K_{51} = -\frac{6EI}{h^2}$$

$$K_{21} = \left(\frac{12EI}{h^3}\right)2 = -\frac{24EI}{h^3} \qquad K_{61} = K_{51}$$

$$K_{31} = \frac{6(2EI)}{h^2} - \frac{6EI}{h^2} = \frac{6EI}{h^2}$$

$$K_{41} = K_{31}$$

  - $u_2 = 1$

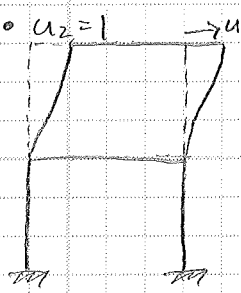

$$K_{12} = -\left(\frac{12(EI)}{h^3}\right)2 = -\frac{24EI}{h^3} \qquad K_{52} = \frac{6EI}{h^2}$$

$$K_{22} = \left(\frac{12EI}{h^3}\right)2 = \frac{24EI}{h^3} \qquad K_{62} = K_{52}$$

$$K_{32} = \frac{6(EI)}{h^2} = \frac{6EI}{h^2}$$

$$K_{42} = K_{32}$$

InfraStructure, LLC
ENGINEERING CONSULTING GROUP

COMPUTED BY C.MB	DATE	SHEET 11 OF 24
CHECKED BY	DATE	PROJ. NO.
PROJECT Chapter 9		
SUBJECT Structural Dynamics (Chopra)		

- $u_3 = 1$

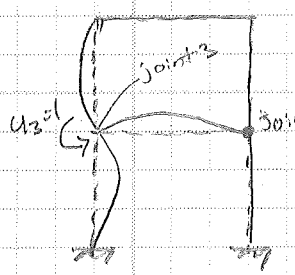

$K_{13} = \frac{6(2EI)}{h^2} - \frac{6EI}{h^2} = \frac{6EI}{h^2}$ * note K_{13} comes from contributions at joint 3 nothing from joint 4

$K_{23} = \frac{6EI}{h^2}$

$K_{33} = \frac{4(2EI)}{h} + \frac{4(2EI)}{2h} + \frac{4EI}{h} = \frac{16EI}{h}$

$K_{43} = \frac{2(2EI)}{2h} = \frac{2EI}{h}$

$K_{53} = \frac{2EI}{h}$ $\quad K_{63} = 0$

- $u_4 = 1$

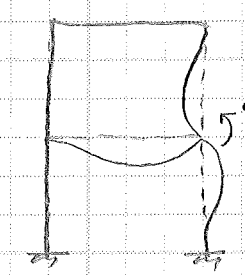

$K_{14} = \frac{6(2EI)}{h^2} - \frac{6EI}{h^2} = \frac{6EI}{h^2}$ $\quad K_{54} = 0$

$K_{24} = \frac{6EI}{h^2}$ $\quad K_{64} = \frac{2EI}{h}$

$K_{34} = \frac{2(2EI)}{2h} = \frac{2EI}{h}$

$K_{44} = \frac{4(2EI)}{h} + \frac{4(2EI)}{2h} + \frac{4EI}{h} = \frac{16EI}{h}$

- $u_5 = 1$

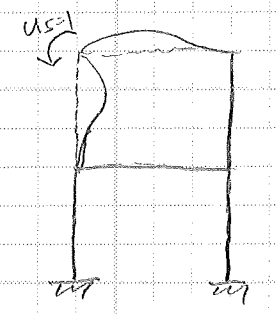

$K_{15} = -\frac{6EI}{h^2}$ $\quad K_{55} = \frac{4EI}{h} + \frac{4EI}{2h} = \frac{6EI}{h}$

$K_{25} = \frac{6EI}{h^2}$ $\quad K_{65} = \frac{2EI}{2h} = \frac{EI}{h}$

$K_{35} = \frac{2EI}{h}$

$K_{45} = 0$

* K_{15} from contributions of Left side 2nd story column

- $u_6 = 1$

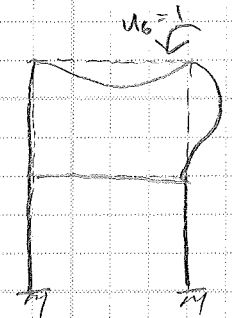

$K_{16} = -\frac{6EI}{h^2}$ $\quad K_{56} = \frac{2EI}{2h} = \frac{EI}{h}$

$K_{26} = \frac{6EI}{h^2}$ $\quad K_{66} = \frac{4EI}{h} + \frac{4EI}{2h} = \frac{6EI}{h}$

$K_{36} = 0$

$K_{46} = \frac{2EI}{h}$

$$[K] = \frac{EI}{h^3}\begin{bmatrix} 72 & -24 & 6h & 6h & -6h & -6h \\ -24 & 24 & 6h & 6h & 6h & 6h \\ 6h & 6h & 16h^2 & 2h^2 & 2h^2 & 0 \\ 6h & 6h & 2h^2 & 16h^2 & 0 & 2h^2 \\ -6h & 6h & 2h^2 & 0 & 6h^2 & h^2 \\ -6h & 6h & 0 & 2h^2 & h^2 & 6h^2 \end{bmatrix}$$

EOM: $[m][\ddot{u}] + [k][u] = [p(t)]$

InfraStructure, LLC
ENGINEERING CONSULTING GROUP

COMPUTED BY CMB	DATE	SHEET 11 OF
CHECKED BY	DATE	PROJ. NO.
PROJECT Chapter 10		
SUBJECT Structural Dynamics (Chopra)		

- mass & stiffness matrices determined in Example 9.1

$$[m] = \begin{bmatrix} 2m & 0 \\ 0 & m \end{bmatrix} \qquad [K] = \begin{bmatrix} 3K & -K \\ -K & K \end{bmatrix} \qquad K = \frac{24EI_c}{h^3}$$

- frequency equation: $(2m^2)\omega^4 + (-5Km)\omega^2 + 2K^2 = 0$
  - $\omega_1 = \sqrt{K/2m}$
  - $\omega_2 = \sqrt{2K/m}$

- after subbing in K
  - $\omega_1 = 3.464\sqrt{\frac{EI_c}{mh^3}}$
  - $\omega_2 = 6.928\sqrt{\frac{EI_c}{mh^3}}$

- natural modes

$$\phi_1 = \begin{bmatrix} 0.5 \\ 1 \end{bmatrix} \qquad \phi_2 = \begin{bmatrix} -1 \\ 1 \end{bmatrix}$$

- to normalize 1st mode, M_1 is calculated

$$M_1 = \phi_1^T[m]\phi_1 = m\begin{bmatrix} 0.5 & 1 \end{bmatrix}\begin{bmatrix} 2 & 0 \\ 0 & 1 \end{bmatrix}\begin{bmatrix} 0.5 \\ 1 \end{bmatrix} = \frac{3m}{2}$$

  - to make $M_1 = 1$, divide ϕ_1 by $\sqrt{3m/2}$ to obtain normalized mode

$$\phi_1 = \frac{1}{\sqrt{6m}}\begin{bmatrix} 1 \\ 2 \end{bmatrix}$$

  - second mode can be normalized similarly

* Example 10.5 *

Determine the natural frequencies & modes of the system shown below & defined in example 9.9. The story height h = 10ft.

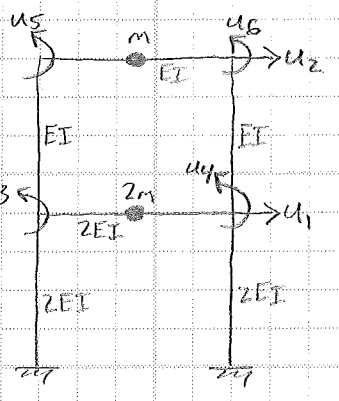

(a)

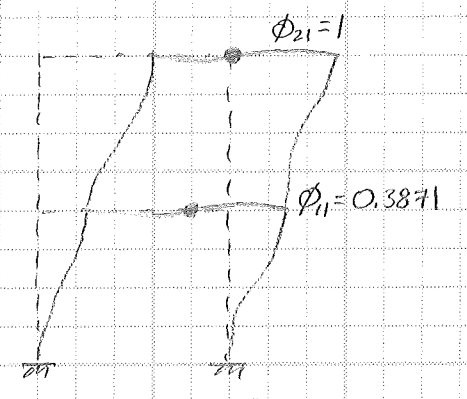

$\omega_1 = 2.198\sqrt{\frac{EI}{mh^3}}$

(b)

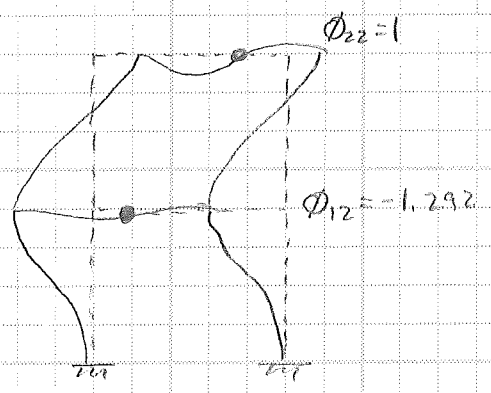

$\omega_2 = 5.850\sqrt{\frac{EI}{mh^3}}$

(c)

InfraStructure, LLC
ENGINEERING CONSULTING GROUP

COMPUTED BY CMB	DATE	SHEET 12 OF
CHECKED BY	DATE	PROJ. NO.
PROJECT Chapter 10		
SUBJECT Structural dynamics (Chopra)		

- mass & condensed stiffness matrix found in example 9.9

$$[m_{tt}] = \begin{bmatrix} 2m & 0 \\ 0 & m \end{bmatrix} \qquad [\hat{K}_{tt}] = \frac{EI}{h^3}\begin{bmatrix} 54.88 & -17.51 \\ -17.51 & 11.61 \end{bmatrix}$$

- frequency equation:
  - $\det\left\{[\hat{K}_{tt}] - \omega_n^2[m_{tt}]\right\} = 0$
  - $\omega_1 = 2.198\sqrt{\frac{EI}{mh^3}}$ • $\omega_2 = 5.850\sqrt{\frac{EI}{mh^3}}$
- this example has flexible beams while 10.4 has rigid beams, notice that the flexible beams lower the natural frequencies, consistent w/ intuition
- natural modes are determined by solving: $\{[K_{tt}] - \omega_n^2[m]\}\phi_n = [0]$

$$\phi_1 = \begin{bmatrix} 0.3871 \\ 1 \end{bmatrix} \qquad \phi_2 = \begin{bmatrix} -1.292 \\ 1 \end{bmatrix}$$

- the natural modes above define the lateral displacements of each floor. The joint rotations associated w/ the first mode are determined by substituting ϕ_1 for $[u_t]$ in the equation below defined in example 9.9
  - $[u_o] = [T][u_t]$

$$\begin{bmatrix} u_3 \\ u_4 \\ u_5 \\ u_6 \end{bmatrix} = \frac{1}{h}\begin{bmatrix} -0.4426 & -0.2459 \\ -0.4426 & -0.2459 \\ 0.9836 & -0.7869 \\ 0.9836 & -0.7869 \end{bmatrix}\underbrace{\begin{bmatrix} 0.3871 \\ 1 \end{bmatrix}}_{[u_t]=\phi_1} = \frac{1}{h}\begin{bmatrix} -0.4172 \\ -0.4172 \\ -0.4061 \\ -0.4061 \end{bmatrix}$$

- similarly joint rotations for 2nd mode are found

$$\begin{bmatrix} u_3 \\ u_4 \\ u_5 \\ u_6 \end{bmatrix} = \frac{1}{h}\begin{bmatrix} 0.3528 \\ 0.3528 \\ -2.0573 \\ -2.0593 \end{bmatrix}$$

* Example 10.6 *

Figure 9.5.1 shows the plan view of a one story building consisting of a roof idealized as a rigid diaphragm, supported on 3 frames A, B, & C as shown. The roof weight is a uniformly distributed magnitude of 100 psf. The lateral stiffness of the frames are $K_y = 75$ K/ft for frame A & $K_x = 40$ K/ft for frames B & C. The plan dimensions are $b = 30$ft & $d = 20$ft, the eccentricity is 1.5 ft, & building height is 12 ft. Determine the natural periods & modes of vibration of the structure.

example105_English.m

```
E = 1149120 %Define modulus of elasticity (kip/ft^2)
I = (pi/4)*(1.5/2)^4 %Define moment of inertia (ft^4)
L = 10 %Define length (ft)
m = (75/32.1740) %Define mass (kip)

%Partition mass matrix
mtt = m*[2,0;0,1]

%Compile stiffness matrix
k = ((E*I)/L^3) * [72,-24,6*L,6*L,-6*L,-6*L;-24,24,6*L,6*L,6*L,6*L;
    6*L,6*L,16*L^2,2*L^2,2*L^2,0;6*L,6*L,2*L^2,16*L^2,0,2*L^2;
    -6*L,6*L,2*L^2,0,6*L^2,L^2;-6*L,6*L,0,2*L^2,L^2,6*L^2]

%Partition stiffness matrix
ktt = k(1:2, 1:2)
kot = k(3:6, 1:2)
kto = k(1:2, 3:6)
koo = k(3:6, 3:6)

%Condense stiffness matrix
kc = ktt - (kot' * koo^-1 * kot)

%Characteristic equation
[phi,w2] = eig(kc, mtt)

%Calculate natural frequencies
w = [sqrt(w2(1,1)); sqrt(w2(2,2))]
f = w/(2*pi)
T = [1/f(1,1); 1/f(2,1)]

%Calculate influence vector
i = [1;1]

%Calculate generalized mass
M = transpose(phi)*mtt*phi

%Normalize modes to Mn = 1
phi_norm = [phi(1,1)/sqrt(M(1,1)), phi(1,2)/sqrt(M(2,2));
         phi(2,1)/sqrt(M(1,1)), phi(2,2)/sqrt(M(2,2))]

%Calculate L vector
LL = transpose(phi)*mtt*i

%Calculate effective modal mass
EMM = [(LL(1,1)^2)/M(1,1); (LL(2,1)^2)/M(2,2)]

%Calculate effective modal mass participation percentage
EMPP = [EMM(1,1)/(mtt(1,1)+mtt(2,2)); EMM(2,1)/(mtt(1,1)+mtt(2,2))]
```